ORGANIC LASING: CORRELATION BETWEEN MOLECULAR STRUCTURE, OPTICAL AND OPTOELECTRONIC PROPERTIES

Dissertation

zur Erlangung des Grades
"Doktor der Naturwissenschaften"
im Promotionsfach Chemie
am Fabereich Chemie, Pharmazie und Geowissenschaften
der Johannes Gutenberg-Universität
in Mainz

vorgelegt von
Hun KIM
geboren in Rüsselsheim
Mainz, 2012

Dekan:

1. Berichterstatter:
2. Berichterstatter:

Tag der mündlichen Prüfung:

ABSTRACT

In this thesis mainly two alternating indenofluorene-phenanthrene copolymers were investigated with a variety of spectroscopic and optoelectronic experiments. The different experimental techniques allowed to retrieve deeper insights into their unique optical as well as optoelectronic properties. The motivation of the research presented in this work was to correlate their photophysical properties with respect to their application in electrically pumped lasing. This thesis begins with the description of optical properties studied by classical absorption and emission spectroscopy and successively describes an overall picture regarding their excited state dynamics occurring after photoexcitation studied by time-resolved spectroscopy. The different spectroscopic methods do not only allow to elucidate the different optical transitions occurring in this class of materials, but also contribute to a better understanding of exciton dynamics and exciton interaction with respect to the molecular structure as well as aggregation and photooxidation of the polymers. Furthermore, the stimulated emission properties were analyzed by amplified spontaneous emission (ASE) experiments. Especially one of the investigated materials, called BLUE-1, showed outstanding optical properties including a high optical gain, a low threshold for ASE and low optical losses. Apart from the optical experiments, the charge carrier mobility was measured with the time-of-flight technique and a comparably high hole mobility on the order of $1 \cdot 10^{-2}$ $cm^2/(Vs)$ was determined for BLUE-1 which makes this material promising for organic lasing. The impact of the high charge carrier mobility in this material class was further analyzed in different optoelectronic devices such as organic LEDs (OLEDs) and organic solar cells.

ZUSAMMENFASSUNG

Im Rahmen der vorliegenden Arbeit wurden mit einer Reihe von verschiedenen spektroskopischen wie auch optoelektronischen Experimenten zwei alternierende Indenofluoren-Phenanthren Copolymere untersucht. Die hier vorgestellten experimentellen Techniken erlauben einen tiefen Einblick in die einzigartigen optischen wie auch optoelektronischen Eigenschaften dieser Materialklasse. Die dabei gewonnen photophysikalischen Erkenntnisse werden in Hinblick auf eine Realisierung eines rein elektrisch betriebenen organischen Lasers diskutiert. Mittels klassischer Absorptions- und Emissionsspektroskopie wurden optisch angeregte Zustände untersucht und deren Dynamiken mit der zeitaufgelösten Spektroskopie bestimmt. Die verschiedenen spektroskopischen Experimente dienten dabei nicht nur zur Beschreibung der optischen Übergänge, sondern auch zum Verständnis von Exzitonendynamiken, Exzitonen-Wechselwirkungen in Bezug auf die Molekülstruktur wie auch Zwischenkettenwechselwirkungen und Photooxidation. Weiterhin wurde diese Klasse von konjugierten Polymeren hinsichtlich der verstärkten spontanen Emission (engl. Amplified Spontaneous Emission, ASE) untersucht. Vor allem ein Material mit der Bezeichnung BLUE-1 stach hervor mit einer für ASE hohen optischen Verstärkung, einer niedrigen Schwelle und geringen optischen Verlusten. Neben den spektroskopischen Methoden, wurde die Ladungsträgermobilität für BLUE-1 mit der Time-of-Flight Methode zu $1 \cdot 10^{-2}$ $cm^2/(Vs)$ bestimmt. Die Auswirkung von hohen Ladungsträgermobilitäten in dieser Materialklasse wurde weiterhin auch in verschiedenen optoelektronischen Bauteilen wie organischen LEDs (OLEDs) und organischen Solarzellen analysiert.

PUBLICATIONS AND CONFERENCE CONTRIBUTIONS

PUBLICATIONS

Scientific publications presented in this work

H. Kim, N. Schulte, I. A. Howard, F. Laquai, "*Spectroscopic Investigation of High Gain Phenanthrene-Indenofluorene Copolymers for Organic Lasing*" in preparation.

H. Kim, N. Schulte, G. Zhou, K. Müllen, F. Laquai, "*A High Gain and High Charge Carrier Mobility Indenofluorene-Phenanthrene Copolymer for Light Amplification and Organic Lasing*." Advanced Materials **2011**, 23(7), 894-897.

Further publications

W. K. Bae, D. Lee, J. Lim, J. Kwak, H. Kim, A. Park, H. Lee, H. Woo, M. Park, F. Laquai, K. Char, C. Lee, S. Lee,"*Bright and Low-Voltage Driven White Light-Emitting Diodes Based on Colloidal Quantum Dots with an Inverted Structure*", in preparation.

K.-S. Kim, H. Kim, J.-H. Kim, J.-H. Kim, C.-L. Lee, F. Laquai, S. I. Yoo, B.-H. Sohn, "*Correlation of Micellar Structures with Surface Plasmon-Coupled Fluorescence in Strategy for Fluorescence Enhancement*", submitted.

K.-S. Kim, J.-H. Kim, H. Kim, F. Laquai, E. Arifin, J.-K. Lee, S.-I Yoo, B.-H. Sohn,"*Switching Off FRET in the Hybrid Assemblies of Diblock Copolymer Micelles, Quantum Dots, and Dyes by Plasmonic Nanoparticles.*", DOI: 10.1021/nn301893e.

M. Tomar, N.T. Lucas, H. Kim, F. Laquai, K. Müllen and J. Jacob, "Facile synthesis of 5,8-linked quinoline based copolymers", Polymer International **2012**, DOI: 10.1002/pi.4211.

M.G. Schwab, T. Qin, W. Pisula, A. Mavrinskiy, X. Feng, M. Baumgarten, H. Kim, F. Laquai, S. Schuh, R. Trattnig, E.J.W. List, K. Müllen:"Molecular Triangles: Synthesis, Self-Assembly, and Blue Emission of Cyclo-7,10-tris-triphenylenyl Macrocycles, Chemistry - An Asian Journal **2011**, 6(11), 3001-3010.

CONFERENCE CONTRUBUTIONS

11/2011	Poster presentation at 12th Pacific Polymer Conference, Jeju Island, Korea
07/2011	Oral presentation at IRTG workshop, Mainz, Germany
03/2011	Poster presentaion at annual meeting of the German Physical Society (DPG), Dresden, Germany
01/2011	Poster presentation at IRTG workshop, Seoul, Korea
12/2010	Oral presentation at Pacifichem 2011, Honolulu, USA
06/2010	Oral presentation at IRTG workshop, Mainz, Germany
08/2009	Poster presentation at IRTG workshop, Mainz, Germany

CONTENTS

LIST OF FIGURES

LIST OF TABLES

ACRONYMS

Alq3 Aluminium-tris(8-hydroxychinolin)

ASE amplified spontaneous emission

CCD charge coupled device

CIE commission internationale de l'éclairage

COT 1,3,5,7-cyclooctatetraene

CT charge-transfer

CW continous-wave

DF delayed fluorescence

DFB distributed feedback

DIO 1,8-diiodooctane

DOS density of states

DSC differential scanning calorimetry

EL electroluminescence

EQE external quantum efficiency

ETL electron transport layer

FF fill-factor

FRET Förster Resonance Energy Transfer

FWHM full width at half maximum

GDM Gaussian Disorder Model

HDMS hexamethyldisilazane

HeCd Helium-Cadmium

HIL hole injection layer

HOMO highest occupied molecular orbital

ICCD intensified charge coupled device

IR infrared

ISC intersystem crossing

ITO indium tin oxide

IV current-voltage

KWW Kohlrausch-Williams-Watts

LED light emitting diode

LiF lithium fluoride

LUMO lowest unoccupied molecular orbital

MEH-PPV poly[2-methoxy-5-(2-ethylhexyloxy)-p-phenylene vinylene]

MTHF 2-Methyltetrahydrofuran

Nd:YAG neodymium-doped yttrium aluminium garnet

NIR near-infrared

OLED organic light emitting diode

OFET organic field effect transistor

OPO optical parametric oscillator

OSC organic solar cell

PCBM [6,6]-phenyl-C61-butyric acid methyl ester

PCE power conversion efficiency

PEDOT:PSS poly(3,4-ethylenedioxythiophene) poly(styrenesulfonate)

PFO poly(9,9-di-n-octylfluorene)

PIA photoinduced absorption

PIF poly(indenofluorene)

PL	photoluminescence
PLQE	photoluminescence quantum efficiency
PTFE	polytetrafluorethylen
SE	stimulated emission
SHG	second harmonic generation
SMU	source-measure-unit
SPA	singlet-polaron annihilation
SSA	singlet-singlet annihilation
STA	singlet-triplet annihilation
TA	transient absorption
TE	transverse electric
Ti:Sa	titanium-sapphire
TM	transverse magnetic
TOF	time-of-flight
TPBI	1,3,5-tris(1-phenyl-1H-benzimidazol-2-yl)benzene
TRPL	time-resolved photoluminescence
TTA	triplet-triplet annihilation
UV	ultra-violett
ZnO	zinc oxide

1 INTRODUCTION

Luminescence of aromatic molecules has been studied intensively over the course of the last century [4, 12]. Their optical properties, for example the potential for color tunability over the whole visible electromagnetic spectrum and their facile synthesis offer a variety of different applications [13]. In 1976, Alan Heeger, Hideki Shirakawa and Alan MacDiarmid first showed electrical conduction in poly(acetylene), tunable across the full range from an insulator to a metal by doping [14, 15]. These findings were of particular importance, since it was until then believed that polymers were insulators and therefore unable to transport charges. Since then, it became possible to combine mechanical properties of plastic with the optical and electrical properties of organic molecules with high molecular absorption cross sections, high quantum yields and charge carrier mobilities. They were awarded the Nobel Prize for Chemistry in the year 2000 and laid the foundation of organic electronics. Nowadays, organic semiconductors have entered our everyday life and the arena of consumer electronics is currently undergoing a transition from inorganic and liquid crystal based technology to different organic technologies. For example, displays of smartphones and televisions based on organic semiconducting molecules are substituting existing technologies and in many cases offer consumers advantages over their inorganic equivalents, including strong color contrast, larger viewing angles and lower power consumption. White light emitting panels have started to replace conventional lighting sources such as light bulbs. Organic field effect transistors (OFETs) have now achieved hole mobilities in the order of $1 \cdot 10\ \mathrm{cm}^2/(\mathrm{Vs})$ [16] and are competing with polycrystalline silicon in the low-tech area [17]. Organic electronics offer technologies, which are impossible with inorganic material such as in the field of bio-electronics [18, 19, 20]. All-organic solar cells currently achieve power conversion efficiencies of over 10 % [21] and will soon enter the market to revolutionize todays way of mobile energy generation.

However, apart from a few products based on organic electronics already available or applications close to market entrance, there are still technologies far away from realization. An electrically pumped laser is such a device and often named "the holy grail" of organic optoelectronics [22]. Following the evolution of inorganic semiconductors, the extension of organic light emitting diode (OLED) technology to the development of an organic laser diode is the most logical step. Such an application would be of great importance for photonics [23], communication [24, 25], sensing [26, 27, 28, 29] and consumer electronics [30] as well as in completely novel applications. Despite successful demonstration of organic lasing occurring after photoexcitation by a pump laser [31] or an LED [32], a purely electrically driven device has not yet been realized. The difficulties in developing such a technology thus far are a consequence of the intrinsic constraints in organic semiconductor materials. The mechanisms inherent to the function of an electrically pumped laser, that is light emission from excited states and charge transport, are different in organic molecules compared to their inorganic equivalents and due to the intrinsic properties of organic molecules are often mutually exclusive. Stimulated emission in organic molecules is achieved from a highly luminescent medium, able to amplify its own emission. Simultaneously, the onset of stimulated emission in such a material requires a high charge carrier mobility to generate a sufficient number of excited states [33]. A high charge carrier mobility is usually achieved by a close packing of adjacent molecules, while such a close spatial arrangement typically quenches the fluorescence, lowering the quantum yield [33] and often leads to unwanted aggregate emission [34]. Only one material has so far been reported that combines a high charge carrier mobility and a high gain, however, still far away from the requirements for a purely electrically driven device [35]. Moreover, finding the right device architecture with electrodes separated from the emission zone is as significant as identifying the right material with high mobilities, high quantum yield and low optical losses [36, 37, 38, 39]. Blue emitting choromophores have so far shown the best advances in the field of organic lasers, achieving low thresholds and high optical gain [40, 41], while the regions of stimulated emission and polaron/triplet absorption are spectrally separated and thus their interaction

with each other is minimized [42, 43, 44].

A deep and fundamental understanding of gain materials for future lasing applications is a prerequisite for further advances. This work confronts the issues addressed in the prospect of an electrically pumped lasing device and suggests material compositions in order to achieve high gains and mobilities. A novel class of conjugated polymers is introduced and polymers combining the two prerequisites for a lasing device are identified, allowing suggestions to be made regarding the ideal material composition for lasing applications. To this end various optical and optoelectronic experiments were carried out to elucidate the polymers' unique properties from a photophysical as well as from an optoelectronic viewpoint. Different dynamic processes were identified by means of time-resolved spectroscopy and discussed in the context of organic lasers.

This thesis consists of five chapters. *Chapter 1* briefly outlines the impact of organic optoelectronics and classifies this work in the field of organic lasers. *Chapter 2* deals with the theoretical concepts on which this thesis is based, starting with the general description of light-matter interaction, the electronic structure of conjugated molecules and illustrating absorption and emission of light in organic systems. Subsequently, the fate of excitons and polarons in the framework of the Gaussian Disorder Model is explained. Finally, a short description of charge injection and light emission in OLEDs is given. *Chapter 3* presents the experimental results on the optical properties of indenofluorene-phenanthrene copolymers, starting with classical steady-state absorption and emission spectroscopy and followed by time-resolved photoluminescence spectroscopy. Amplified spontaneous emission (ASE) characteristics are analyzed for this class of materials and the stimulated emission cross sections determined. *Chapter 4* concentrates on the electronic and optoelectronic properties of the same class of copolymers, determining the charge carrier mobility and correlating high charge carrier mobilities to device performance in OLEDs as well as in organic solar cells. *Chapter 5* summarizes this thesis and gives an outlook for future material compositions in order to finally achieve the ultimate goal of a purely electrically driven lasing device.

2

THEORETICAL BASICS

2.1 ABSORPTION AND EMISSION OF LIGHT

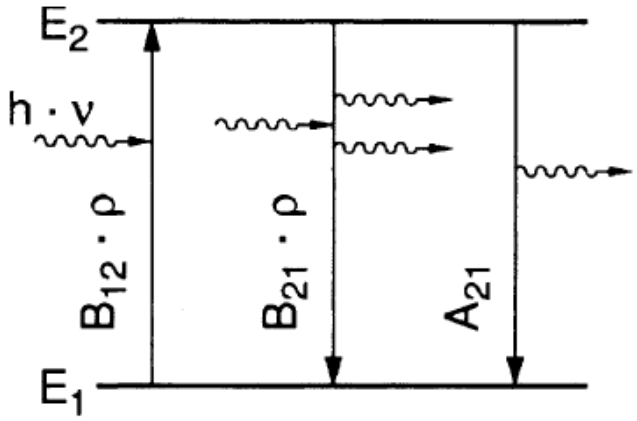

Figure 1: Absorption and emission of light in a two-level system. Reprinted from Ref. [1] with permission.

The quantum-mechanical description of light was first carried out by Albert Einstein in his pioneering work "Zur Quantentheorie der Strahlung" [45] in 1916. His work was based on Planck's law and the postulation of discrete energy levels. A thermal radiation field of photons induces in a molecule a transition ($E_1 \rightarrow E_2$) with $E_1 < E_2$ when the photon energy is equal to the energetic difference between the transition:

$$E = h\nu = E_2 - E_1 = \frac{h \cdot c}{\lambda},$$

h is the Planck's constant, c is the speed of light, ν the frequency of light and λ the wavelength. This process is also known as *induced absorption*. Light-matter interaction is generalized into three different processes. Apart from induced absorption, there is *spontaneous emission* and *induced emission*. The propability P_{ij} that a molecule undergoes one of these processes per second is given by:

$$P_{12}(\text{induced}) = B_{12} \cdot \rho(\nu)$$
$$P_{21}(\text{induced}) = B_{21} \cdot \rho(\nu)$$
$$P_{21}(\text{spontaneous}) = A_{21} \cdot \rho(\nu),$$

the constants B_{12}, B_{21} and A_{21} are known as the Einstein coefficients of *induced absorption*, *induced (or stimulated) emission* and *spontaneous emission*, respectively. *Induced emission* releases photons from E_2 by the stimulation of the transition from the excited state. Incoming photon and released photon have the same phase, frequency and direction. Emission of photons from E_2 can additionally occur *spontaneously* without the presence of an external radiation field [1]. The photons from this process are not in a relationship to each other and thus released photons are non-coherent. At thermal equilibrium the ratio of the population density between N_1 and N_2 and their statistical weights g_1 and g_2 are given by the Boltzmann distribution:

$$\frac{N_2}{N_1} = \frac{g_2}{g_1}\, e^{-\frac{E_2 - E_1}{kT}} = \frac{g_2}{g_1}\, e^{-\frac{h\nu}{kT}}$$

From the three relations of the Einstein coefficients the following equations are deduced:

$$B_{12} = \frac{g_2}{g_1} B_{21}$$
$$B_{21} = \frac{8\pi h\nu^3}{c^3} B_{21}.$$

For $g_1 = g_2$, the rate of induced emission is equal to that of induced absorption, which exemplifies that induced emission cannot occur from a two-level system as both have the same strength. In order to achieve induced emission the population density of the upper level has to exceed the lower level with $N_2 >> N_1$. Induced emission is then more likely to occur than absorption. This is also known as population inversion, which can only be achieved with ancillary levels and not from the two levels E_1 and E_2 alone. When spontaneous emission allows different transition paths with $A_i = \sum_k A_{ik}$, the change of population density of photoluminescence dN at a time interval dt can be calculated with:

$$dN_i = A_i\, N_i\, dt$$
$$\Rightarrow N_1(t) = N_{i0}\, e^{-A_i t} = N_{i0}\, e^{-\frac{t}{\tau_i}},$$

where N_{io} is the population density at t=o and τ_i represents the mean spontaneous emission lifetime, where the popluation density N_i has decreased to $1/e$ [1].

Considering the two-level system, absorption of light is determined by the absorption coefficient $\alpha(\omega)$ and is connected to the absorption cross section $\sigma_{12}(\omega)$ with:

$$\alpha(\omega) = (N_1 - (g_1/g_2)N_2)\sigma_{12}(\omega).$$

2.2 ELECTRONIC CONFIGURATION OF CARBON ATOMS IN MOLECULES

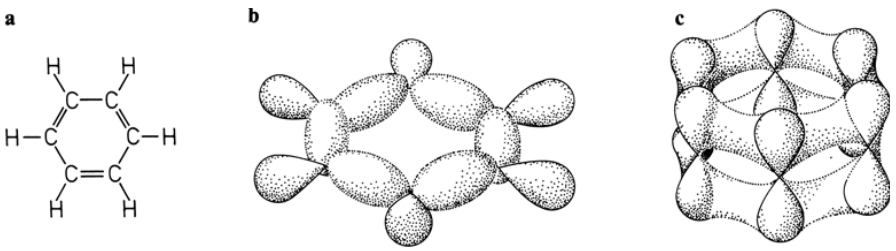

Figure 2: Molecular structure of (a) benzene, (b) probability distribution of σ-orbitals and (c) probability distribution of π-electrons. Reprinted from Ref. [2] with permission.

Carbon belongs to group four of the periodic table with an electron configuration of $1s^2 2s^2 2p^2$. Four electrons reside in the outer electronic level. The two s electrons are paired and the the two p electrons are unpaired [5]. Three possible types of hybridization occur in carbon namely sp, sp^2 and sp^3. Carbon atoms are covalently bonded to each other, however depending on the type of bonding, different orbitals are involved. Single bonds between carbon atoms are formed by sp^2-sp^2 overlap and also known as σ-bonds and are spatially confined along the internuclear axis [46]. Double bonds also known as π-bonds, result from the overlap of p_z-orbitals and sp^2-orbitals. In conjugated systems, alternation of single and double bonds causes delocalization of π-electrons. With the extension of the π-electron system such as in conjugated polymers the delocalization along

the polymer backbone provides a "highway" for charge carriers [47]. The simplest form of a conjugated polymer is polyacetylene. Its energy levels are depicted in Figure 3.

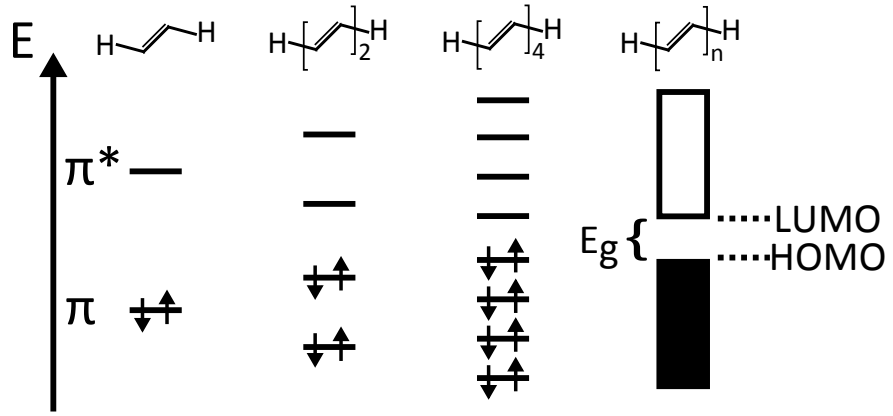

Figure 3: Molecular structure of acetylene derivatives and their corresponding orbital energies.

As the conjugation increases the bandgap E_g decreases and the density of states increases. These effects are caused by changes in electron-electron interaction [8].

2.3 OPTICAL PROPERTIES OF ORGANIC MOLECULES

2.3.1 *Optical transitions in organic molecules*

Electronic transitions in organic molecules from $E_1 \rightarrow E_2$ are characterized by the transition dipole moment $\vec{d}_{21}$, which describes the coupling strength of a transition. For $\vec{d}_{21} = 0$, the given transition is dipole forbidden [48]. The classical treatment of the electric dipole moment for two electric charges with opposite polarity at a distance $\vec{r}$ is given by $\vec{d} = e \cdot \vec{r}$. A quantum mechanical definition of the dipole moment operator is defined as the sum over all dipole moments of a number of i electrons ($\vec{d} = \sum_i e\vec{r}_i$). The transition dipole moment is:

$$\langle \vec{d}_{21} \rangle = \langle \psi_2 | \vec{d} | \psi_1 \rangle = \int \psi_2^* \cdot \left(\sum_i e\vec{r}_i \right) \cdot \psi_1 \, dV,$$

where ψ_1 and ψ_2 denote the wavefunction of the respective eigenstates.

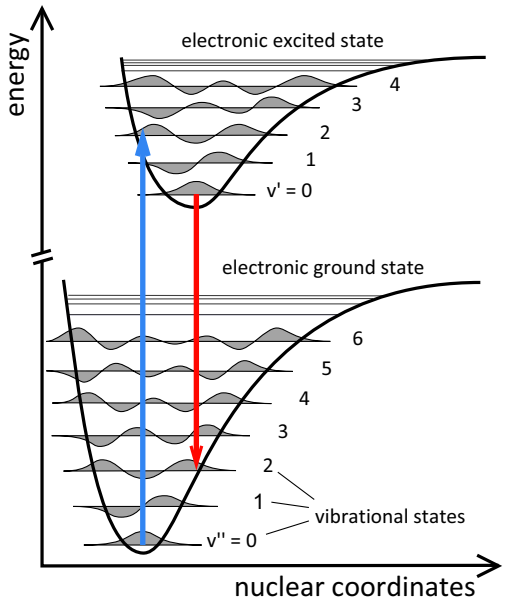

Figure 4: Electronic transitions in organic molecules obey the Franck-Condon principle. The energy surface potentials of ground and excited state are drawn as a function of their internuclear distance. Adapted from Ref. [3].

The Born-Oppenheimer approximation allows to separate the total wavefunction of a molecule into their constituent parts of electronic ψ'_e, vibrational χ_v and rotational ψ_r components. This simplification allows to express the overall wavefunction of a molecule as the product of the individual vibrational, electronic wavefunctions ($\psi = \psi'_e \cdot \chi_v \cdot \psi_r$). For optical transitions the rotational part does not play a significant role and is neglected. Furthermore the electronic wavefunction can be divided into two noninteracting terms, one depending only on the spatial coordinates of the electron and the other depending on the spin coordinates ($\psi'_e = \psi_e \psi_s$) [5]. The probability to excite a molecule is then given by:

$$
\begin{aligned}
|\langle \vec{d}_{21} \rangle|^2 &= |\langle \psi_2 | \vec{d} | \psi_1 \rangle|^2 \\
&= \underbrace{|\langle \psi_{e2} | \vec{d} | \psi_{e1} \rangle|^2}_{\text{Orbital selection rules}} \cdot \underbrace{|\langle \chi_{v2} | \chi_{v1} \rangle|^2}_{\text{Franck Condon factor}} \cdot \underbrace{|\langle \psi_{s2} | \psi_{s1} \rangle|^2}_{\text{Spin selection rules}}
\end{aligned}
$$

The dipole moment operator $\vec{d}$ only appears at the orbital term, since rearrangement of nuclei is slow compared to electronic transitions and the spin is insensitive to the electric field

[5]. Each factor of the above equation has to be non-zero, for a transition to be allowed. Therefore different selection rules for each factor apply. Electronic transitions have to obey the *symmmetry* selection rules. The Franck-Condon factor describes the *spatial overlap* of the wavefunctions between ground and excited state as illustrated in Figure 4. The spin selection rules forbid transitions, where the spin of the electron changes. The ground and excited state of a molecule can be presented by their energy surface potentials with their corresponding vibrational sublevels. The internuclear distance between both states determines absorption and emission and the strength of the transition, which is determined by the oscillator strength and is directly connected to the dipole moment with:

$$f = \frac{8\pi_0 \nu}{3he^2} |\langle \vec{d}_{12} \rangle|^2$$

Only if the Franck-Condon factor is non-zero, the transition is allowed to occur. In aromatic systems, the transition of $\pi \rightarrow \pi^*$ has the highest oscillator strength and $n \rightarrow \pi^*$ the lowest. Based on Kasha's rule, emission occurs only from the vibronic ground level ($\nu = 0$) of the excited state. Therefore, excitations into the manifold of higher lying vibronic sublevels relax by radiationless internal conversion into $\nu = 0$ before they further relax to the electronic ground-state S_0. As illustrated in Figure 4, electronic transitions only occur vertically. Absorption and fluorescence spectra of rigid small molecules, such as anthracene are thus mirror imaged with well resolved vibronic sublevels with a very small energetic offset between the 0-0 transitions, namely Stoke's Shift [12]. The reason is that the change of internuclear distance of the ground and excited state is very small. A Stoke's Shift is not only a result of geometric reorganization in the excited state, but can also be caused by the environment such as solvent molecules.

2.3.2 *Absorption of light in organic molecules*

The absorption of light in organic molecules is given by the relation between the light intensity $I_0(\lambda)$ entering and $I(\lambda)$ leaving the absorbing medium described by the Beer-Lambert Law, from which the absorption coefficient $\alpha(\lambda)$ can be calculated [4]:

$$I(\lambda) = I_0(\lambda) \cdot e^{-\alpha(\lambda)l}$$
$$\Leftrightarrow \alpha(\lambda) = \frac{1}{l} \cdot \ln\frac{I_0}{I} = \ln 10 \cdot \epsilon(\lambda) \cdot c = 2.303 \cdot \epsilon(\lambda) \cdot c,$$

where $\epsilon(\lambda)$ is the molar decadic absorption coefficient (in L/mol·cm), c the concentration (in mol/L) of the chromophore and l the absorption path length (in cm). The molecular absorption cross section $\sigma(\lambda)$ (in cm^2) characterizes the photon-capture area of a molecule [4]

$$\sigma(\lambda) = \frac{\ln(10) \cdot \epsilon(\lambda)}{N_A},$$

N_A is the Avogadro number with $6.0234 \cdot 10^{23}$ mol^{-1}. The "strength" of an optical transition is calculated by integrating over the molar absorption coefficient $\epsilon(\lambda)$ and is also known as the oscillator strength:

$$f = 2303 \cdot \frac{mc^2}{N_a \pi e^2 n} \int \epsilon(\tilde{\nu})\, d\tilde{\nu},$$

where m and e are the mass and charge of an electron, c is the speed of light, n the refractive index and $\tilde{\nu}$ the wavenumber (in cm^{-1}).

Absorption and emission of light in molecules causes an electronic transition between their molecular orbitals. Ground state absorption causes the promotion of an electron from a bonding orbital to an anti-bonding orbital [4]. This transition can occur from a σ-orbital, π-orbital or a non-bonding n-orbital. The σ-σ^* transition has the highest energy gap and n-π^* the lowest:

$$n \to \pi^* < \pi \to \pi^* < n \to \sigma^* < \sigma \to \pi^* < \sigma \to \sigma^*$$

When the spin of an electron remains unchanged during the transition, it has a total spin quantum number of $S = \sum_i s_i = -\frac{1}{2} + \frac{1}{2} = +\frac{1}{2} - \frac{1}{2} = 0$ and a multiplicity of $M = S + 1 = 1$. Therefore this state is also known as the singlet state. Molecules in the excited state can undergo intersystem crossing (ISC) by spin flipping resulting in a pair of electrons with parallel spin. Due to the Pauli exclusion principle both electrons reside in two different quantum states. The total spin quantum number

is $S = 1$ and hence the multiciplicity is $M = 3$. This quantum state is also called triplet state. Intersystem crossing (ISC) is a forbidden transition due to the spin selection rule. Still, it occurs on a finite timescale by spin-orbit coupling. The efficiency of this coupling varies with the fourth power of the atomic number and therefore ISC is most likely occurring in the presence of heavy atoms. According to Hund's rule the triplet state is lower in energy compared to the singlet state.[4].

The excited singlet state S_1 and excited triplet T_1 can recombine to the ground state S_0 by emission of light as depicted in Figure 5. Emission from S_1 and T_1 can be distinguished by their spectral position and by their intrinsic lifetimes.

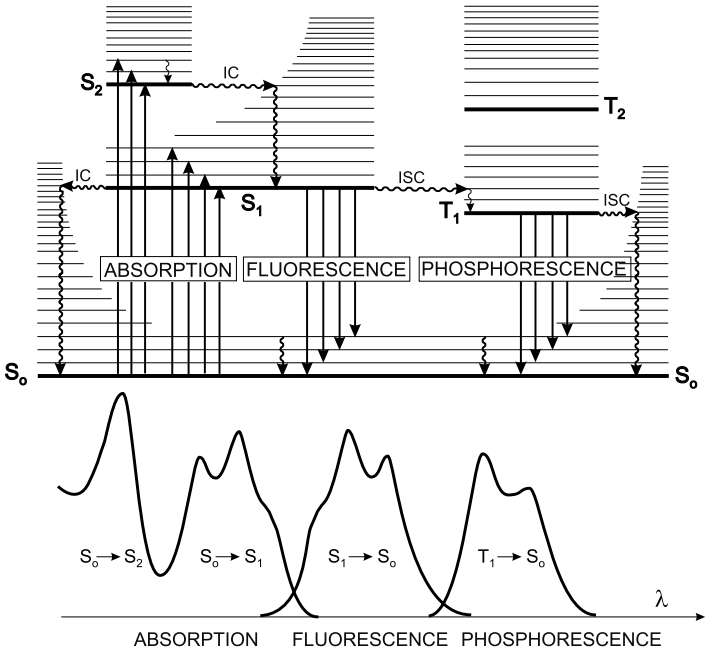

Figure 5: Perrin-Jablonski diagram. Reprinted from Ref. [4] with permission.

The emission from S_1 is also known as fluorescence, which typically has a lifetime between 10^{-10} s and 10^{-7} s. In contrast, emission from T_1 occurs from a lower energy state and therefore is red-shifted to the fluorescence. This process is also known as phosphorescence. The time constant of this process is in the order of 10^{-6} s to 1 s and in some cases can even last up to several to days. Transitions from $S_1 \rightarrow S_0$ or $T_1 \rightarrow S_0$ do not

necessarily occur by emission of a photon. They can also occur non-radiatively and the excess energy is dissipated as heat.

2.3.3 *Spectral lineshapes in organic molecules*

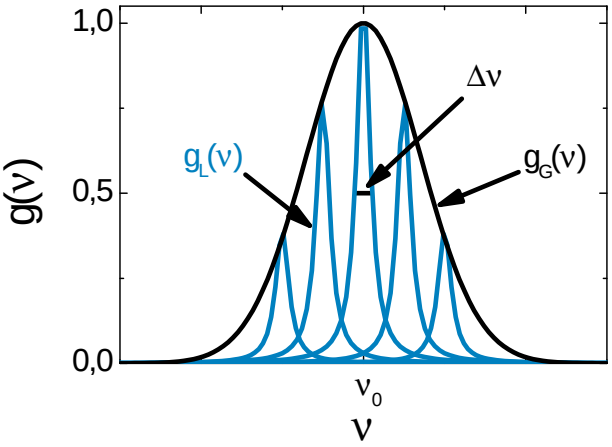

Figure 6: Gaussian lineshape caused by a distribution of different chromophore sites.

Spontaneous emission has a finite lifetime of the excited state E_2, which consequently limits the linewidth of this transition. From the uncertainity principle $\Delta E \simeq h/(2\pi\tau_2)$, the ultimate limit for the spectral linewidth $\Delta\nu$ can be derived:

$$\Delta\nu = \frac{\Delta E 2\pi}{h} = \frac{1}{\tau_2}.$$

In organic molecules τ_2 is the fluorescence lifetime. This mechanism of line broadening is also referred to as *homogeneous line broadening*. Its line shape is described by a Lorentzian function:

$$g_L(\nu) = \frac{\Delta\nu/2}{(\nu-\nu_0)^2 + (\Delta\nu/2)^2},$$

where ν_0 is the center frequency. Another mechanism that causes homogeneous line broadening is heat. Furthermore spectral lines are also broadened by *inhomogeneous* broadening. It is always present when a distribution of chromophores are probed and is related to static disorder. Static disorder occurs since molecules are located in different environments and have different positions with respect to each other. The line shape caused

by inhomogeneous broadening can be described by a Gauss function:

$$g_G(\nu) = \frac{1}{\sqrt{2\pi\sigma^2}} \cdot \exp\left(-\frac{(\nu-\nu_0)^2}{2\sigma^2}\right).$$

Hence, the energy of electronic transitions of an ensemble of molecules or chromophores are statistically distributed as experimentally evidenced by an envelope of a Gaussian function, corresponding to a distribution of chromophore sites.

2.3.4 *Photoluminescence quantum efficiency*

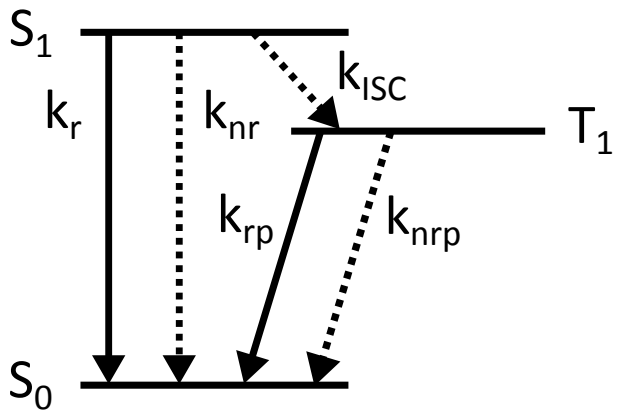

Figure 7: Energy level and depopulation paths in organic materials.

The photoluminescence quantum efficiency Φ is defined as the ratio of the number of photons that are emitted N_{em} and the number of photons N_{abs} that are absorbed by a medium:

$$\Phi = \frac{N_{em}}{N_{abs}},$$

where $0 < \Phi \leqslant 1$. The reason is that different depopulation channels are present in a molecule, which are of radiative and nonradiative nature as illlustrated in Figure 7. The lifetime of the S_1 state is given by the inverse sum of all decay rates that occur from that state [5]:

$$\tau_{S_1} = (k_r + k_{nr} + k_{ISC})^{-1},$$

where k_r, k_{nr} and k_{ISC} are the radiative and nonradiative and the intersystem crossing rate, respectively. The photoluminescence quantum efficiency of the state S_1 is hence defined as the

ratio of the radiative decay rate (k_r) divided by the sum of all decay rates of the S_1 state:

$$\Phi_F = \Phi^* \frac{k_r}{k_r + k_{nr} + k_{ISC}} = \Phi^* \frac{\tau_F}{\tau_r},$$

where Φ^* is the generation efficiency of the fluorescent state S_1.

2.3.5 *Intermolecular interactions of molecules*

The formation of aggregates is a consequence of the spatial arrangement of identical molecules, which do not form a chemical bond though. The simplest form of aggregation is also known as dimer, where only two molecules are involved. When two molecules are brought close together, the dipoles of the molecules start interacting with each other and new transition bands are observed [49]. Based on the type of aggregation they can affect the emission spectrum and absorption spectrum differently. Typical characteristics are displacement of emission and absorption bands with respect to the individual chromophore emission and the appearance of new transition bands. The ground-state energy of a dimer is given by:

$$E_g = E_1 + E_2 + W,$$

where E_1 and E_2 are the ground state energies of the individual molecules and W is the coulombic binding energy. For W<o, the aggregate state is called dimer and for W>o excimer. Generally, the excitation energy of a dimer is not localized on one single molecule anymore and oscillates coherently between the molecules [5].

For two molecules with a dipole moment parallel to each other, the net dipole moment is zero. The transition to the lower state E' is thus dipole forbidden as illustrated in Figure 8. Only E'' has a nonzero transition moment, is therefore allowed and observed as a hypsochromic shift of the absorption. This type of aggregate is also known as *H-aggregate*. They exhibit in most cases very weak or no fluorescence [6]. When the dipole moments are oriented head-to-tail, only the lower lying transition to E'' is allowed, causing a bathochromic shift compared to the monomer transition. This type of aggregation is also known as *J-aggregate*. The two type of aggregates are only the two extreme

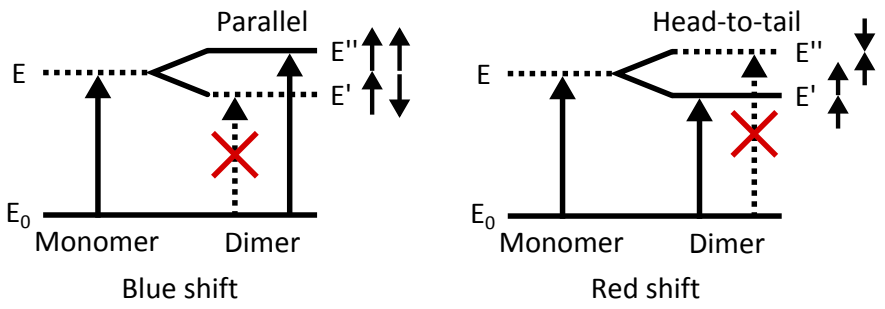

Figure 8: Transition bands of monomers and dimers with respect to the orientation of their dipole moments. Dipole-forbidden transitions are denoted by dotted lines. Adapted from [5].

cases. In reality molecules are oriented to each other with different angles, resulting in more complex spectral changes for instance in the case of band-splitting [49].

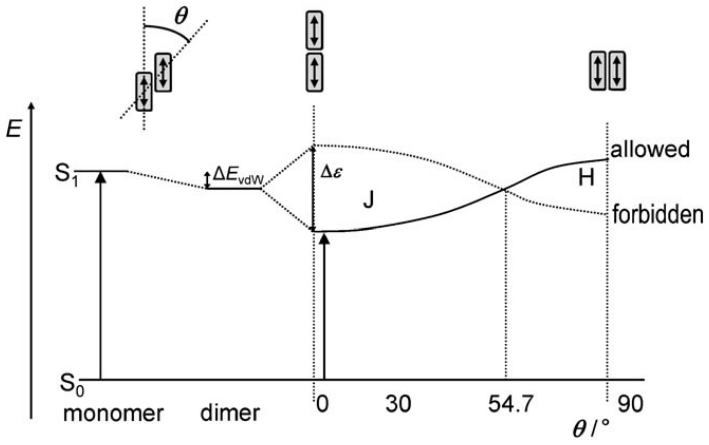

Figure 9: Relation between orientation of transition dipole moments and transition energies in dimers. Reprinted from Ref. [6] with permission.

A special case of intermoleuclar interaction is an *excimer*. Excimer aggregates only exist in the excited state and a ground state of a monomer. Their emission is broad and structureless. An excimer state E_1^* is generated by interaction between a molecule in an excited singlet state S_1^* and a ground state S_0. The excited state excimer E_1^* decays radiatively to the ground state. In principle, every organic crystal can show excimer emission by applying pressure [5].

2.4 MOTION OF EXCITONS AND CHARGES DESCRIBED BY THE GAUSSIAN DISORDER MODEL

In inorganic semiconductors an electron is elevated from the occupied valence band into the conduction band by the absorption of a photon. In this process a defect electron is left in the valence band, which is also known as a hole. At room temperature electron and hole are quickly decoupled from each other due to their low binding energy of less than 25 meV. At very low temperatures however, electrons and holes attract each other by Coulomb forces and a bound state is created known as an electron-hole pair. They are also referred to as Mott-Wannier excitons in inorganic semiconductors.

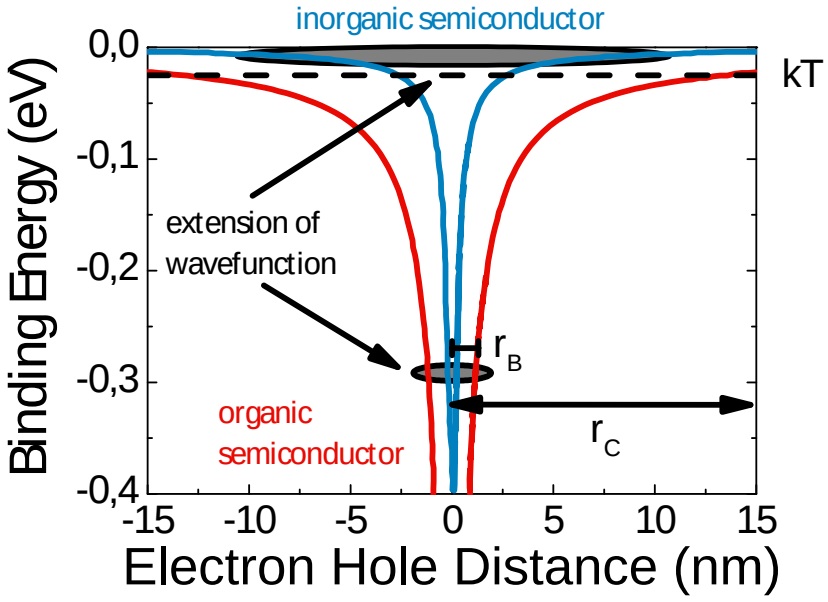

Figure 10: Coulomb potential in inorganic and organic semiconductors. In organic semiconductors the exciton radius r_B is considerably smaller than the Coulomb radius r_C. Adapted from Ref. [7].

In contrast, the absorption of photons in organic semiconductors creates electron-hole pairs that are created and localized within one molecule. This class of electron hole pairs is also known as Frenkel excitons. The reason for this highly localized state is the weak intermolecular coupling as well as the low dielectric constant ϵ_r ranging between 3 and 4. In comparison, inorganic materials such as silicon have a dielectric constant of

ϵ_r=12. Electron-hole pairs, which are bound by Coulomb attraction have typically a binding energy of about E_b=650 meV at an average distance of r_0=0.6 nm. A comparison of the extension of their exciton wavefunctions can be found in Figure 10. Only at a distance of about 20 nm between electron and hole, the binding energy is similar to the thermal energy (E=kT) at room temperature and excitons can be separated. Bound excitons can either be singlet or triplet excitons depending on their spin-multiplicity.

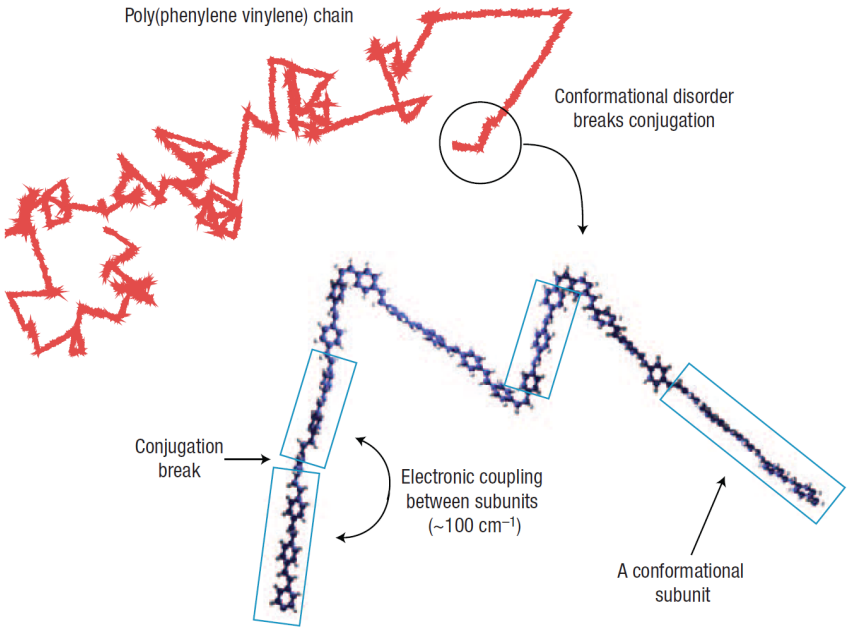

Figure 11: Representative scheme of a polymer chain of PPV. Reprinted from Ref. [8] with permission.

Conjugation along the polymer chain as illustrated in Figure 11 is disturbed by breaks such as chemical defects, torsional motions and kinks of the polymer backbone. The conjugation length is typically between 5 and 15 monomer units [50]. This leads to a distribution of conjugation lengths and therefore a distribution of energies. The density of states (DOS) of conjugated polymers is best described by a Gauss function [51]:

$$\rho(E) = \frac{1}{\sqrt{2\pi\sigma^2}} \cdot \exp\left(-\frac{E^2}{2\sigma^2}\right).$$

$\sigma(E)$ is the standard deviation of the Gauss distribution and is also known as disorder parameter. In organic semiconductors σ typically varies between 50 to 100 meV [52]. The Gaussian shape

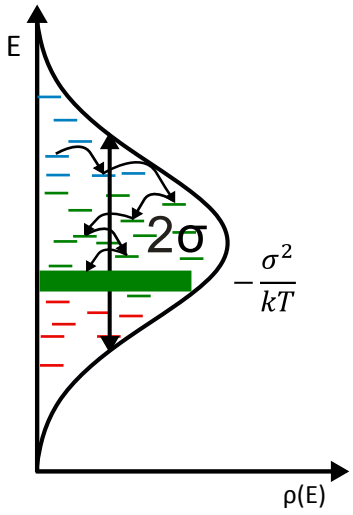

Figure 12: Typical representation of the DOS in conjugated polymers. The relaxation pathway of an exciton is illustrated.

of the DOS has been verified experimentally and theoretically [53, 54, 55]. A relaxation process of an exciton is schematically shown in Figure 12. When an excitation is generated in the DOS, exciton migration takes place between localized, i.e. discrete energy sites. The exciton moves by a hopping process to states lower in energy until it reaches its thermal quasi-equilibrium. Subsequently, the exciton resides in states below the center of the DOS, around an equilibrium energy of $E_\infty = -\sigma^2/(kT)$. The motion of hopping between two sites i and j of different energy is described by the Miller-Abrahams rate ν_{ij}. It outlines that hopping occurs by phonon-assisted tunneling with a rate of [56, 57]:

$$\nu_{ij} = \nu_0 \cdot \exp(-2\alpha R_{ij}) \cdot \begin{cases} \exp\left(-\frac{E_j - E_i}{kT}\right), & E_j > E_i \\ 1, & E_j < E_i, \end{cases}$$

where ν_0 is the phonon vibration frequency, R_{ij} the electronic wave function overlap factor and α the inverse localization radius (result of the overlap intergral of the wavefunctions assuming exponential decay with distance [58]). Jumps upwards in energy $E_j > E_i$ include a Boltzmann factor. The formula also implies that electron-phonon coupling is weak enough to render polaronic effects negligible. There is no other activation energy except the energy difference in electronic site energies that has to be overcome in order to hop [51]. Spectroscopically, the migration of the excitation towards the tail of the DOS in

conjugated polymers is observed as a red-shift of the photoluminescence spectrum with time [59, 60]. Spectral diffusion occurs on a timescale between ps and ns [61]. At very low temperatures ($T \rightarrow 0K$) the migration is kinetically frozen and thus the excitation decays before the equilibrium energy E_∞ is reached by relaxation [53, 62]. The Gaussian Disorder Model is not only applicable to exciton motion in disordered systems, but also to the motion of charge carriers. The charge carrier mobility in conjugated polymers is influenced by two different types of disorder. The *diagonal disorder* is related to the fluctuations of energies of the highest molecular orbitals (HOMO) and lowest unoccupied molecular orbital (LUMO) levels of the chain segments. *Off-diagonal disorder* describes the fluctuations of the strength of interaction between adjacent chain segments based on their relative positions and orientations [63]. The off-diagonal disorder is also known as positional disorder. The charge carrier mobility in dependence of both paramters is given by:

$$\mu(T,F) = \mu_0 \cdot \exp\left[-\left(\frac{2\sigma}{3kT}\right)^2\right] \cdot \exp\left[\left(C\left(\frac{\sigma}{kT}\right)^2 - \Sigma^2\right)\sqrt{F}\right].$$

where $C{=}2.9 \cdot 10^{-4}$ $(cm/V)^{1/2}$ is an empirical constant. When the mobility is extrapolated to the zero-field limit, it leads to following equation [51]:

$$\mu(T) = \mu_0 \cdot \exp\left[-\left(\frac{2\sigma}{3kT}\right)^2\right] = \mu_0 \cdot \exp\left[-\left(\frac{T_c}{T}\right)^2\right]$$

T_c describes the extent of energetic disorder and is connected to the disorder with $kT_c = 2\sigma/3$. When $T_c < T$, the charges will not reach their dynamic equilibrium and the description of the mobility with the given formula is not valid anymore. The field dependence follows a Poole-Frenkel-type behavior with $\log(\mu) \propto \beta F^{1/2}$, where β is a material constant. The external electric field lowers the energy barrier for hops upwards in energy and allows charge carriers to leave the tail of the DOS [63].

Table 1 summarizes the main differences between band-like tranport and the transport behavior decribed by the Gaussian Disorder Model (GDM).

Dependence	Band-like transport	GDM
Temperature	negative	$\mu(T) \propto \exp\left[-\left(\frac{2\sigma}{3kT}\right)\right]$
Time	none	yes - stronger at low T
Carrier density	none	mobility increases
Electric field	none	Poole-Frenkel dependence

Table 1: Comaprison between different transport models [11].

2.5 LASING IN ORGANIC SEMICONDUCTORS

Lasing is generated by stimulated emission, leading to coherent radiation. In general, a laser consists of a gain material incorporated into an optical feedback structure. The type of optical feedback, in combination with the gain material determines the wavelength, optical linewidth and laser threshold. When light is emitted in the gain medium, it propagates forward and backward within the resonator. If the amplification exceeds the losses of the resonator, stimulated emission is dominating spontaneous emission and lasing begins [64].

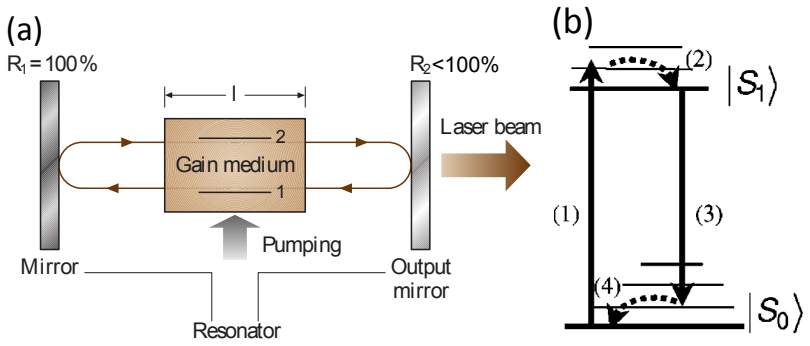

Figure 13: (a) Schematic drawing of a laser oscillator. Reprinted from Ref. [9] with permission. (b) Four-level laser scheme of an organic gain material. Reprinted from Ref. [10] with permission.

Stimulated emission in organic semiconductors occurs by population inversion and follows the same mechanism as in dye lasers, where lasing is achieved by a four-level system as depicted in Figure 13. Photoexcitation of the electronic ground state S_0 of a molecule to the vibration manifold of the first excited singlet state S_1, is followed by rapid thermalization to the vibronic ground state ($v = 0$) of S_1. From there, laser action

occurs by stimulated emission between S_1 and S_0 with $\nu > 0$. For organic solid state lasers, various types of resonators have been used for laser emission [10, 65, 66, 67]. The amplification of light is defined by the gain coefficient g of the emissive medium. As light travels through this medium the stimulated emission intensity $I(l)$ increases exponentially with the distance l [10]:

$$I(l) = I_0 \cdot e^{(g-\alpha)l}.$$

The gain coefficient of a medium is dependent on the stimulated emission cross section $\sigma_{SE}(\lambda)$ and the number of excited states N of the material. The product of both parameters determines the gain with $g(\lambda) = \sigma(\lambda) \cdot N$. Therefore a high stimulated emission cross section is essential for efficient laser output. $\sigma_{SE}(\lambda)$ is defined as follows [68]:

$$\sigma(\lambda) = \frac{\lambda^4 f(\lambda)}{8\pi n^2 c_0 \tau_r},$$

$f(\lambda)$ is the normalized spectral distribution of the photoluminescence, n the refractive index, c_0 the vacuum speed of light and τ_r the radiative lifetime of the involved optical transition. $\sigma(\lambda)$ can experimentally be accessed by transient absorption spectroscopy as outlined and discussed in chapter 3.6.

2.6 ORGANIC LIGHT EMITTING DIODES

The operation principle of organic light emitting diodes (OLED) is divided into five different processes:

1. Injection of charge carriers from the electrodes
2. Charge carrier transport in the organic layer
3. Recombination of charge carriers and exciton formation
4. Exciton diffusion
5. Recombinaton of excitons

A typical layout of an OLED structure can be found in chapter 4.4. The simplest architecture consists of an organic layer sandwiched between two electrodes of different work functions. As a first step at the interface between electrode and organic layer

charge carriers are injected into the highest occupied molecular orbital (HOMO) and LUMO levels, respectively. The injection barriers ϕ are given by the energy levels of the organic semiconductor and the Fermi levels of the electrodes that need to be overcome by tunneling [69]. The thermionic emission is also known as Richardson-Schottky-injection. The maximum current density J_s that can be injected is limited by the energy barrier ϕ and the externally applied voltage :

$$J = J_S \cdot \exp\left(\frac{\Delta\phi}{kT}\right), \text{with } J_S = A \cdot T^2 \exp\left(-\frac{\phi}{kT}\right).$$

The applied voltage generates at the interface an electric field F and decreceases the barrier heigt by $\Delta\phi = e\left(\frac{eF}{\epsilon\epsilon_0}\right)^{1/2}$, also known as Schottky-Effect [70]. A is the Richardson constant with $A = \frac{4\pi k^2 e}{h^3} = 1.2 \cdot 10^6 \frac{A}{m^2 K^2}$. The energy offset between both materials determines the current flow inside the bulk material. If the injection barrier is vanishingly small, the current is not injection limited and the contact is ohmic. Therefore electrodes and interlayers are chosen that lower the injection barrier into the HOMO and LUMO levels. For cathodes, metals with low workfunctions are required. Typically lithium fluoride (LiF) or calcium in combination with aluminium is used [71]. An often used anode is indium tin oxide (ITO). The advantage of this metal oxide is that it has a high transperancy in the visible. It shows a high reflectance in the infrared (IR) region and is thus often used as thermal isolation in windows. Another anode that is currently attracting a lot of attention is graphene [72, 73]. After injection, carriers follow the transport mechanisms as described in chapter 2.4. Recombination of free charge carriers follows Langevin recombination [74]. The bimolecular recombination process of electrons and holes results in the formation of excitons. Spin statistics restricts the formation of singlet excitons to a fraction of 0.25 and triplets to 0.75. The singlet:triplet ratio has also been verified experimentally [75]. The extension as well as the position of the recombination zone is dependent on the injection, transport and recombination properties of the organic material [76]. Ideally an electron-hole pair is formed that emits light. Different processes can however quench the exciton such as chemical defects [77], metal-electrode quenching [78], annihilation processes [79, 80], high electric fields [81, 82], unbalanced charge transport [83, 84] and exciton-polaron quenching [85].

Light emission in electroluminescent devices is determined by two different parameters. The internal quantum efficiency η_{int} is the ratio of emitted photons relatively to the electrons injected. Not every radiative exciton is detected due to losses by the metal-electrode, surface plasmons and waveguide modes confined in the organic layers [86]. Therefore the external quantum efficiency (EQE) is easier to be determined and is also more significant for display applications. It describes the ratio of electrons injected N_e to the photons detected N_{ph} and is described by:

$$\begin{aligned}\eta_{ext} &= \frac{N_{ph}}{N_e} \\ &= \eta_{int} \cdot \eta_{out},\end{aligned}$$

where η_{out} is the outcoupling efficiency with $1/(2n^2)$ and n being the refractive index. With a refractive index of typically 1.6 for organic materials and a triplet-singlet ratio of 3:1 in electroluminescent devices, the upper limit for singlet emitters is therefore at about 5 % and triplet emitters at 25 % [87]. OLEDs that use emission from triplet states can achieve $\eta_{int} \approx 100\%$ [88].

3

OPTICAL SPECTROSCOPY ON INDENOFLUORENE COPOLYMERS - STEADY-STATE AND TIME RESOLVED CHARACTERISTICS

3.1 THE CLASS OF POLY(INDENOFLUORENES)

3.1.1 *Introduction*

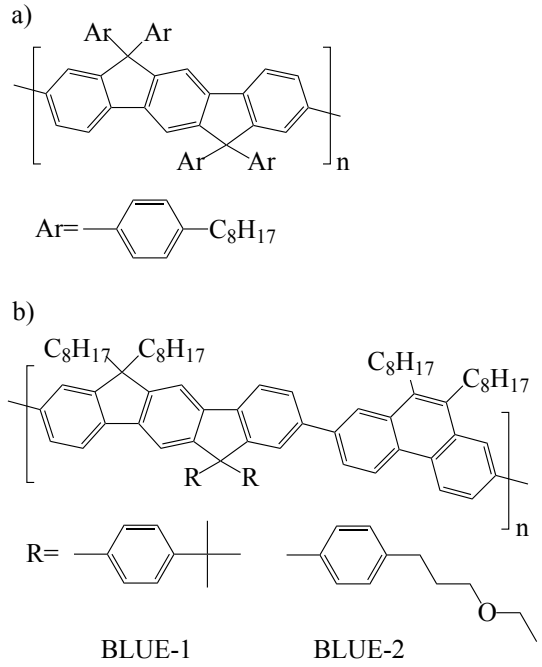

Figure 14: Molecular structures of a) Poly(indenofluorene) and b) Poly(indenofluorene)-phenanthrene copolymers discussed in this chapter

The development of blue light emitting materials that combine a high chromophore density as well as good electroluminescence properties is still a hot topic of research for OLEDs. Especially blue emitters deployed in optoelectronic devices often have a short lifetime and low stability. Ladder-type polymers have shown versatile properties for various organic optoelectronic applications. Poly(indenofluorene)s for instance, are well-known

as stable blue emitters with good thermal and oxidative stability, are soluble in common organic solvents and have good film forming properties. Copolymers based on indenofluorene units with different other monomeric units have proven to be suitable for various optoelectronic applications such as OLEDs [89], organic solar cells (OSCs) [90] and organic field effect transistors (OFETs) [91, 92].

The molecular structures of the three materials investigated in this thesis are sketched in Figure 14. Aryl-poly(indenofluorene) (PIF) served as reference material for comparison with previous studies. Both copolymers, namely BLUE-1 and BLUE-2, consist of strictly alternating units of substituted indenofluorene and phenanthrene, while they differ in the side chains attached to the indenofluorene unit. All of them are blue-emitters and have been designed for OLEDs. They have excellent solubility in common organic solvents such as toluene. Phenanthrene is known as a polycyclic aromatic compound with absorption and emission properties outside the visible region centered in the ultraviolett (UV) range [93]. Steady-state as well as time-resolved experiments were performed for a deeper understanding of their optical transitions, their excited state dynamics and their intermolecular interaction.

3.2 EXPERIMENTAL

3.2.1 *Sample preparation*

All polymer films for optical spectroscopy were prepared from toluene solution with a concentration typically of 10 mg/ml. Films were spincast with a Süss Micro Tec Delta 80 spincoater on precleaned fused silica substrates. Prior to spincoating the substrates were cleaned in an ultrasonic bath of an alkaline liquid (Hellmanex II) and subsequently in ethanol and isopropanol for 10 minutes each. Typical spinning speeds for thin film preparation were 2000 rpm for 120 s. Film thicknesses were determined by a Dektak surface profiler and were in the range between 120 nm and 170 nm. Measurements in solution were carried out in pre-cleaned quartz cuvettes with an optical path length of 1 mm.

3.2.2 *Steady-state spectroscopy*

Absorption spectra were recorded with a Perkin-Elmer Lambda 2 UV/VIS spectrometer. For *steady-state photoluminescence* studies, a TIDAS 3D fluorescence spectrometer was used.

Photoluminescence quantum efficiency (PLQE) measurements were carried out on films spincoated on quartz. The samples were placed inside a polytetrafluorethylen (PTFE) coated integrating sphere and excited with a LED (Hamamatsu, LC-L2) at a wavelength of 365 nm (3.40 eV). The PL signal was dispersed by a spectrograph (Shamrock SR303i) and read out by an intensity calibrated charge coupled device (CCD) line array camera (Ames Photonics, Larry-2048). The photoluminescence quantum efficiency (PLQE) values were evaluated as described in [94].

Quasi steady-state *photoinduced absorption (PIA)*, was measured on films. The spectra were taken at 77 K with excitation at 365 nm (3.40 eV) provided by a light emitting diode (LED) light source at a modulation frequency of 317 Hz. The resulting change in transmission was monitored at each wavelength with a dispersed tungsten-halogen light source as a probe and by using Si and Ge detectors with lock-in detection.

Refractive indices were determined by refractometry. Thin films of BLUE-1 and BLUE-2 were measured with a UV/VIS absorption spectrometer (Perkin-Elmer, Lambda 900) in absorbance mode and at perpendicular incidence in reflectrometry mode. The refractive index in transverse electric (TE) and transverse magnetic (TM)-polarization was determined by a thin film polarizing filter incorporated inside the spectrometer. The refractive indices were calculated by means of Fresnel's equation as described in Campoy-Quiles et al. [95]

3.2.3 *Time-resolved spectroscopy*

Time-resolved photoluminescence (TRPL) spectra were measured with a C4742 Hamamatsu streak camera system. Depending on the time scale of the dynamics, samples were excited with two different laser systems. For short processes up to several nanoseconds, samples were excited with the frequency doubled

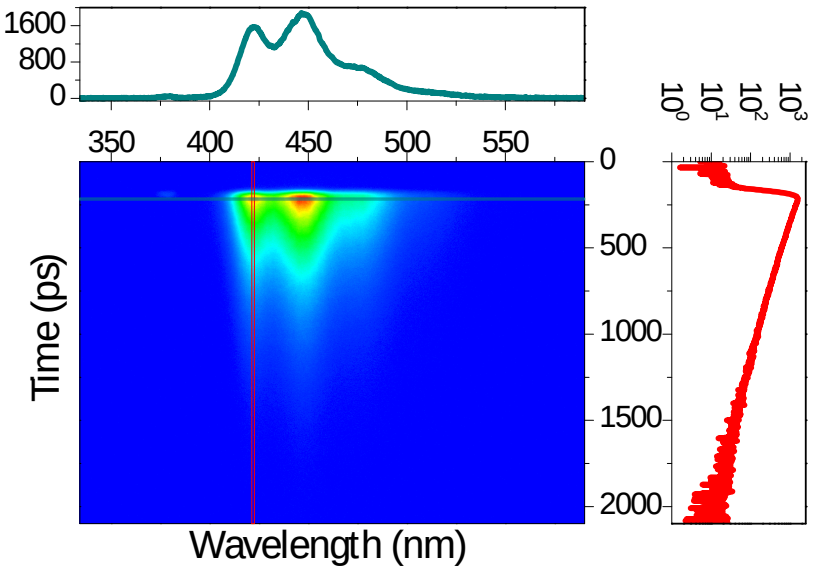

Figure 15: Streakcamera image comprising spectral and temporal information.

output from a mode-locked titanium-sapphire (Ti:Sa) oscillator (Mira 900 Duo, Coherent) operating at a repetition rate of 80 MHz with a pulse width of 200 fs. The excitation wavelength was tunable in the range from 370 nm (3.35 eV) to 430 nm (2.88 eV). For longer lifetimes up to 1 ms, samples were excited with the output of an optical parametric amplifier (OPerA Solo, Coherent), itself pumped by a Ti:Sa (Libra, Coherent) amplifier system at a repetition rate of 1 kHz and a pulse width of 100 fs. Spincast films were kept in a home-built cryostat under a dynamic vacuum of typically around 10^{-6} mbar. The streak system allowed to measure and analyze time dependent luminescence spectra. Photons emitted from the sample are at first spectrally dispersed by a spectrometer before they reach a photo cathode that translates the incoming photons to electrons. The released electrons are subsequently accelerated in a time-dependent electrical field. Depending on the time at which these electrons enter the electric field, they are projected to a phosphorous screen at different positions. This allows to conserve spectral and temporal information as well as intensity in a form of a three dimensional image. In-plane coordinates comprise spectral and temporal information and the out-of-plane coordinate includes the corresponding signal intensity. The temporal

resolution is about 15 ps.

Delayed fluorescence (DF) experiments were carried out at liquid nitrogen temperature of 77 K. Sample preparation followed the description of the low temperature time-resolved photoluminescence (TRPL) experiments in chapter 3.4.1. Materials were excited with the third harmonic (355 nm (3.49 eV)) of a nanosecond neodymium-doped yttrium aluminium garnet (Nd:YAG) laser (INDI Ray Spectra Physics) with a pulse width of 8 ns. The pump fluence was controlled with a series of neutral density filters. Emission was collected with a telescope, dispersed by a spectrograph (Shamrock SR-303i) and detected with a gated intensified CCD detector (Andor IStar DH740 ICCD camera).

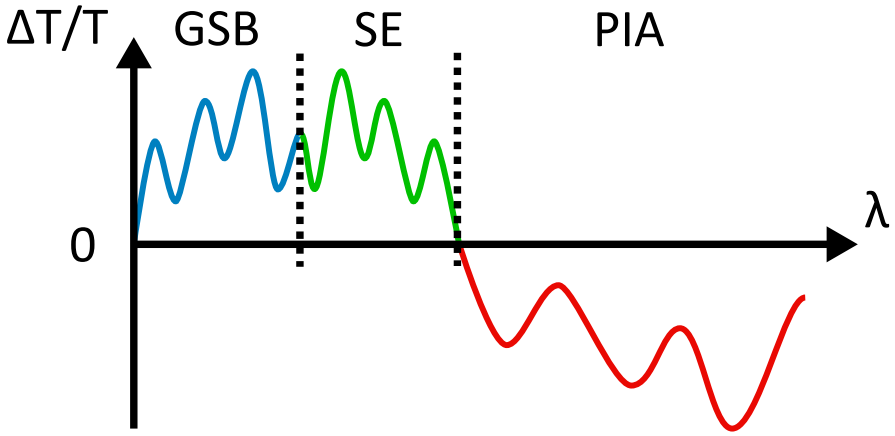

Figure 16: Illustration of a typical transient absorption spectrum. Positive ΔT/T signals are caused by the ground state bleach (GSB) or by stimulated emission (SE). A negative ΔT/T signal is assigned to photoinduced absorption (PIA).

Transient absorption TA spectroscopy measurements were performed with a home-built pump-probe setup. The output of a commercial Ti:Sa amplifier (Coherent LIBRA HE, 3.5 mJ, 1 kHz, 100 fs) operating at 800 nm (1.55 eV) was split into two different pathways to generate pump and probe beam. The beam of the amplifier was focused on a c-cut 3 mm thick sapphire plate, which generated the supercontinuum white light in the visible region. The excitation pump beam at 380 nm (3.26 eV) was supplied from an optical parametric amplifier (Coherent OPerA Solo). The beam was guided on a broadband retroreflector mounted on a mechanical delay stage before it hit the

sample. The delay stage allows varying the optical pathlength of the pump beam, which enables the beam to hit the sample at different time delays with respect to the probe beam. The length of the stage allowed covering a time range up to 4 ns with a resolution only restricted by the pulse width of the excitation pulse. The repetition frequency of the pump beam was reduced from 1 kHz to 500 Hz by a chopper. Both beams were then overlapped on the sample. The probe signal was then dispersed and read out by a linear photodiode array at 1 kHz. The read-out frequency of the photodiode array allowed to collect a signal with the pump and probe pulse present on the sample T_1 and only the probe pulse T_2. The different states of pump beam "'on"' (T_1) and pump beam "'off"' (T_2) determines $\Delta T/T = (T_2 - T_1)/T_2$. Films were kept in a dynamic vacuum at typically $1 \cdot 10^{-6}$ mbar during measurements.

3.2.4 *Amplified spontaneous emission and lasing*

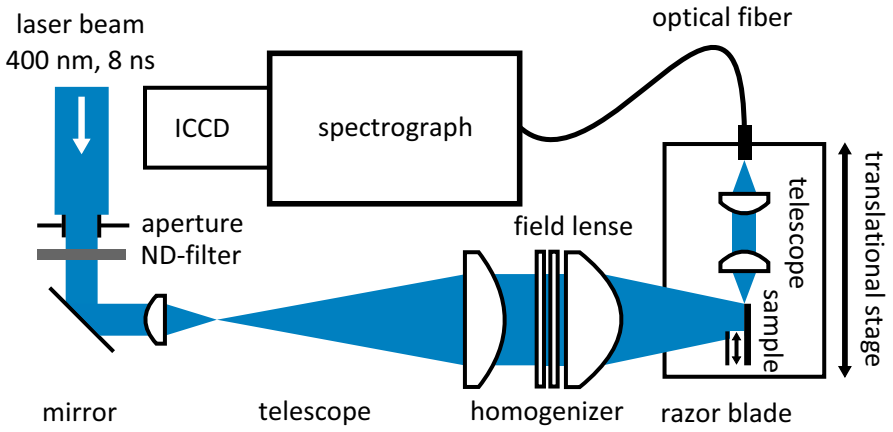

Figure 17: Schematic drawing of the experimental set-up used for ASE experiments.

A straightforward and practical method to investigate amplified spontaneous emission (ASE) is the variable stripe length method. A laser typically with a pulse width in the ns range is used and tuned to the absorption of the studied material. A set of optical components transforms the initial laser beam into a striped shape with which the ASE threshold, loss and gain parameter can be determined. In the following, excitation of the samples during ASE experiments was provided by the tunable

output (410-700 nm) (3.02-1.77 eV) of an optical parametric oscillator (OPO) from GWU Lasertechnik itself pumped by the third harmonic (355 nm (3.49 eV)) of an Nd:YAG nanosecond laser (10 Hz INDI Ray Spectra Physics). For accessing the wavelength range from 260 - 410 nm (4.77-3.02 eV) the output of the OPO could be frequency-doubled with a second harmonic generation (SHG) unit. The output beam was transformed with a beam homogenizer consisting of two crossed cylindrical micro lens arrays (LIMO Lissotschenko Mikrooptik) to achieve a 8 x 1 mm^2 flat top beam profile. The edge-emitted ASE emission was dispersed by a Shamrock SR-303i spectrograph and detected by a gated intensified charge coupled device (ICCD) detector (Andor IStar DH740 ICCD camera). For the bi-layer ASE experiments HIL-2 was spincoated from a toluene solution of 5 mg/ml with 1000 rpm for 60 s on a precleaned quartz substrate. After crosslinking the film inside a dry N_2-glovebox at 180 °C for one hour, BLUE-1 was spincoated on top of the injection layer from a 10 mg/ml toluene solution with a spinning speed of 2000 rpm for 120 s.

In order to achieve true *laser* action, an optical feedback for the organic fluorescent medium is needed. Therefore a 1D sinusoidal distributed feedback structure with a periodicity of 283 nm was fabricated. The grating structures were etched into pre-cleaned fused silica substrates via interference lithography. In a two-step process, first a Microposit primer on hexamethyldisilazane (HDMS) basis and subsequently a Microposit S1805 photoresist that was diluted in a 1:1 ratio with Microposit EC solvent were spincast each with 4000 rpm for 60 s. After baking the films for 30 minutes at 90 °C, they were exposed to a Helium-Cadmium (HeCd) Laser at 442 nm (2.81 eV) with a power of 1.8 mW. The beam spot size on the sample position was about 2 cm in diameter. The sample was mounted on a rotating stage with a mirror positioned perpendicular to it. The grating structure was made by exposing the laser beam on to the mirror and the sample. The angle of exposure defines the spacing of the 1D interference pattern. After developing the films with a ma-D 330 Microresit Technology developer, they were baked at 110 °C for 30 minutes. The grating structures on the photoresist were then transferred onto the underlying substrate by reactive ion etching. Polymers were spincast on the

fused silica gratings with 2500 rpm for 120 s from a 7.5 mg/ml solution of toluene. Samples were kept under high vacuum conditions and excited with the frequency doubled output of an ultrafast femtosecond amplifier (Coherent Libra HE) at 400 nm (3.10 eV) and under an angle of 20 ° perpendicular to the film plane. The laser emission was detected perpendicular to the film plane with an OceanOptics 2000 CCD spectrometer.

3.3 ABSORPTION AND EMISSION SPECTROSCOPY

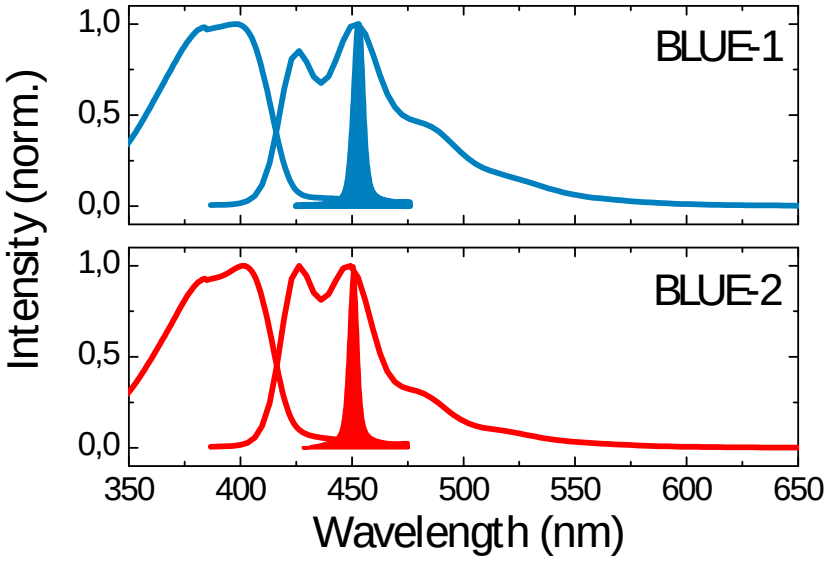

Figure 18: Steady-state absorption and emission spectra of thin films of BLUE-1 and BLUE-2. The filled curves correspond to the ASE spectra.

Figure 18 shows the room temperature PL, absorption and ASE spectra of the two copolymers spincast on quartz. The thickness of the films was typically between 120 nm and 170 nm. As common for many conjugated polymers, absorption spectra are broad and nearly featureless, which is a consequence of inhomogeneous broadening occurring at room temperature. In contrast, the fluorescence spectra exhibit clear vibronic progressions. Both polymers emit in the blue spectral region and have similar vibronic features. Absorption and emission spectra show a Stokes shift of about 180 meV, which results from a loss of energy during the reorganization of the polymer chain in the excited state

[13]. By optical excitation, electronic transitions from the ground state to the excited state occur throughout the DOS. In the first singlet excited state S_1, vibrational relaxation has to occur before any transition between electronic levels takes place. The emission spectra are less broadened and the vibronic structure is conserved (strong coupling between electrons and vibrational degrees of freedom) [96]. Ladder-type polymers typically show a pronounced vibronic structure. The rigid and planar polymer backbone causes also small Stokes shifts. The filled curves in Figure 18 correspond to the ASE spectra obtained after pulsed laser excitation in slab waveguide structures (polymer film on quartz substrate with the glass and air forming the cladding layers) well above the ASE thresholds, which will be discussed in detail in chapter 3.5.

3.3.1 *Quasi steady-state excited state absorption*

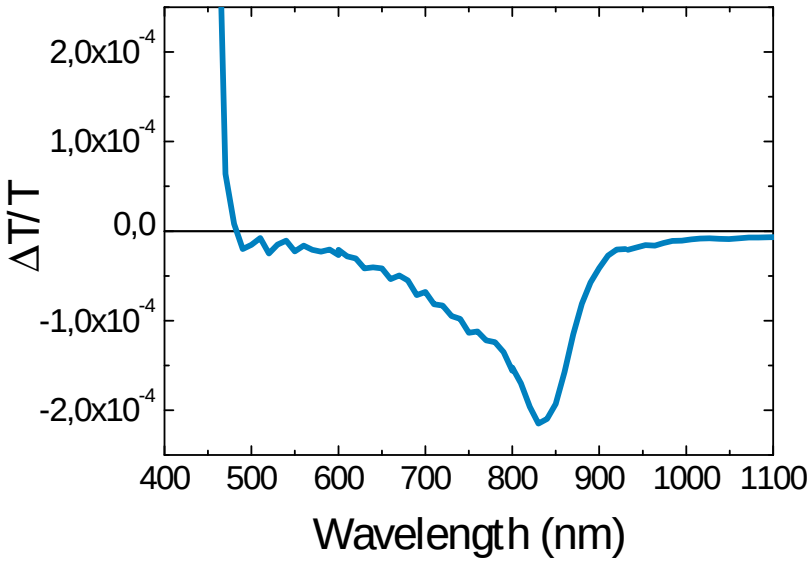

Figure 19: Quasi steady-state PIA spectrum of BLUE-1 on film. The sample was excited with 365 nm (2.40 eV).

Quasi steady-state PIA is highly sensitive to long-lived excited states. The measurement signal obtained by this technique is the fractional change of transmission $\Delta T/T = -N_{exc} \cdot \sigma \cdot d$, with N_{exc} comprising the steady-state density of photoinduced species, σ

the absorption cross section and d the sample thickness. This experimental technique allows to determine dipole-coupled electronic transitions in quasi steady-state (modulation frequency at 317 Hz). From the measurements carried out on BLUE-1, two different PIA bands are observed in the visible to near-infrared (NIR) region. A rather featureless broad band between 480 nm (2.58 eV) and 750 nm (1.65 eV) followed by a distinct absorption band peaking at 820 nm (1.51 eV). The measurement technique does not allow to distinguish between different long-lived species. Transient absorption (TA) spectroscopy shown in chapter 3.6 demonstrates that the broad absorption feature most likely occurs from the singlet exciton. The distinct feature at 750 nm (1.65 eV) is assigned to triplet excitons and was also observed in poly(para-phenylene) and PIF [42, 97].

3.4 TIME-RESOLVED FLUORESCENCE SPECTROSCOPY ON BLUE-1 AND BLUE-2 - THE INFLUENCE OF INTERMOLECULAR INTERACTION

3.4.1 *Fluorescence spectroscopy*

The origin of the blue emission and the exciton dynamics were studied by streak camera measurements. Solutions with different concentrations as well as thin films were investigated at room temperature as well as at liquid nitrogen temperatures of 77 K.

Fluorescence decay transients of both polymers in toluene at a concentration of 0.1 mg/mL are depicted in Figure 20. When comparing prompt and delayed spectra at a time delay of 4 ns, BLUE-1 has a different spectral shape at later times compared to the prompt fluorescence spectrum. The 0-0 transition is reduced, while the lower vibronic modes experience a slight spectral red shift. The change of the spectral appearance is observed only at later times. The transient spectrum at delays of 1.2 ns resembles the prompt photoluminescence. A decrease in fluorescence intensity of the 0-0 transition has been often reported and assigned to reabsorption, especially if the Stokes-shift is relatively small. Usually reabsorption occurs in films or concentrated solutions [98]. Instead BLUE-2 shows no spectral shift at delay times of 4 ns. A featureless emission is superimposed on the fluorescence, which will be discussed later. Since both materials have simi-

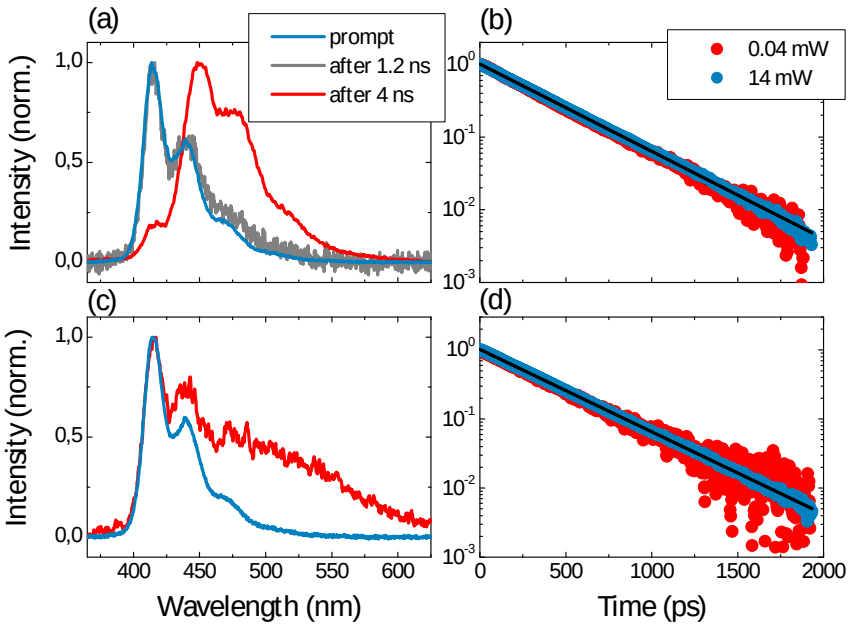

Figure 20: Time dependent photoluminscence spectra of (a) BLUE-1 and (c) BLUE-2 and their corresponding decay dynamics (d), (e) respectively in toluene at a concentration of 0.1 mg/ml. The polymers were excited with a pump power of 0.04 mW.

lar steady-state absorption and emission spectra, reabsorption in this particular case can be excluded. Decay constants were elucidated by fitting the transients with a single-exponential function. The lifetimes were found to be τ_1=361 ps and τ_2=364 ps for BLUE-1 and BLUE-2 respectively. The spectrum of BLUE-1 changes with time. The decay constant is not affected by this spectral shift as indicated by a single-exponential decay pattern.

A different decay pattern can be observed for both materials spincast on fused silica. At a pump power as low as 0.04 mW, the decay pattern of BLUE-1 deviates from a single-exponential function. Higher pump intensity does not change significantly the kinetics of the material. In contrast, BLUE-2 shows a transition from a single-exponential decay to a bi-exponential behavior with increasing the pump power as illustrated in Figure 21. The change of decay pattern can be assigned to energy transfer and is reflected in the photoluminescence spectra at different time delays, shown in Figure 22. At low pump power, the prompt

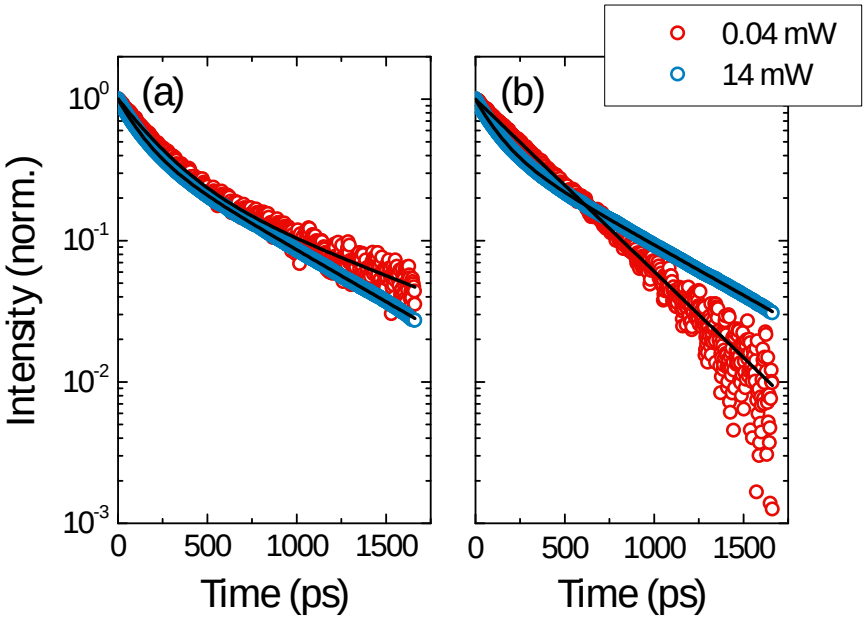

Figure 21: Fluorescence transients of (a) BLUE-1 and (b) BLUE-2 as film at different pump fluences.

and delayed spectra of BLUE-2 show no difference. In contrast, BLUE-1 behaves differently implying the presence of two states. The prompt spectra of BLUE-1 and its delayed emission spectrum after 1.2 ns originate from two different emission sites. Both emission species have a vibronic spacing of about 180 meV, which can be ascribed to carbon-carbon double bond stretching modes of the polymer. At higher pump power, the delayed emission shifts slightly to the red by about 3 nm (20 meV) with the vibronic features remaining. The second emissive species was observed in all of the experiments. The transient luminescence spectrum of BLUE-2 however, when excited with 14 mW transforms after 1.2 ns into a broad featureless emission, with a peak centered at around 492 nm (2.89 eV), which has also been observed in solution. In addition a decrease of the 0-0-transition intensity takes place. Defect emission observed from fluorenone groups within the polymer backbone of ladder-type polymers has been extensively studied and will be further discussed in chapter 3.4.2. However, fluorenone defects are not the origin of this emission due to a mismatch of the spectral position. Since defect emission from fluorenone groups can be excluded, the band at 492 nm (2.52 eV) in BLUE-2 appears to be from an aggregate, which forms as the sample gets locally heated by the high pump power. This process is irreversible once the

sample is excited with high powers and accounts for the dynamics as well as the spectral characteristics. Glass transition temperatures were found to be 270 °C and 71 °C for BLUE-1 and BLUE-2 (see Appendix) respectively and can explain the stronger tendency of BLUE-2 to undergo local morphological changes at high pump powers. Even though BLUE-1 shows no trace of aggregation when spincast from toluene, it is possible to tune the morphology of the polymer as well. For instance, if BLUE-1 is embedded into an optical inactive matrix (Zeonex 480R) in a ratio of 100:1, prepared from a toluene solution with a concentration of 10 mg/ml, an aggregate band appears in transient luminescence spectroscopy (see appendix). Polarizing optical microscopy recordings show that birefringent domains are formed with a size of up to 10 µm, which most likely cannot be referred to crystalline domains, but are a consequence of a change of local packing (see appendix). Pristine films that were spincast showed no birefringent behavior and such domains were not present anymore. Time-resolved measurements show that these domains behave very similar to BLUE-2 with an aggregate band occurring at the same spectral position position. Aggregation most likely occurs during the spincoating process of the blend, where both materials start to solidify at different times and demixing is thus stronger.

The decay kinetics of BLUE-1 and BLUE-2 are significantly different from each other, in solution as well as in bulk comparing the dynamics and spectra at delayed times. The evidence of a second spectral component appearing in BLUE-1 and its impact on ASE properties were in focus of this study. TRPL measurements were conducted at low temperatures. Therefore samples were kept in a dynamic vacuum. A cold finger thermally connected from the outside of the cryostat to the internal body of the sample holder ensured the thermal conduction with liquid nitrogen. The cold finger was constantly filled with liquid nitrogen for about 30 min prior to the start of the measurement. Films were spincoated with the same parameters as for steady-state absorption and emission spectroscopy and subsequently fixed onto a home built copper sample holder. A heat transfer paste was spread between the backside of the quartz substrate and the sample holder for better thermal conduction. Low temperature solution measurements were conducted with a home-built cuvette.

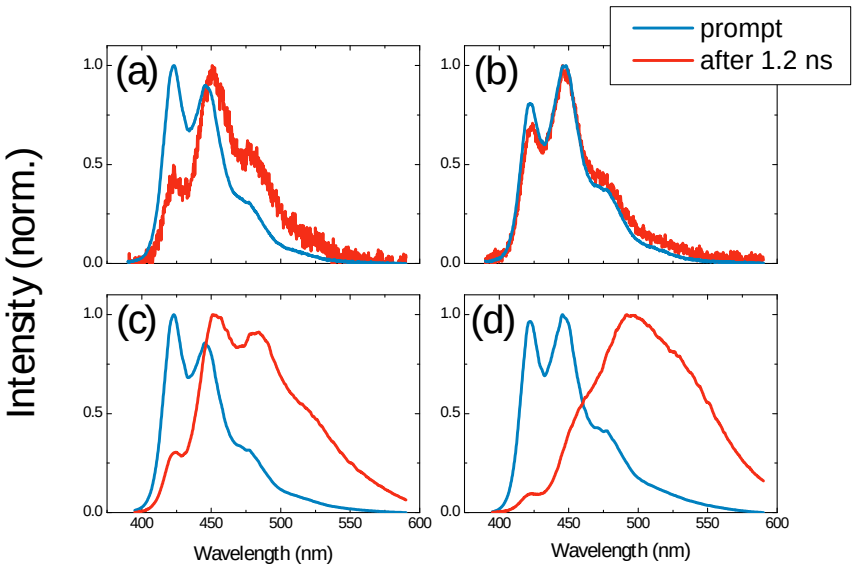

Figure 22: Transient PL spectra of BLUE-1 and BLUE-2 in film, excited with different pump fluences. (a) BLUE-1 (0.04 mW), (b) BLUE-2 (0.04 mW), (c) BLUE-1 (14 mW), (d) BLUE-2 (14 mW).

The main body was made out of copper. On the front and back face of the copper block two quartz windows were embedded with distance of 4 mm. For low temperature measurements at 77 K, BLUE-1 was dissolved in 2-Methyltetrahydrofuran (MTHF), which forms a glassy matrix at 77 K.

To study the effect of low temperatures on the fluorescence lifetimes, BLUE-1 was dissolved in MTHF at a concentration of 0.01 mg/ml. MTHF tends to create a glassy matrix at 77 K and thus the polymer chains are separated at dilute concentrations. Figure 23 compares the dynamics and emission spectra at room temperature and at 77 K. The fluorescence spectra show that the vibrational modes are narrower at low temperatures and experience a red shift of 3 nm (24 meV). Low temperatures in conjugated systems freeze the molecular motion of the molecules, which results in a narrower groundstate DOS and thus a lower disorder. Exciton dynamics resemble at dilute concentrations of 0.01 mg/ml in MTHF similar dynamics compared to the measurements in toluene with a concentration of 0.1 mg/ml. The single-exponential decline of the PL intensity shows that only one excited state is involved in this process originating from

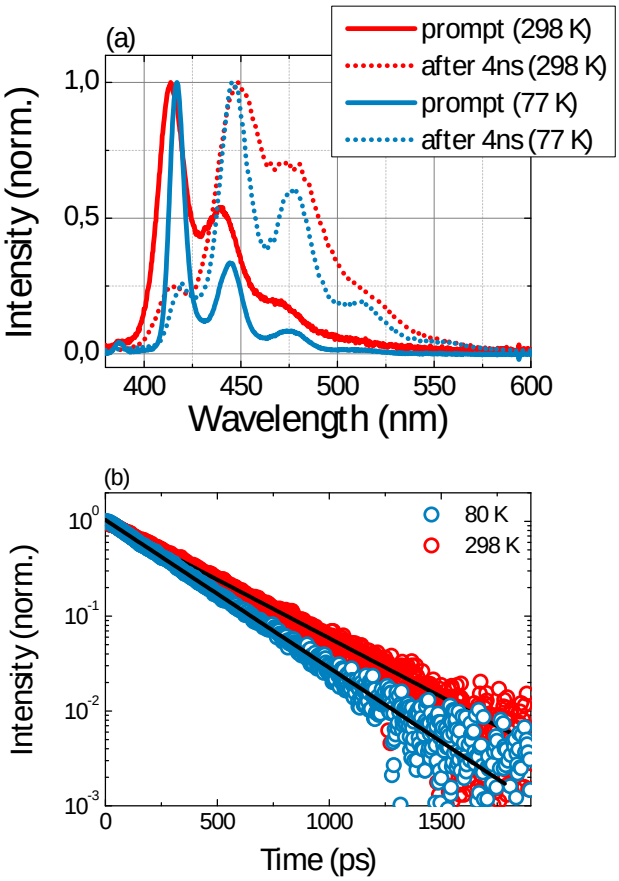

Figure 23: Fluorescence and dynamics of BLUE-1 in a dilute MTHF solution at a concentration of 0.01 mg/ml. Measurements were carried out at room temperature and 80 K.

singlet excitons. The prompt spectrum of BLUE-1 is caused by excitation in the tail of the DOS. Exciton dynamics in disordered materials are well described in the framework of the Gaussian Disorder Model. The process of exciton transport occurs by a hopping mechanism. At low temperatures, hopping occurs as a downhill energy transfer process towards the tail of the DOS, which then is observable as a bathochromic (red shift) of the spectrum with time after excitation.

3.4.2 *Defect emission*

Green emission bands in blue emitting polyfluorenes have been extensively studied in the past [99, 100, 101]. These defect sites, also known as the g-band, are centered at around 535 nm (2.32 eV) and are found in solution and in solid-state. It is accepted that the g-band arises from on-chain keto-defects attributed to

Material	Conditions	A1	A2	t1 (ps)	t2 (ps)
BLUE-1	Toluene 0.1 mg/mL (298 K)	1		361	
BLUE-2	Toluene 0.1 mg/mL (298 K)	1		364	
BLUE-1	MTHF 0.01 mg/mL (298 K)	1		352	
BLUE-1	MTHF 0.01 mg/mL (77 K)	1		278	
BLUE-1	Film (298 K)	0.89	0.11	268	1185
BLUE-1	Film (77 K)	0.91	0.09	281	915

Table 2: Summary of dynamics of BLUE-1 and BLUE-2 measured under different conditions and solvents.

a fluorenone group within the polymer backbone. They can arise from photo-oxidative degradation, thermal degradation or during synthesis [102]. In addition to defect emissions, Lupton et al. observed an emission band at 480 nm (2.58 eV), which was not the result of the keto defect and thus assigned to aggregation [99, 103]. Green emission features in the singlet fluorescence have previously been reported for poly(indenofluorenes) as well [104, 105]. Keivanidis et al. have described a class of poly(indenofluorenes) with different side chains. A spectral component centered at around 517 nm (2.40 eV) was observed in the delayed luminescence and assigned to interchain interaction of the polymer backbones. Oxidative emission effects were not observed though, as the chemical synthesis led to defect-free materials.

Parasitic emission defects originating either from fluorenone groups or from aggregate sites are undesired in light emitting diodes as they affect the color purity of the blue emission. In addition they can act as trap sites in these devices and therefore change charge transport and charge recombination characteristics as will be discussed later in chapter 4. Both emission sites, i.e. g-band or aggregation, are detrimental for organic lasers. In order to achieve stimulated emission, the materials have to sustain a high photon flux without other competing emission processes occurring. The relation between keto-defects and their influence on ASE will be discussed in chapter 3.5.4. Pristine samples of BLUE-1 and BLUE-2 were also studied after they were illuminated with UV-light and stored under ambient conditions for two months. Steady-state as well as time-resolved measure-

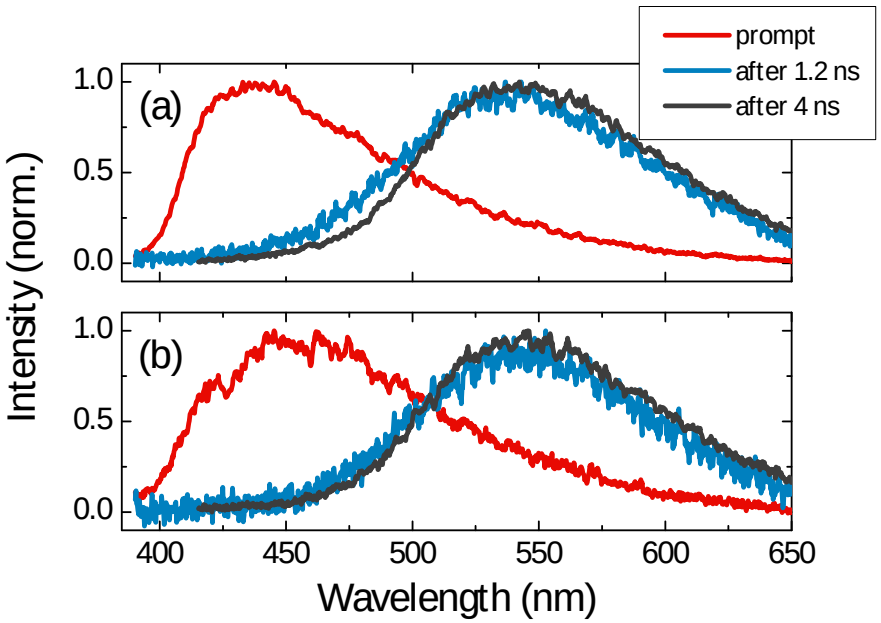

Figure 24: Transient photoluminescence spectra at different delay times from aged films of (a) BLUE-1 and (b) BLUE-2.

ments, illustrated in Figure 24, show that the blue emission of both polymers is largely suppressed and a new dominant emissive species is observed with the spectral characteristics of a g-band, which was not present in the pristine films. The prompt spectra in transient experiments show a featureless blue emission, which shifts within the first 100 ps to the g-band position without any trace of the intrinsic blue fluorescence. The g-band has a rather long lifetime and is still present at 4 ns after excitation.

Steady-state fluorescence measurements reveal that g-band luminescence is the most dominant, broad and featureless emission in the visible spectrum. The 0-1 transition appears in both materials as a weak emissive feature. However, it is worth to mention that only films stressed with UV-light showed g-band characteristics. Films stored for 18 months under ambient conditions, which were not exposed to any UV-radiation, kept their initial blue spectral characteristics and their vibronic modal distributions. Aggregate emission band and g-band emission characteristics are separated by around 45 nm (240 meV) with respect to each other and thus can clearly be distinguished. Both bands show broad and featureless emission spectra and have a longer lifetime compared to the singlet exciton lifetime.

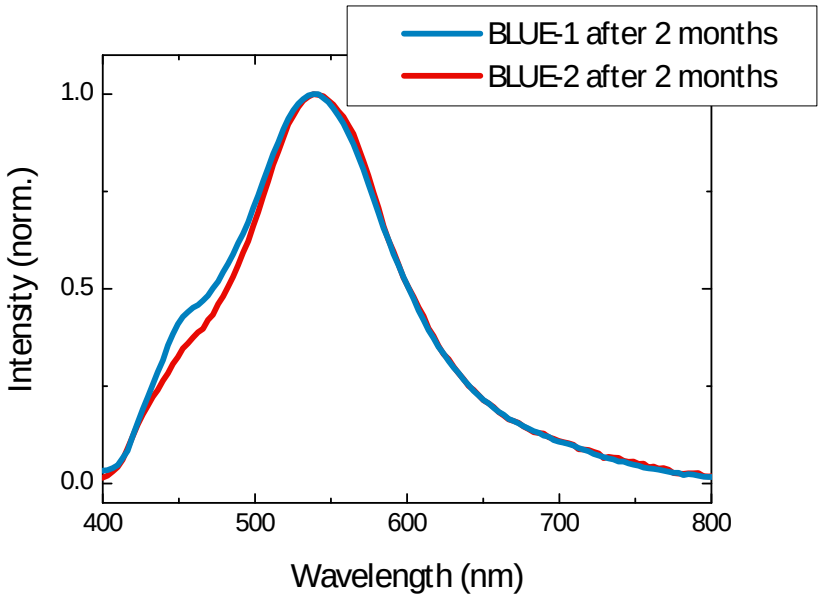

Figure 25: Steady-state fluorescence spectra of BLUE-1 and BLUE-2 after UV light stressing and storing them under ambient conditions for two months.

3.4.3 *The origin of non-monoexponential dynamics in BLUE-1*

Non-monoexponential fluorescence dynamics in conjugated polymers can have various reasons. A deviation from a single-exponential decay can either be caused by interaction with the environment or by the existence of more than one excited species. The former can be influenced by the choice of solvent, concentration and temperature. As intermolecular interaction increases, from an isolated polymer chain to the solid-state, the influence of neighboring chromophores has to be taken into account. For polymers, a distribution of relaxation times can occur that can be analyzed with a stretched exponential function also known as the Kohlrausch-Williams-Watts (KWW) function, which is an empirical description, originally used to define dielectric relaxation in polymers given by [13]:

$$I(t) = I_0 \cdot \exp(-[t/\tau]^{\beta}),$$

where $0<\beta \leqslant 1$ is related to the distribution of lifetimes. In the presence of Förster Resonance Energy Transfer (FRET), the donor molecules obey the stretched exponential law with $\beta=1/2$. In contrast, a multi-exponential function is applied when more than one decay channel is present. Also different chain confor-

mations that contribute distinctively to the photoluminescence can be the reason for a bi-exponential decay [106].

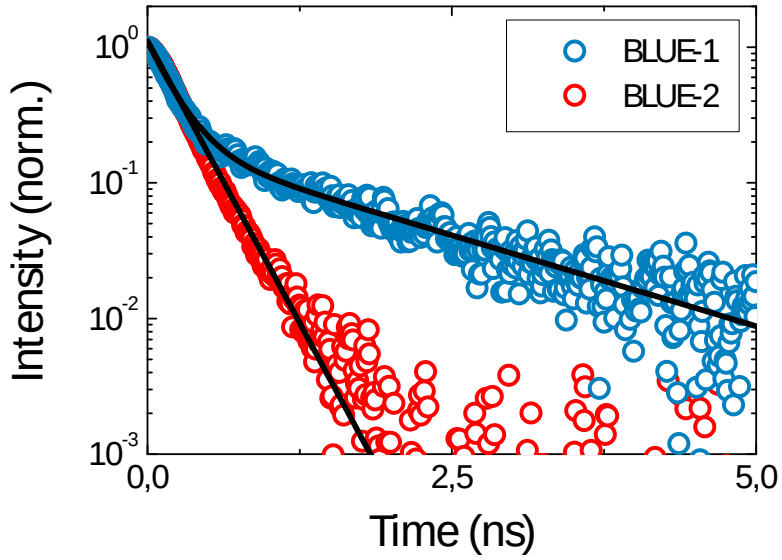

Figure 26: Fluorescence dynamics of BLUE-1 and BLUE-2 in film at room temperature.

Figure 26 shows the fluorescence decay transients in the solid-state. Only BLUE-1 deviates from a single-exponential decay pattern. As it has been discussed in the previous chapter, thin films show this behavior, concomitantly with a red-shift of the fluorescence spectrum at later times after excitation. The bathochromic shift is not caused by spectral relaxation. The former is a relaxation process within the DOS to lower energy sites and is observed as a red-shift of the entire spectrum in time [107]. Here however, as depicted in Figure 22, the 0-0 transition remains at its initial spectral position, whereas only the 0-1 and 0-2 transitions experience a red-shift. Measurements at low temperatures show that the feature remains at its spectral position, whereas the prompt fluorescence experiences a slight red-shift of its vibronic satellites as depicted in Figure 23. Since the second feature is more prominent and influences the decay transients in solid-state, it is assigned to an interchain excited species. Interactions of this kind can originate from various kinds of effects. Bound polaron pairs for instance, can cause a persistent, long-lived PL, attributed to geminate recombination of bound pairs [108]. Pairs are formed in packed regions of the chains, where

the charge only needs to hop a few angstroms onto adjacent conjugated segments [109]. The non-exponential behavior is assumed to originate from a distribution of energies and hence a distribution of barriers to reform the singlet exciton [109]. The reformation has been detected on a timescale up to 1 ms [110]. Furthermore a reduction of the PLQE is observed with the creation of bound pairs. However, different to the findings presented in the scope of this theses, geminate pairs reform singlet excitons and have the same spectral characteristics as the normal fluorescence. Furthermore, formation of polaron-pairs is typically accompanied by a second polaron absorption band with a distinct spectrum that overlaps with the region of stimulated emission. Thus, they are malicious for materials for organic lasing [111]. Such a band was not witnessed in transient absorption (TA) spectroscopy as described in chapter 3.6. Also the high gain parameter with the low threshold as described in chapter 3.5, excludes that the second feature originates from polaron pairs.

Another emission feature that was quite intensively studied in blue emitting poly(fluorenes) is the so called β-phase [112]. This state is introduced when the polymer is dissolved in poor solvents or by slowly heating spincast films from 77 K to room temperature. Spectroscopically the β-phase is recognized by a distinct peak in the absorption spectrum red-shifted to the π-π^* transition. The fluorescence spectrum shows well-defined vibronic replicas with nearly no Stokes-shift and has similarities to ladder-type polymers. It was concluded that the β-phase consists of rigid planar segments of the polymer. Even small fractions of this phase can already dominate the fluorescence spectrum due to efficient energy transfer or by singlet-exciton migration [113]. ASE experiments with small β-phase contents show higher gains and lower thresholds in comparison to the amorphous phase. ASE transition of the β-phase is exclusively occurring at the 0-0 transition [41]. In poly(fluorenes) this feature is only observed for alkyl side-chains with a length between six and nine carbon atoms. It is believed that the side chains of adjacent polymer chains causes interchain "zipping" and planarizes the poly(fluorene) backbone [114]. The fluorescence lifetime of the β-phase in dilute solutions of methylcyclohexane is described by a double-exponential function with a lifetime

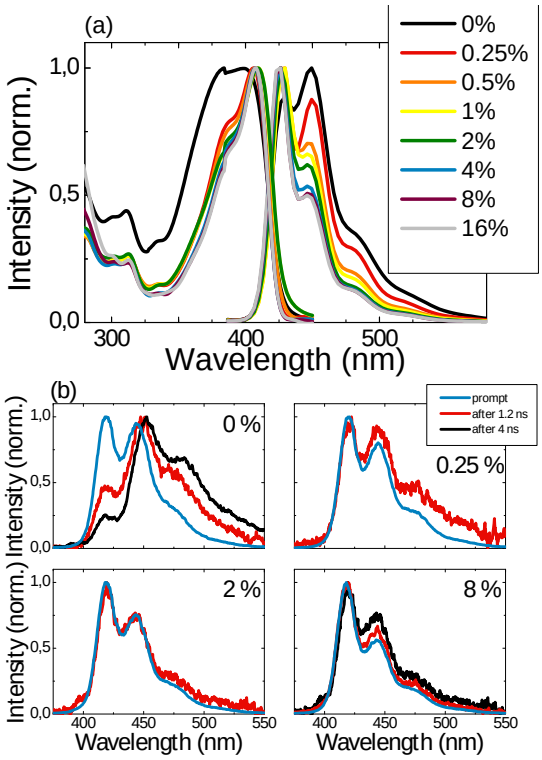

Figure 27: (a) Steady-state spectra of BLUE-1 in film spincast from different DIO/o-xylene volume fractions. (b) Transient photoluminescence spectra as film at different time delays. Note that the second spectral component disappears completely when DIO was added to the soution.

of 130 ps and 270 ps which is shorter than the fluorescence of the amorphous polymer with 340 ps [115]. High β-phase concentrations in spincast films up to 45 % have been obtained by dissolving poly(9,9-di-n-octylfluorene) (PFO) in o-xylene and adding a few volume percent of 1,8-diiodooctane (DIO) [116]. DIO is often used in organic solar cell (OSC)s as an additive. The high boiling point of the solvent at 168 °C causes slower drying during spincoating, resulting in a better packing [117]. Following the procedure described by Peet et al. [116], a solution of BLUE-1 was prepared in o-xylene with different fractions of DIO and subsequently spincast on quartz. The absorption and fluorescence spectra can be found in Figure 27. The additive concentrations were varied, starting with a DIO fraction of 0 % and increasing the concentration up to 16 %. Already small amounts of 0.25 %, change the absorption and emission. Absorption of films spincast from a pure o-xylene solution had no vibronic replica and was rather broad and featureless. With the addition

of the additive the spectrum reveals a distinct absorption peak at 408 nm (3.03 eV) and weak vibronic replicas. The vibronic fine structure of the emission spectra are better resolved with higher DIO content with an increase of 0-0 transition intensity and a decrease of the 0-1 transition. This leads to the conclusion that higher DIO content supports the conformational order of the polymer chains, leading to a better planarization. Steady-state absorption and emission spectra with DIO showed similarities compared to the spectra measured in a dilute solution of toluene (see Figure 71). Even though the spectra indicate a better conformational order of the polymer chains, absorption and emission characteristics do not reveal additional transition bands, which could be assigned to β-phase formation. The time-resolved fluorescence spectra show that the second spectral component, which was typically present in toluene as well in films at larger time delays, vanished completely when DIO is added to the solution. The time-resolved spectra at different time delays are plotted in Figure 27 (b). When BLUE-1 was spincast from pure o-xylene or toluene solutions, the transients of the 0-1 transition always had a non-single-exponential decay with the appearance of a second chromophoric component. With the additive, this feature vanished and the decay transients could be fitted with a single-exponential function as it can be found in Figure 28. The additive seems on the one hand to support better order of the polymer chains, on the other hand suppresses interchain interaction preserving the spectral characteristics of the intrinsic fluorescence without any appearance of the second feature even at time delays of 4 ns, at which this feature was dominating the emission spectrum in solution as well as solid-state. This clearly shows that the second spectral component in BLUE-1 cannot be assigned to β-phase formation.

From the observation, that two different spectral components exist in BLUE-1 films prepared without additives, a bi-exponential function can be applied. The lifetime of the singlet exciton matches the measurements carried out in dilute solutions in toluene or MTHF as depicted in Figure 23 and Figure 20, where only the contribution of the singlet exciton is seen. The lifetime of the second feature was found to be $\tau_2 = 1.6$ ns. It is noteworthy that the decay characteristics of the 0-0 transition regardless of concentration and temperature always follow a

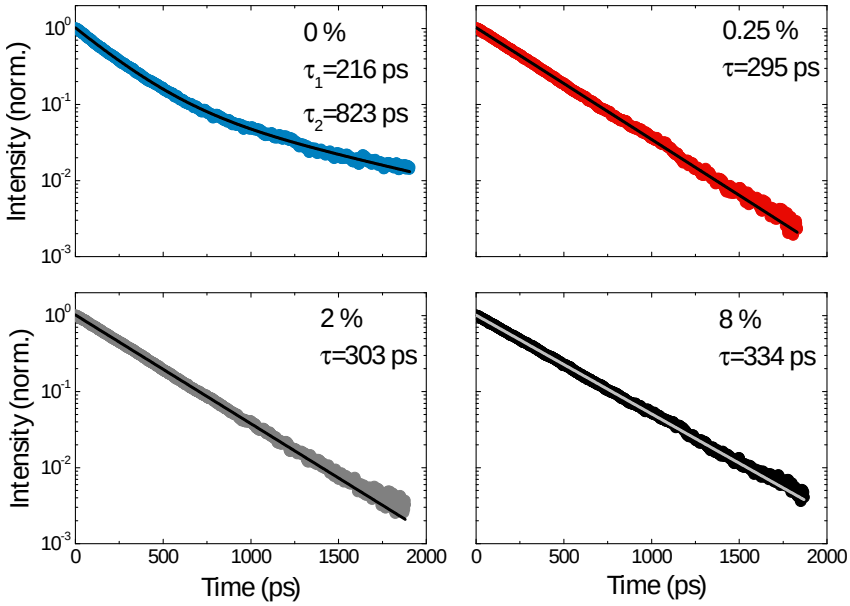

Figure 28: Transient characteristics and their fitted decay constants of BLUE-1 in film with different DIO fractions prior they were spincast.

single-exponential and exhibit the characteristics of the singlet exciton. The decay properties of the vibronic progressions such as the 0-1 transition depend on the concentration, i.e. on the interchain interaction.

3.4.4 *Delayed fluorescence of BLUE-1*

3.4.4.1 *Introduction*

There are two types of delayed fluorescence (DF) that can be distinguished in conjugated materials and occur from the interaction of triplet states [4]. Both show the same spectral distribution as the prompt fluorescence and are caused by triplet states that are created by ISC from $S_1 \rightarrow T_1$. Thus delayed fluorescence has larger decay time constants compared to the prompt fluorescence. *Thermally activated DF* is a consequence of a small energy gap between S_1 and T_1 in the order of several kT. Hence, at higher temperatures the efficiency of the DF increases. In aromatic hydrocarbons such as conjugated polymers the energy gap between S_1 and T_1 is typically about 0.7 eV and thus thermally activated DF cannot be observed with the exception of fullerenes [118, 119]. DF can also be caused by *triplet-triplet*

annihilation (TTA). The rather long lifetime of the triplet states allows them to annihilate. In this process two triplet states are involved and therefore the intensity of DF is proportional to the square of the triplet exciton density n_T. TTA-DF has usually half the lifetime of the intrinsic phosphorescence. Both processes, thermally activated DF and TTA-DF are believed to enhance the EQE of electroluminescent singlet emitters above their classic upper limit of 5 % [120, 84]. In the following DF in BLUE-1 was studied in solution.

3.4.4.2 *Results and discussion*

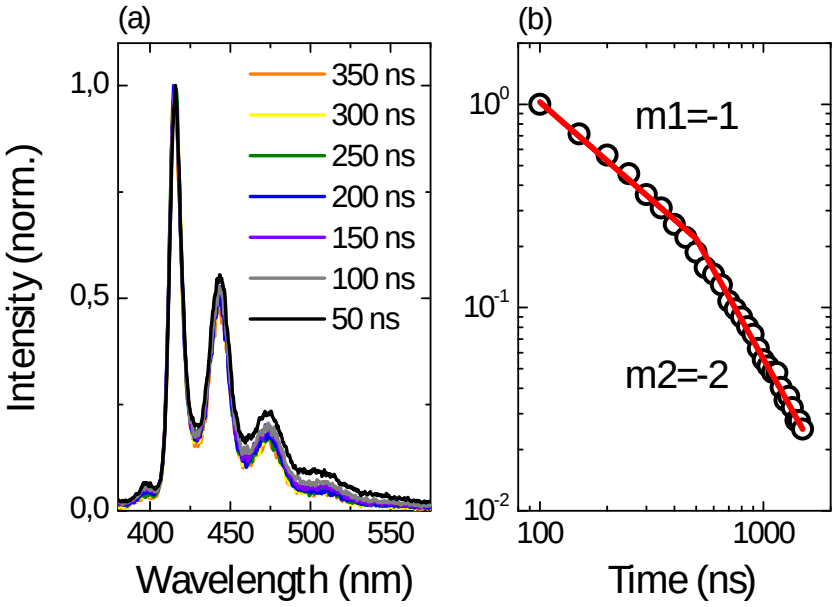

Figure 29: (a) Delayed fluorescence spectrum and (b) decay of BLUE-1 at 77 K in MTHF with a concentration of 0.01 mg/ml. The red lines in Figure (b) are linear fits and describe their power law behavior.

Fluorescence measurements in dilute frozen solution at a concentration of 0.01 mg/ml in MTHF are depicted in Figure 29. The spectra were recorded at a temperature of 77 K. As mentioned above, the DF spectrum resembles the prompt fluorescence with a longer decay time. The DF spectra reveal no change compared to the prompt fluorescence recorded immediately after pulsed excitation. No sign of intermolecular interaction at this concentration could be observed. Figure 29 (b) depicts the DF intensity

decay as a function of the delay time. The DF decay follows a power law of $I_{DF} \propto t^{-m}$, where m defines the order of the process occurring. Two different regimes are identified. Before triplets reach the thermal equilibrium, the DF intensity decays with an order of m=-1. After thermal equilibrium has been reached, the DF decays with m=-2, which has been verified by Monte-Carlo simulations [121]. Excitons execute a random walk migrating towards tail states of the DOS. The relaxation of triplet excitons takes place on a much longer timescale than compared to singlet excitons that are mainly transferred by (long-range) FRET. Triplets are transferred by Dexter-type electron exchange interaction, where both electrons are exchanged simultaneously [62]. Both triplet states need to be localized on the same chain so that they can annihilate in dilute solution. In measurements at a higher polymer concentration of 0.1 mg/ml, the transition from m=-1 to m=-2 occurs on a similar timescale. Higher concentrations generate again interchain excitons (see Figure 74).

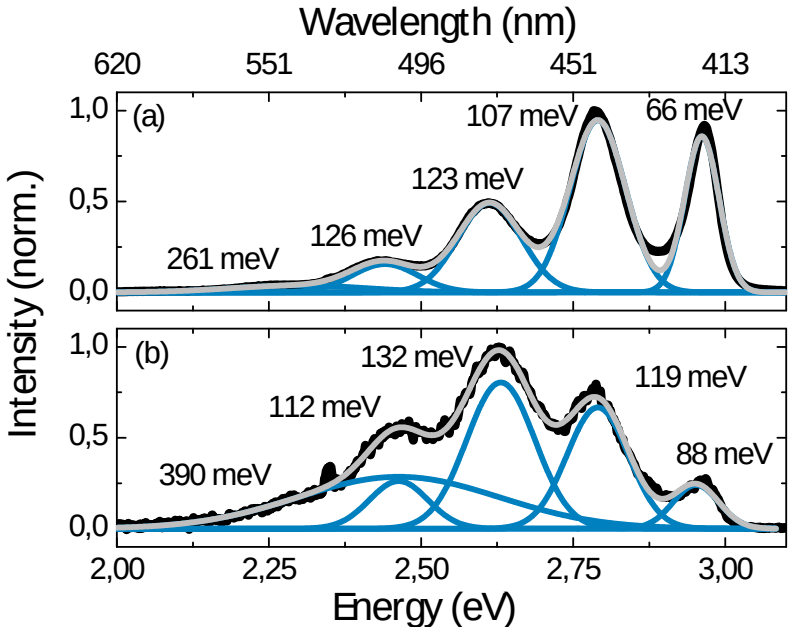

Figure 30: Prompt (a) and delayed (b) PL spectra of BLUE-1. The measurements were recorded at a concentration of 0.1 mg/ml in MTHF at 77 K.

The emission of the interchain excitons, depicted in Figure 30 was recorded 10 ns after pulsed excitation and with a gate width of 2 ns. The emission decays before DF becomes more dominant. The spectral fingerprint of the prompt fluorescence and thus

the interchain exciton does not contribute to DF by TTA. At gate delays of 10 µs and a gate width of 10 ms of the intensified CCD system, phosphorescence could be observed. Photoluminescence was recorded from BLUE-1 dissolved in MTHF at concentration of 0.1 mg/ml. The phosphorescence spectrum can be found in Figure 31. The optical transition $T_1 \rightarrow S_0$ occurs at 558 nm (2.22 eV) with a singlet-triplet gap of Δ_{ST} =0.74 eV, which is similar to previous findings for conjugated polymers [122]. In addition to the phosphorescence spectrum, delayed fluorescence appears simultaneously.

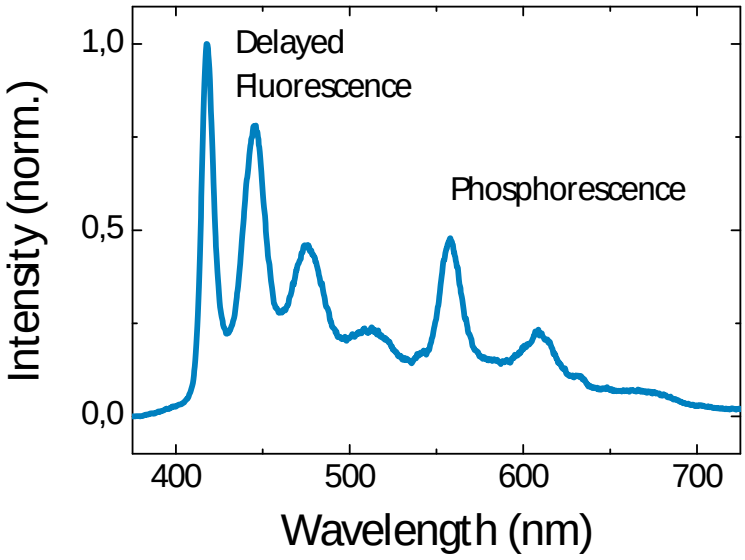

Figure 31: Delayed fluorescence and phosphorescence spectrum of BLUE-1 dissolved in MTHF at a concentration of 0.1 mg/ml.

3.5 AMPLIFIED SPONTANEOUS EMISSION AND LASING

3.5.1 *Introduction*

A particularly challenging application of conjugated polymers is as active materials in organic laser devices. Although optically pumped organic lasing from various feedback structures has already been demonstrated more than a decade ago [123, 124, 125], the successful realization of an electrically pumped laser using a conjugated polymer remains an open issue, despite their favorable photophysical properties such as high fluorescence quantum yields, high chromophore densities in the solid state combined with large stimulated emission cross-sections and long excited state lifetimes. A prerequisite for lasing is the occurrence of ASE. However, only a fraction of the vast number of conjugated polymers show ASE at reasonably low pump energy density thresholds. This is often a consequence of a low gain caused by an overlap of the region of stimulated emission (gain region) with the ground state absorption or the photoinduced absorption of excited states [126]. Furthermore, scattering processes at film imperfections or waveguide leaking into the cladding layers can cause detrimental waveguide losses. The latter plays an important role in devices, since quenching of excited states in the vicinity of metal electrodes severely diminishes the concentration of excited states. Recently, Wallikewitz et al. reported that this issue can be overcome by adding thick hole and electron transport layers to separate the gain material from the metal electrodes. In combination with a cross-linkable active material, which was patterned with a corrugated feedback structure, an electrically addressable device was demonstrated, that still exhibited lasing, though only upon optical excitation [127]. However, a major issue preventing the successful realization of lasing from conjugated polymers in typical device structures is the high number of excited states that has to be generated within the organic layer for amplification of light to occur. This can be easily achieved by optical excitation, but similarly high excitation densities upon electrical excitation require high charge carrier mobilities to allow for fast transport of injected charges to the recombination zone and to avoid build-up of space charges at the interfaces, which would otherwise suppress further charge injection. Thus, the conjugated polymer has to

fulfill many requirements, which are interconnected and can exclude each other. A promising approach is to search for suitable polymers among highly efficient OLED materials. Yap et al. [35] have recently shown that careful tuning of the composition of polyfluorene copolymers cannot only enhance the PL and ASE properties, but also the charge carrier mobility. Following the approach of tuning the optical properties by variation of the polymer structure, a series of step-ladder-type polymers have been previously reported, which have originally been developed for blue OLEDs [126]. Within the series of step-ladder polymers a fully-arylated poly(indenofluorene) homopolymer exhibited the lowest threshold value for ASE, however, only moderate gain coefficients were obtained. Stimulated by these results investigation towards novel copolymers were extended to further optimize the optical and electrical properties for organic lasing. In this respect stimulated emission of copolymers BLUE-1 and BLUE-2 was further analyzed and their performance was compared to the homopolymer PIF.

ASE from organic semiconductors occurs after excitation by pulsed light sources. The ASE peak for both materials occurs at the S_{0-1}-position at around 450 nm (2.76 eV). When the pump fluence is increased, a typical blue shift of the ASE peak emission is observed as a consequence of depopulation of the excited states before they can relax into the tail states of the DOS. ASE in organic materials occurs at the optical 0-1 transition from the first singlet excited state S_1. In order to observe ASE, population inversion is required that induces stimulated emission within a waveguide. Therefore ancillary levels are necessary to finally reach the threshold of ASE. This can be understood in terms of a four-level energy scheme.

A continous-wave (CW) operation has not been demonstrated yet. The reason is that only the first excited singlet state S_1 contributes to stimulated emission. Upon photoexcitation, a certain fraction of singlet excitons undergo ISC to the triplet state T_1. T_1 however does not participate in the induced emission process. Since the transitions are spinforbidden, triplets have relatively long lifetimes of µs to s. Triplet states have distinct absorption features that can overlap with the fluorescence and thus suppress stimulated emission. Continuous photopumping will

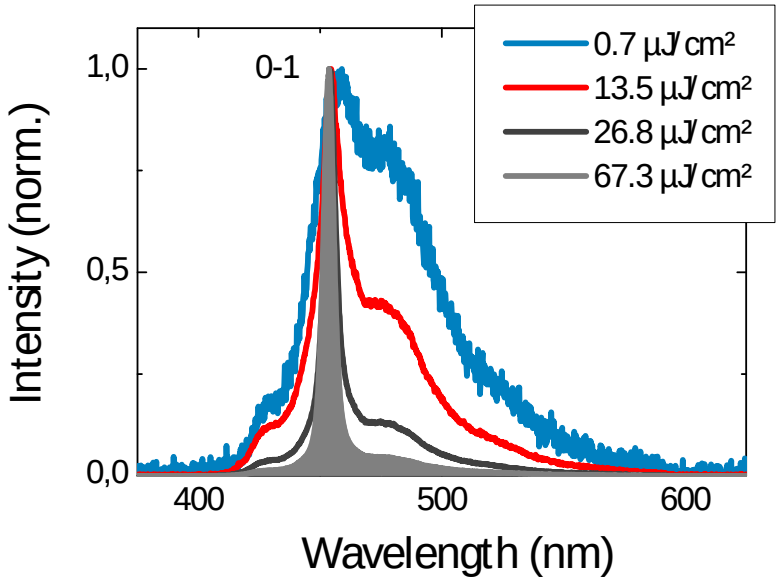

Figure 32: Spectral narrowing of BLUE-1 under different pump fluences. The spectrum collapses at the 0-1 position as pump fluence is increased in a waveguide structure.

accumulate triplet excitons which hampers stimulated radiation. However, CW operation in dye lasers can be achieved. The liquid dye solution needs to be continuously pumped through the resonator cell. Molecules in T_1 are thereby removed from the cavity. Another approach is to add a triplet scavenger to the dye solution. The latter scavenges the triplet state of the dye molecules by energy transfer to lower triplet states. A molecule that is typically used for this purpose is 1,3,5,7-cyclooctatetraene (COT) [128]. The build-up of T_1 in solid state organic semiconductors allows amplification of light only up to several tens of ns. Zhang and Forrest have recently reported a quasi CW operation by deploying a triplet scavenger in a guest-host system. By this approach, they were able to reach laser durations of up to 100 µs [129].

3.5.2 *Results and discussion on PIF, BLUE-1 and BLUE-2*

The ASE threshold, net gain and loss coefficients were determined for PIF, BLUE-1 and BLUE-2. The full width at half maximum (FWHM) of the ASE peak at the 0-1 vibronic progression was monitored as a function of the pump pulse energy density

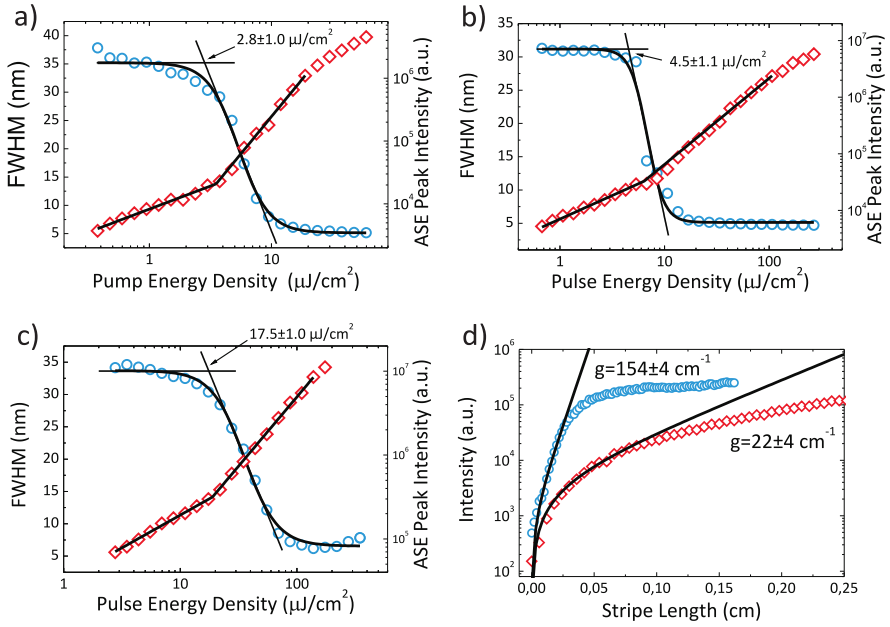

Figure 33: ASE Threshold of a) PIF, b) BLUE-1 and c) BLUE-2 and d) gain measurements of BLUE-1 in comparison to PIF.

upon excitation into the absorption maximum. ASE thresholds were determined at the pump fluence at which the PL spectrum collapsed into one single peak identically to a previously described method [130]. A sigmoidal function according to

$$I(x) = A_2 + \frac{A_1 - A_2}{1 + (x/x_0)^p}$$

was used to fit the dependence of the FWHM of the ASE peak on the pulse energy density, where A_1 and A_2 denote the upper and lower level of the FWHM, x_0 defines the inflection point and p represents the steepness of the function. Additionally, the transition from a linear to a superlinear dependence of the ASE peak intensity on the pump fluence was used as an indication of the ASE threshold values. Both methods were applied to compare and confirm the obtained ASE thresholds. Threshold values of 17.5 ± 1.0 µJ/cm^2 and 4.5 ± 1.1 µJ/cm^2 were determined for BLUE-2 and BLUE-1, respectively. Gain parameters were determined by the variable stripe length method as previously reported by Laquai et al. [131]. A minimum of three different pump energy densities were used to determine the gain values. Typical gain curves representing the maximum achievable gain for PIF and BLUE-1 are shown in Figure 33. The gain parameter

g was determined by fitting the stripe length dependence l of the ASE peak intensity according to:

$$I_g(l) \propto \frac{1}{g}(e^{-g \cdot l} - 1)$$

A maximum gain value of $154 \pm 7\ cm^{-1}$ was determined for BLUE-1, which is the highest gain coefficient determined with the variable stripe length method for a conjugated polymer at the time this thesis was written. For comparison, gain coefficients previously reported for PFO and a PFO copolymer were found to be between $74\ cm^{-1}$ and $87\ cm^{-1}$, respectively [40, 35]. For implementation in light amplifiers and organic lasers low waveguide loss coefficients and high PLQE are also a prerequisite. The loss coefficients were evaluated by fitting the ASE peak intensity as a function of the non-pumped region between the sample edge and the excitation stripe according to:

$$I_\alpha(x) = I_0 \cdot e^{-\alpha x},$$

where I_0 is the amplitude of the function, α the loss coefficient and x describes the distance to the sample edge. All polymers showed very low loss coefficients of about $1\ cm^{-1}$. The measurements of the loss coefficients for BLUE-1 and PIF can be found in Figure 34. Waveguide losses are usually a result of intrinsic absorption and scattering at interfaces caused by the surface roughness and particles or grain boundaries potentially present in the polymer films [132]. The small loss coefficients show that both copolymers have excellent film forming and waveguide properties. Additionally, much higher PLQE values of $(55 \pm 4)\%$ were observed for BLUE-1 and $(66 \pm 2)\%$ for BLUE-2 than for Aryl-PIF $(35 \pm 2)\%$, which makes the copolymers more attractive than the homopolymer for light amplification. The PLQE of Aryl-PIF is slightly lower than previously reported [131], probably due to an entirely different experimental setup used for the present study. Furthermore, the loss coefficient obtained for the new batch of Aryl-PIF is lower than obtained previously [131], which is believed to be due to better film formation of the new polymer batch. However, the ASE threshold and gain coefficients are in excellent agreement with previously observed values and verify comparability [131].

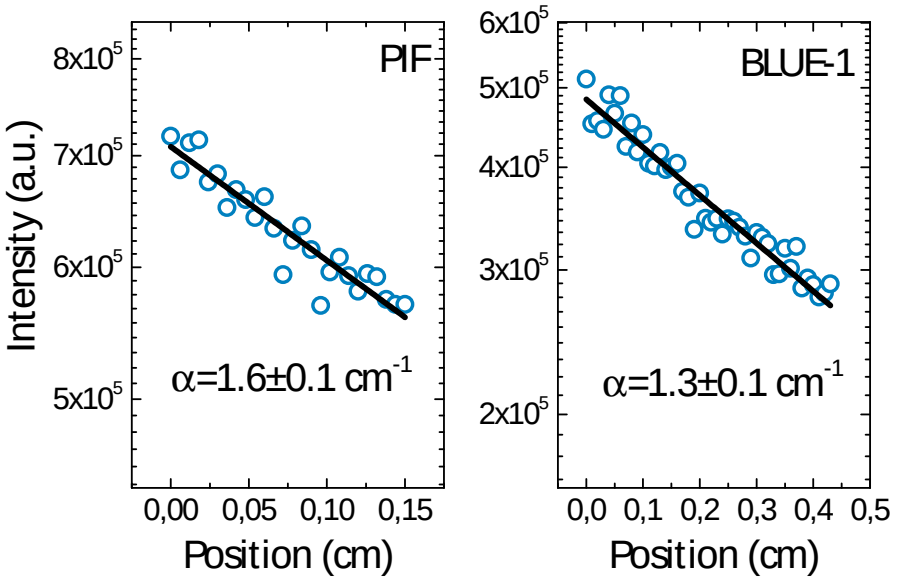

Figure 34: Determination of ASE loss coefficients.

In OLEDs, waveguiding is recognized as a loss channel since it hinders the outcoupling of light and thus reduces the external quantum efficiency. One approach to overcome this problem is to deploy high refractive index lenses that support a better outcoupling of substrate modes trapped inside the organic layer [133]. A waveguide is generally a dielectric structure that due to its refractive index distribution allows lightguiding. The simplest waveguide is onedimensional, consistent of three different layers with three different refractive indices. The lightguiding layer has to have a higher refractive index than its surrounding cladding layers. BLUE-1 and BLUE-2 both can be considered as the core of a waveguide when spincoated on quartz, in which quartz and air act as cladding layers with refractive indices of $n_{SiO_2@450nm} = 1.47$ and $n_{O_2} = 1.00$ respectively. Different to OLEDs, waveguiding is essential for ASE to occur. If the amount of spontaneously emitted photons propagating along the film direction of the polymer is higher than the optical losses, amplification occurs while light travels through the medium. As a consequence, the emission spectrum narrows at the position where the net gain is highest, which is typically at the 0-1 transition in organic materials [134]. The refractive index of the TE-polarization, the mode parallel to the film plane as well as their cladding layers, determine the percentage of light traveling along a waveguide. The intensity profile $I(x)$ of the TE_0 mode

and the resulting confinement factor Γ determined by the mode confined in film direction x with a thickness d are connected as follows:

$$\Gamma(x) = 100 \times \frac{\int_0^d |E(x)|^2 dx}{\int_0^\infty |E(x)|^2 dx} = \frac{\int_0^d I(x) dx}{\int_0^\infty I(x) dx}$$

Confinement factors Γ were found to be 44% and 43% for BLUE-1 and BLUE-2 respectively. The thickness of the polymer films were set to 120 nm which is close to the film thickness used for ASE measurements. The calculations were done with a semi-analytical freeware program [135]. The resemblance of the optical constants for both materials indicate that they support waveguiding and a sufficient amount of light is guided along the film plane to support ASE. Previously reported confinement factors for blue emitting polymers with ASE characteristics and a thickness of 100 nm are within the same range. A series of fluorene based homopolymers and copolymers showed Γs ranging between 37% and 61% [136].

Furthermore, both material possess intrinsic optical anisotropy ($\Delta n = |n_0 - n_e| = |n_{TE} - n_{TM}|$) showing that there is a preferential alignment of the polymers within the substrate plane [95]. Optical anisotropy in conjugated polymers results from different oscillator strengths in different directions due to particular molecular ordering of transition dipoles. Anisotropy can even arise from different processing procedures, molecular weights and film thicknesses. Typical variations of Δn for conjugated polymers are in the range between 0 (isotropic) and 0.4 [137]. The degree of alignment in this particular case is very high, peaking at the π-π^* transitions of the polymers. It is proven that highly aligned conjugated polymers can enhance the gain and reduce the ASE threshold. Martini et al. found that by incorporating poly[2-methoxy-5-(2-ethylhexyloxy)-p-phenylene vinylene] (MEH-PPV) into aligned mesoporous silica templates, they were able to order the polymer chains parallel to the substrate plane. By orienting the polymer chains, they were able to lower the ASE threshold more than a factor of 20 with respect to spincast polymer films and increase the gain [138]. They finally concluded that chain alignment and the minimization of interchain electronic coupling improves the gain and reduces the loss. On the contrary, the chromophore density scales expo-

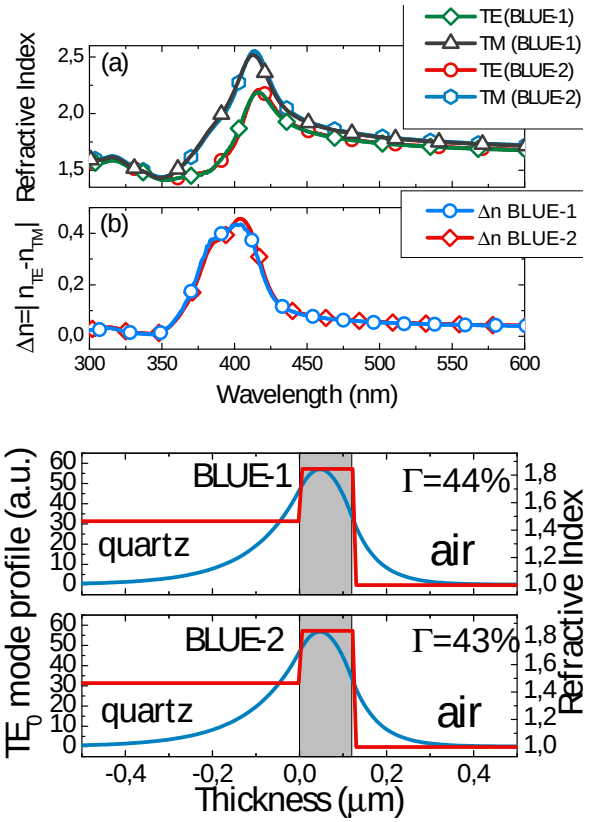

Figure 35: (a) Wavelength dependence of the refractive index of BLUE-1 and BLUE-2 in TE and TM mode determined and their (b) optical anisotropy. (c),(d) Intensity profile of the TE_0-mode in the slab waveguide structure for BLUE-1 and BLUE-2.

nentially with the gain [139]. However, if conjugated polymers are more densely packed so that interchain coupling occurs as it is the case for BLUE-1, one has to cope with further photophysical processes that will occur. It is claimed that a closer spatial arrangement of the molecules will lead to formation of aggregates that facilitate singlet-singlet annihilation (SSA) and thus diminish line narrowing [34].

As discussed in the previous chapter 3.4.1, BLUE-1 shows two spectral components. The TRPL measurements in Figure 37 show an intramolecular species appearing in solid-state. The intramolecular species is red-shifted compared to the initial fluorescence and the transients were fitted with a bi-exponential function. The high optical anisotropy as well as the dense packing can explain the higher chromophore density and thus the higher gain of the material. Nevertheless, the malicious byprod-

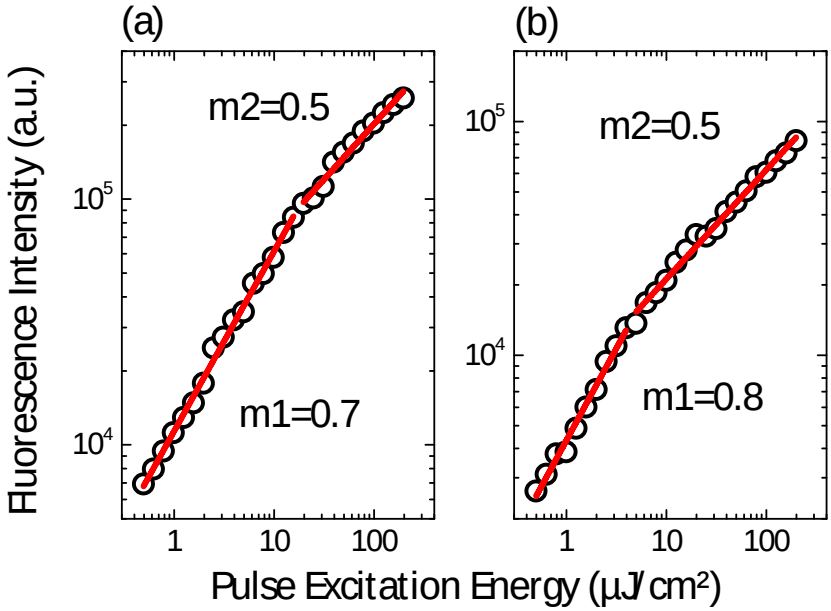

Figure 36: Fluorescence fluence dependence in film of (a) BLUE-1 and (b) BLUE-2.

uct of enhanced chain packing, where the existence of aggregates or polaron pairs is more likely to occur, usually suppresses the gain and polaron pairs seems not to occur. Figure 36 depicts the fluorescence intensity as a function of the pump fluence. The data were extracted from the ASE threshold experiments illustrated in Figure 33. Instead of tracing the 0-1 transition, with which the ASE threshold parameter can be extracted, the 0-0 transition was traced to retrieve more information on the fluorescence. Both graphs were plotted in a double logarithmic fashion. A clear kink can be observed and each region was linearly fitted. SSA is at higher fluences indicated by the square-root dependence on pump fluence. For BLUE-2 this regime is reached even before the ASE threshold. In the previous chapter, it was shown that aggregation can be induced by photopumping BLUE-2. BLUE-1 seems to sustain high pump fluences and the onset of SSA starts occurring at higher exciton concentrations. Even though BLUE-1 is densely packed and has a higher chromophore density, the chromophoric backbones are still very well isolated so SSA occurs at higher exciatition densities. As discussed in chapter 3.4.1 the glass transition temperature of both materials affects the stability. For BLUE-2 there is evidence that aggregation can be induced by the pump pulse and affects

the ASE characteristics.

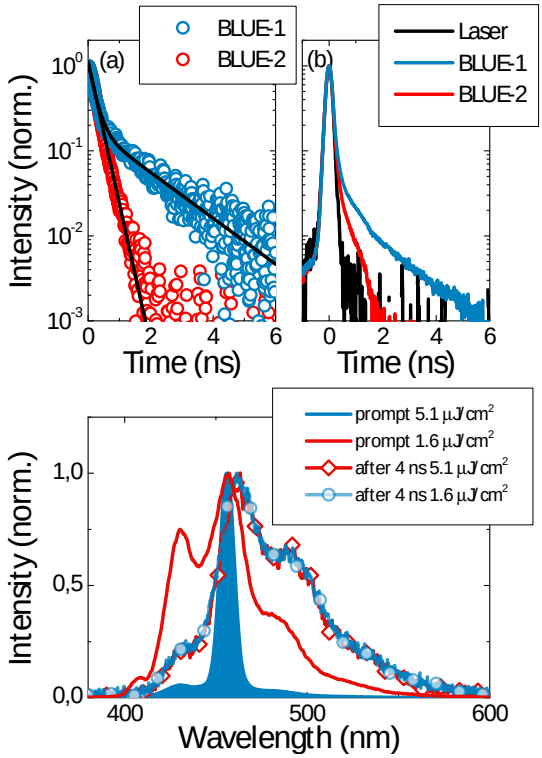

Figure 37: Decay transients of BLUE-1 and BLUE-2 recorded at (a) 1.6 µJ/cm^2 and at (b) 5.1 µJ/cm^2. Graph (c) illustrates transient photoluminescence spectra of BLUE-1 at different delay times. The prompt spectrum shows at higher pump fluences ASE. The spectral characteristics at a delay time of 4 ns are not affected by the pump fluence and the occurence of ASE.

The second spectral component that was discussed in chapter 3.4.3 with a lifetime of τ_2=1.6 ns is not influenced by ASE. At higher pump fluences above the ASE threshold at 13 µJ/cm^2, where ASE depletes the majority of the excited states within the resolution of the streakcamera experiment as illustrated in Figure 37 (b). The second component feature with its spectral characteristics occurs regardless of the pump fluence.

3.5.3 *Lasing characteristics*

While for ASE, a slab waveguide is sufficient and amplification of light occurs after spontaneous emission, true lasing needs incorporation of the material into an optical feedback structure,

for instance in a cavity. Within such a cavity, light gets amplified by multiple forward and backward reflections, thus stimulating emission of photons. If at a certain excited state density optical losses are overcome, the output emission gets amplified by up to several orders of magnitude, a situation where stimulated emission overcomes spontaneous emission, expressed by a clear lasing threshold. Besides, true laser emission shows a substantially narrower linewidth than ASE, since a lower number of modes are involved in this process. To demonstrate lasing from the copolymers, a 2nd order distributed feedback (DFB) structure was chosen. The lasing mechanism of a DFB laser relies on Bragg scattering within the waveguide. Instead of using conventional cavity mirrors, laser operation is supported by an 1D interference grating causing a periodic perturbation of the refractive index of the medium [140]. Mode selectivity occurs at the Bragg wavelength λ_{Bragg}, where the confined light experiences a back and forward scattering. The laser wavelength can be tuned either by changing the effective refractive index n_{eff}, the order of refraction m or the grating constant Λ according to following relation:

$$2 \cdot n_{eff} \cdot \Lambda = m \cdot \lambda_{Bragg} \; ; \qquad m = 1, 2, ...$$

For practical use a grating structure of 2nd order was chosen. Advantage of the 2nd order is that the periodicity of the grating can be easily fabricated by interference lithography and the laser emission is detected perpendicular to the substrate plane. In 1st order gratings light cannot escape the substrate and lasing can only be detected from the sample edge.

Figure 39 compares the typical laser emission obtained from a thin film of BLUE-1 and BLUE-2 to the ASE spectrum observed from the same film, but excited outside the grating region. The lasing linewidth is limited by the spectral resolution (2 nm) of the fiber-coupled CCD spectrometer.

Similar to the ASE experiments, the pump fluence of the excitation laser was varied with a set of reflective neutral density filters and the evolving lasing peak was recorded. A clear kink can be seen when stimulated emission overcomes the optical waveguide losses. ASE and lasing spectra were obtained from a thin film spincoated onto a quartz glass grating structure.

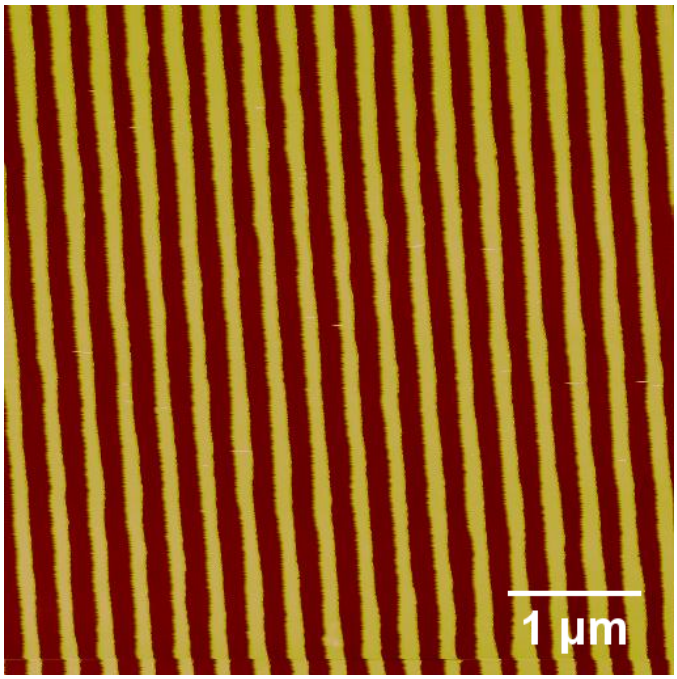

Figure 38: Topography of the grating structure etched on a quartz substrate. The image was determined by atomic force microscopy.

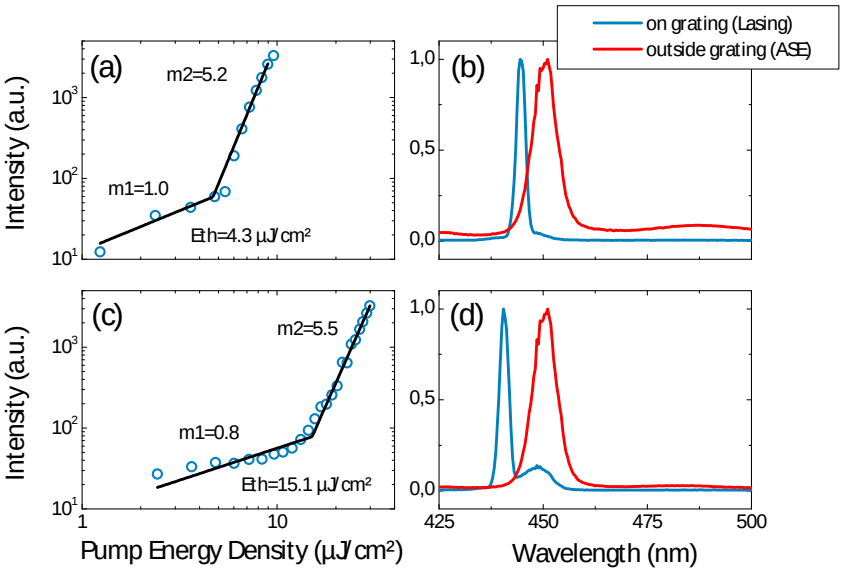

Figure 39: Lasing characteristics for BLUE-1 (a), (b) and BLUE-2 (c), (d)

The ASE spectrum was obtained from the region of the polymer film outside the grating area, whereas the lasing spectrum was observed on the grating. The thresholds are comparable to the ones obtained by ASE experiments in both cases, however the higher power law dependence as well as the linewidth clearly demonstrate the difference to ASE. Both lasing peaks do not coincide with the ASE peak which is caused by the Bragg condition of the DFB laser.

3.5.4 *ASE from a PIF-triphenylamine copolymer*

3.5.4.1 *Spectroscopic properties and ASE*

A further study was carried out with different PIF-based copolymers. The aim of this investigation was to analyze two different PIF-copolymers with the purpose to deploy them as hole injection layers in OLED structures. Therefore typical hole transporting units were incorporated into the backbone of the polymer. The molecular structure of both materials is depicted in Figure 40. Both contain hole transporting units based on triarylamine, whereas HIL-2 features also crosslinkable parts. The crosslinking process starts upon thermal heating of the sample above 180 °C and is finished within an hour. HIL-1 and HIL-2 have optical steady-state characteristics more similar to the PIF homopolymer than to BLUE-1 or BLUE-2. During optical characterization it has been found that HIL-2 exhibits ASE characteristics, which will be discussed in the following. The backbone is rather isolated from other neighboring units due to the bulkiness of the molecule and thus exciton-exciton interaction is expected to be reduced.

The optical properties of HIL-1 and HIL-2 in steady-state are very similar. They possess similar optical features in absorption and emission. In contrast to the novel polymers investigated in the previous section, their fluorescence spectra are red-shifted and have very similar vibronic progressions compared to the PIF homopolymer. Hence, the comparison of both material systems suggest that PL for both originates mainly from the indenofluorene chromophore. Concerning the steady-state absorption and emission, it is noteworthy that upon heating them above 180 °C for over one hour under ambient conditions, the emission characteristics are dramatically changed and an additional spec-

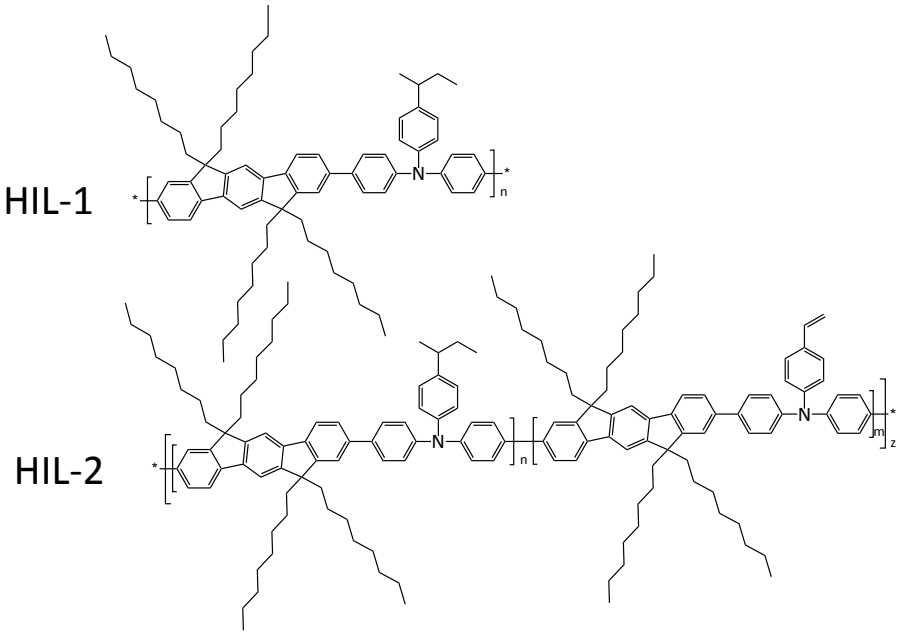

Figure 40: Molecular structure of HIL-1 and HIL-2.

tral feature appears. The absorption spectra are not affected by thermal heating. The additional emission that appears in both materials has the same characteristics as discussed in chapter 3.4.2 and is also depicted in Figure 41.

HIL-1 served as a reference for the crosslinkable HIL-2. Both exhibit a defect band, however the bands appear at slightly different positions. Defect emission of HIL-1 appears at around 550 nm (2.58 eV) and lies far apart from the singlet fluorescence. In contrast, the emission band that additionally occurs for HIL-2 is superimposed with the emission at about 530 nm (2.68 eV) and thus the emission bands of the 0-1 and 0-2 transition appear more dominant compared to the initial spectrum. Defect fluorescence was only observed when the samples were heated to over 180 °C under ambient conditions, while heating in inert conditions such as in a dry N_2-glovebox did not affect the fluorescence characteristics and thus defect emission could not be observed. The keto-defect emission was not only activated by heating the samples under atmospheric conditions. Samples stored in a dynamic vacuum and exposed to high pump fluences of a mode-locked laser shared similar changes of the emission spectra. The spectral dynamics changed similarly to the one discussed in chapter 3.4.2. At a fluence as low as 0.2 mW, there was

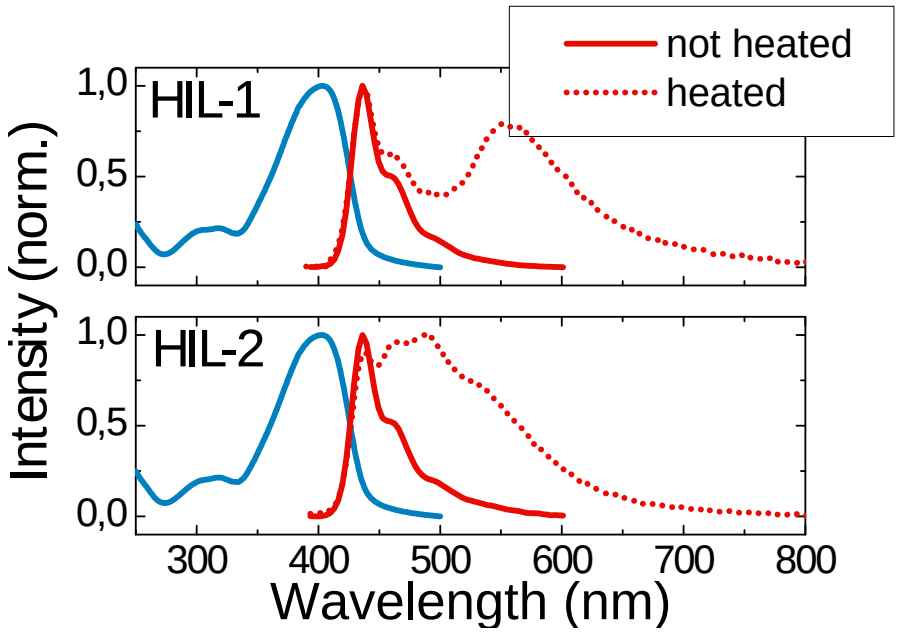

Figure 41: Absorption and emission spectra of HIL-1 and HIL-2. Both materials under the influence of heat at 180 °C in ambient condtions show defect emission.

no time dependent change of the spectrum occurring. Constant irradiation at high fluences of 16 mW transforms the spectrum with time. The prompt spectrum does not differ from the singlet fluorescence excited with 0.2 mW. With increased delay times the spectrum transforms until at delays of 4 ns, a broad and structureless feature appears at the keto-defect position. Similar to the blue emitting polymers, the creation of structural defects within the bulk material changes the transients irreversibly, once illuminated with high excitation powers.

The instability of the hole injection layers does not allow them to be used as emitters in electroluminescent devices. Additionally to the purpose to use them as injection layers in OLED structures, they also show ASE when spincast on quartz. The materials were processed similarly as in the previous ASE experiments. Samples were prepared from solution of a concentration of 10 mg/ml in toluene and spincoated on pre-cleaned quartz substrates with a spinning speed of 2000 rpm for 120 s. The thicknesses were found to be around 70 nm. Two samples of HIL-2 were prepared under the same conditions and one of them was crosslinked and the ASE performances compared to the other. Figure 43 depicts the ASE characteristics after the

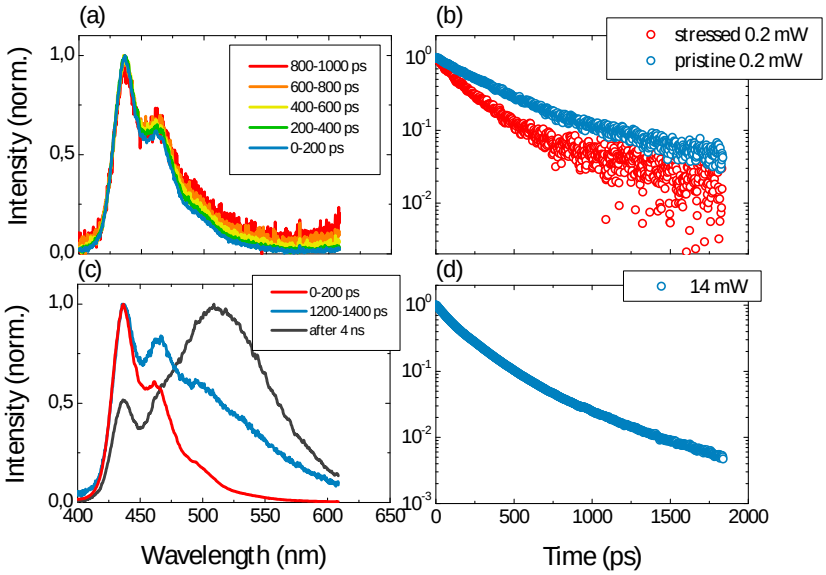

Figure 42: Time-resolved photoluminescence (a) spectrum and (b) transients excited with 0.2 mW. Graph (c) and (d) show the spectrum and transients respectively when excited with a pump power of 14 mW. Higher fluences induce defects.

crosslinking process. A slight change of the ASE parameters was observed. An increase of the threshold value from 1.5 $\mu J/cm^2$ to 3.4 $\mu J/cm^2$ and of the gain value from 9 cm^{-1} to 15 cm^{-1} was determined from a pristine film to a crosslinked film. The slight difference could be caused by the crosslinking process that most likely changes the morphology of the film and thus the chromophore distribution. The latter induces the difference in ASE performance, which is quite small, but still larger than the error of the experiment. In both cases at higher pump fluences above the ASE threshold a kink from a superlinear increase to a sublinear behavior as a function of the excitation power can be recognized. Differently to what was discussed in the previous chapter, where for BLUE-1 and BLUE-2 the superlinear dependence decreased to a linear one at around an order of magnitude above the threshold power, HIL-2 shows a power law dependence of m=0.6. As pump fluences are increased in the waveguide, further processes in addition to ASE are occurring in such disordered materials. SSA for instance, can take place as a secondary process competing with ASE when exciton densities are high enough. A deviation to a sublinear slope dependence

with m=0.5 indicates the regime of SSA.

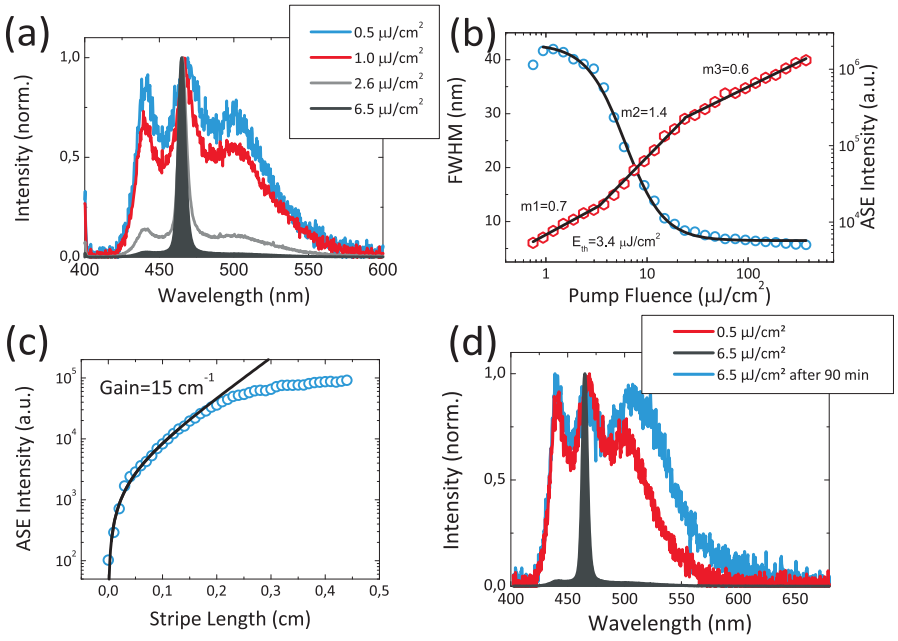

Figure 43: ASE characteristics of HIL-2. (a) Spectral narrowing under different pump fluences, (b) threshold measurements, (c) gain measurements and (d) photo-degradation.

However, the sublinear dependence in the hole injection layers suggests that a different process prior to ASE and SSA are present. Figure 43 (d) illustrates the PL spectra of HIL-2 after being crosslinked. The spectra were collected from ASE experiments and show singlet fluorescence taken below the ASE and another spectrum excited above the ASE threshold with 6.5 $\mu J/cm^2$. After about 90 minutes of constant photoexcitation of the slab waveguide structure, ASE was not observed anymore at a pump fluence of 6.5 $\mu J/cm^2$, where previously ASE occurred. Furthermore, the spectral shape changed to the one of the keto defect state. There is a high tendency for keto defect emissions to occur in these polymers as their molecular structure allows thermal- and photodegradation. The results suggest that keto defect emission is detrimental to organic lasers and leads to a suppression of ASE in a waveguide. Even though threshold values of HIL-2 are lower than for the polymers studied in the previous chapter, the gain parameters are far below the ones found for the phenanthrene-indenofluorene copolymers. Studies on MEH-PPV processed from different solvents report that chromophores isolated by bulky side chains have reduced interchain

interaction, which eventually is advantageous to gain build-up [141]. This suggests that the triarylamine groups together with the hole crosslinking units isolate the chromophores, so interchain interaction of different chromophoric backbones is reduced and this is beneficial to ASE characteristics. Still, the lower gain parameter of HIL-2 is a direct cause of the instability of the material. The interplay of SSA and finally the photodegradation leads only to moderate gain values while the threshold value is as low as 1.5 $\mu J/cm^2$. The molecular structure also suggests that fully-alkylated indenofluorene-copoylmers have a higher tendency of photodegradation that suppresses in turn ASE in ambient conditions. Alkylated-arylated and fully-arylated indenofluorenes that were studied in the previous chapter, have neither shown a suppression of ASE nor was a keto-defect band present, even after photoexcitation for several hours.

3.5.4.2 *Towards an optoelectronic device - Investigation of ASE on a bilayer of HIL-1 and BLUE-1*

One prerequisite for a purely electronically driven injection laser is that the absorption band of the injected charges should not overlap with stimulated emission of the active medium. Otherwise the injected polarons will interact and quench the stimulated emission.

To determine the polaron absorption band, quasi steady-state PIA measurements were performed on both materials. The polymers were blended with [6,6]-phenyl-C61-butyric acid methyl ester (PCBM) in a ratio of 50:50 and successively spincast on quartz from a toluene solution, while the polymer concentration in both cases was 10 mg/ml. The blend was excited with a UV-LED peaking at 365 nm (3.40 eV). Photoexcitation creates highly localized Frenkel-type excitons within the polymer. If a polymer/PCBM interface resides within the exciton diffusion length, the offset of the LUMO levels between both materials allows to create a charge-transfer state, which can split into free charges. Quasi steady-state PIA allows to probe long-lived states such as polarons, which will give rise to an additional absorption feature indicated by a negative signal when the change of transmission $\Delta T/T$ is plotted versus the wavelength as shown in Figure 44. An absorption band is visible at around 700 nm (1.77 eV) that arises from the states present in the film. Singlet states

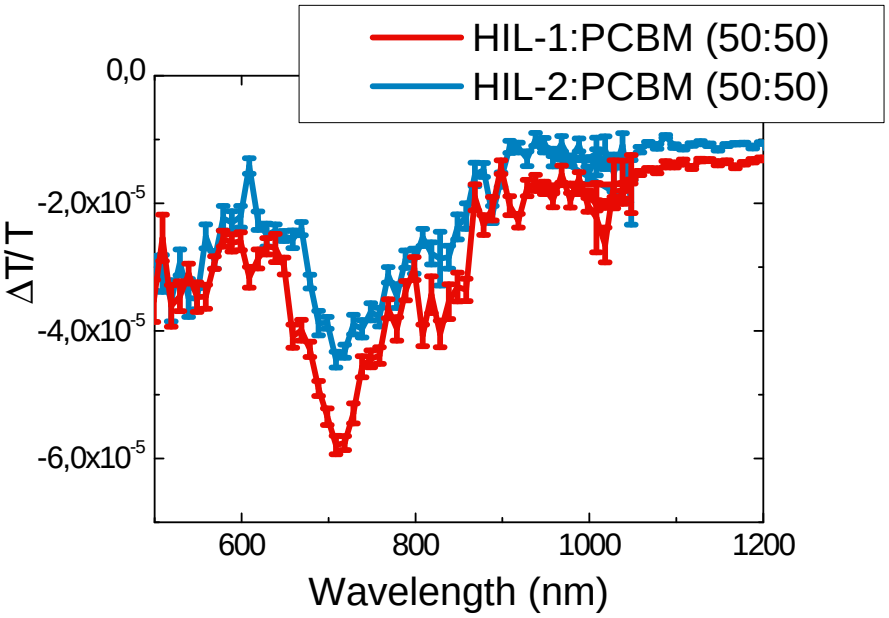

Figure 44: Photoinduced absorption spectrum of both hole injection layers mixed in a ratio 50:50 with PCBM.

and polarons absorb far apart from each other, which is one of the prerequisites for ASE in organic semiconductors. PIA studies show that interaction and thus reduction of gain is not expected by polarons. Since the polaron absorption of HIL-2 is separated to the singlet fluorescence of BLUE-1, it is unlikely that both species will interact. For any organic light emitting device, e.g. an OLED or an organic electrical injection laser, the spectral overlap has to be as small as possible [125]. For the device layout it is essential that excitons created by injected charges are separated from the electrodes before they recombine in the active medium. Excitons created close to an electrode can be quenched by the metal and finally will not contribute to light emission. Interlayers between the electrodes have proven to be beneficial to increase the quantum efficiency in such devices. Not only do they separate exciton creation from the electrode, but also they support hole or electron transport that increases the rate of exciton formation. Similarly to OLED devices, interlayers are essential to achieve an organic injection laser to finally support high excitonic densities, which then can lead to lasing if amplification overcomes the optical losses. Schols et al. for example realized an OLED with field-effect to transport electrons, separating the cathode from the light-emission zone by a distance of 1 µm. They were able to achieve current densities of up to

10 A/cm^2 with an EQE similar to conventional structures [142]. Wallikewitz et al. on the other hand realized ASE and lasing in an OLED structure when optically excited [127]. Crosslinking HIL-2 allows to spincoat BLUE-1 on top and investigate if ASE is supported in device like architectures similarly to Wallikewitz approach. Figure 45 illustrates the absorption and emission spectra in steady-state as well as the emission spectra recorded with different experimental setups.

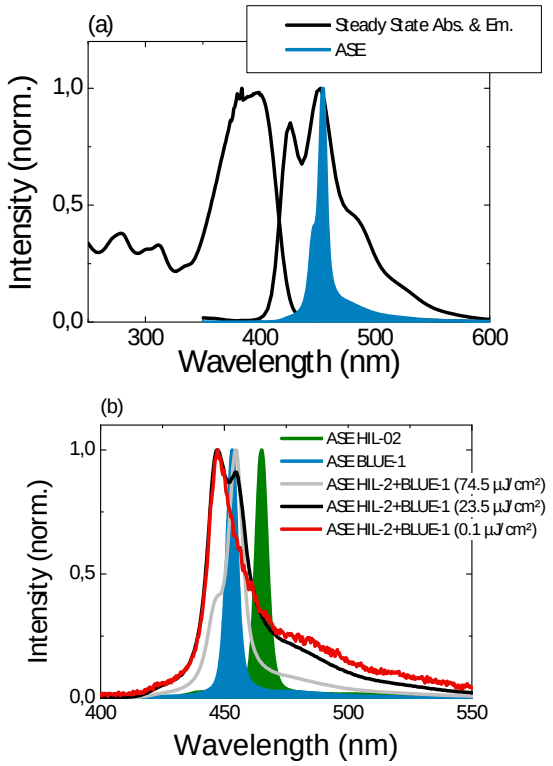

Figure 45: (a) Steady-state absorption and emission spectra of a bilayer of BLUE-1 and HIL-2. The filled curve corresponds to the ASE spectrum. (b) Comparison of ASE spectra between single layer structures of BLUE-1 and HIL-2 and as a bilayer.

Figure 45 (a) shows PL and ASE spectrum of the bilayer structure. The steady-state spectrum, recorded with a 3D TIDAS fiber spectrometer resembles the PL spectra of the top-layer when excited with 350 nm (3.54 eV). The low excitation power and the high absorption coefficient of BLUE-1 presumably do not allow the excitation light to penetrate into the deeper lying layer and therefore the PL might only be the emission spectrum of BLUE-1.

From the ASE experiments on the bilayer, illustrated in Figure 45, a complete collapse of the spectrum, which occurred in all the former experiments was not observed in the present case, even with the maximum pump energy that the SHG laser unit supplied. The ASE peak remained at the position of BLUE-1. However, different to the observation on BLUE-1 at low pump fluences, where optical losses are still suppressing ASE, the luminescence spectrum is simply one relatively broad peak different to the steady-state spectrum. As soon as the fluence is increased, a double peak structure can be seen with positions 8 nm apart from each other. The initial peak is further suppressed at higher pump energies, until ASE occurs at the 0-1 transition of BLUE-1.

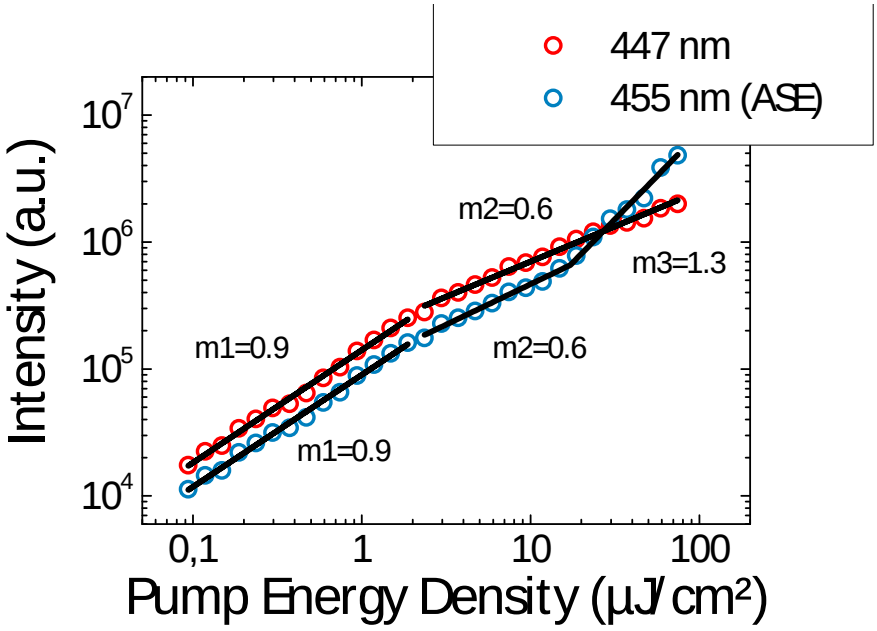

Figure 46: Determination of the ASE threshold at 455 nm (2.77 eV). The evolution of the ASE peak as well as the peak occurring at 447 nm was monitored.

Following the evolution of both peaks as a function of the pump energy density, only the peak appearing at 455 nm (3.1 eV) shows a superlinear increase with a power law dependence of $m_3 = 1.3$ as illustrated in Figure 46. Both peaks show an almost linear increase of the luminescence signal until a transition is visible at several $\mu J/cm^2$. The linear dependence drops and a power law dependence of $m = 0.6$ is obtained. Only the ASE peak follows a non-linear increase with a visible kink, from which the ASE threshold was evaluated, by determining the in-

tersection of both straight lines giving $E_{th} = (17.2 \pm 5.6)\mu J/cm^2$. The transition to a sublinear increase points to the onset of SSA at 2 $\mu J/cm^2$ indicated by the sublinear power-law behavior at low pump fluences and before the ASE threshold exciton densities are reached. Even in the presence of SSA, the bilayer can still exhibit ASE.

3.6 TRANSIENT ABSORPTION SPECTROSCOPY ON BLUE-1

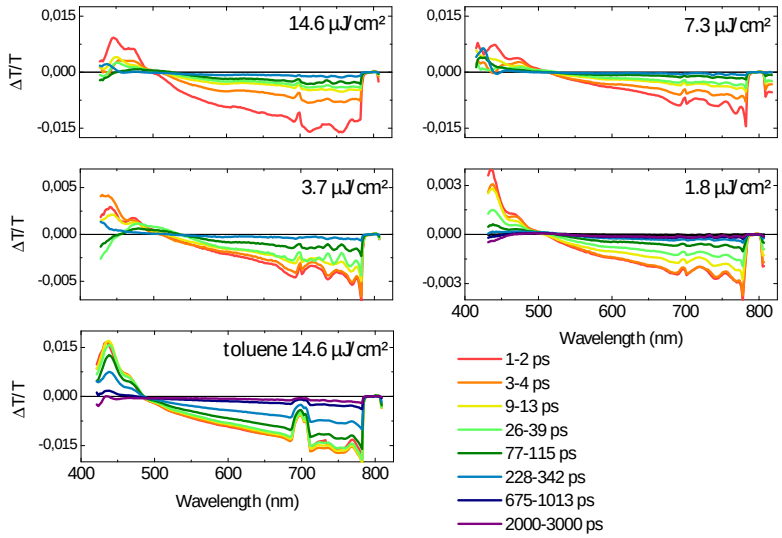

Figure 47: Transient absorption spectra of BLUE-1 as film and in toluene at different pump fluences.

The amplification of light is dependent on the stimulated emission cross section σ_{SE} of the material. Via pump-probe spectroscopy σ_{SE} can be accessed. Transient absorption (TA)-spectroscopy allows to trace excited state dynamics after photoexcitation. This is achieved by a pump pulse, which will change the level occupation if resonantly coupled to an electronic transition. The quantity of the measurement that will be determined by pump-probe spectroscopy is the change of the transmission of the probe, assuming an electronically dipole coupled transition from level $i \to j$ with $i > j$ [111]:

$$\frac{\Delta T}{T} = -\sum_{ij} \sigma_{ij}(\omega) \cdot \Delta N_j \cdot d.$$

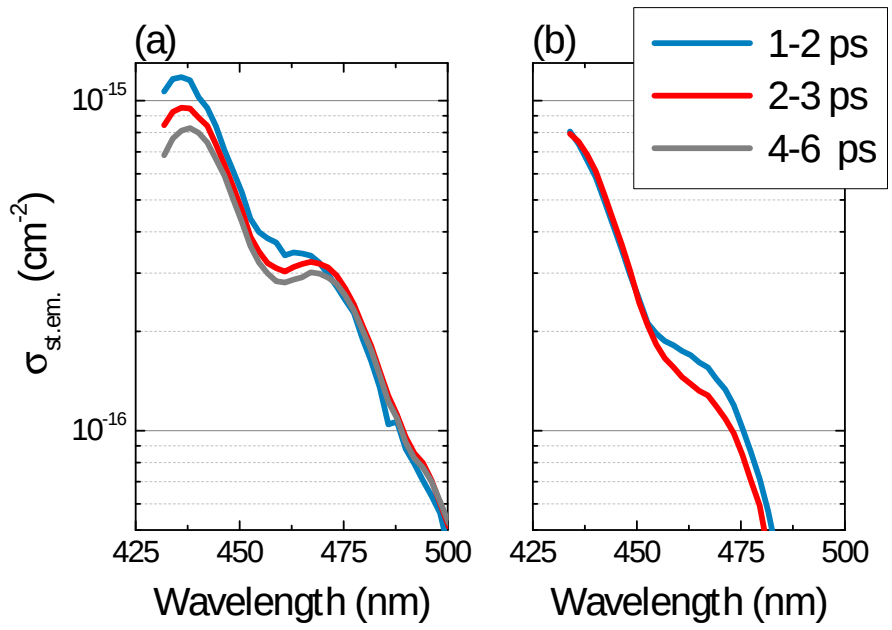

Figure 48: Stimulated emission cross sections of (a) BLUE-1 and (b) BLUE-2 determined by pump-probe spectroscopy.

$\sigma_{ij}(\omega)$ is the cross section (in cm^2) of the transition and contains the information of the dipole moment of the transition and the line shape. ΔN_j describes the change of level occupation and d is the sample thickness. As already mentioned in chapter 3.5, BLUE-1 achieved the highest gain value that so far has been reported as determined by the variable stripe length method with g=154 cm^{-1}. Figure 49 depicts the transient absorption spectrum of BLUE-1 in thin film at different delay times as well as in toluene, recorded at different pump fluences. For the determination of σ_{SE}, BLUE-1 was excited with a pump fluence of $E_P = 1.8 \mu J/cm^2$ to avoid ASE. A positive $\Delta T/T$ signal corresponds here to stimulated emission (SE), which resembles the steady-state PL spectrum. The negative $\Delta T/T$ signal is caused by PIA. Both regions are separated by an isosbestic point at around 510 nm (2.43 eV), whose position remains constant in time. This is typical for the presence of one major species in the excited polymer film [126]. The SE cross section can be determined from the following equation:

$$\sigma_{SE} = \frac{\Delta T/T}{N_{exc} \cdot d},$$

with N_{exc} being the volume density of the excited singlet states. σ_{SE} is found to be $1.2 \cdot 10^{-15} cm^2$. Typically, cross sections

of blue emitting polymers with ASE characteristics have been reported to be in the range of $1 \cdot 10^{-16} cm^2$ [143, 126, 144]. The optical gain can be calculated from the cross section according to $g=\sigma_{SE} \cdot N_{exc}$. The gain value obtained from transient absorption spectroscopy is found to be $g = 197 cm^{-1}$. Compared to the gain value determined by ASE measurements, this value is slightly higher. Apart from a high oscillator strength, a high chromophore density and luminescence efficiency, the absence of spectral overlap between SE and PIA is essential in order to achieve a high gain value [68]. An overlap between SE and PIA can be very detrimental for organic lasers and can completely suppress SE.

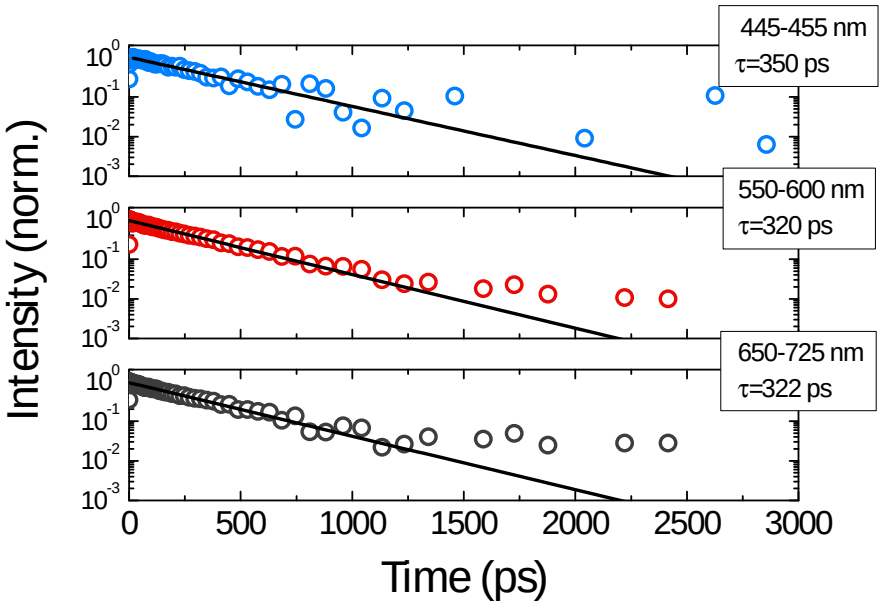

Figure 49: Dynamics of BLUE-1 in toluene obtained by TA-measurements and monitored at different wavelengths.

The PIA spectrum of BLUE-1 is broad and structureless, which is very typical for conjugated polymers. The excited state dynamics of BLUE-1 in film are illustrated in Figure 50. The dynamics of the PIA band in toluene are similar to the SE dynamics and have nearly the same time constants compared to the fluorescence lifetime measurements. Since the decay constants in the whole PIA spectrum do not differ from the SE kinetics, they are assigned to singlet S_1 excitons. In solid-state, the SE dynamics compared to the PIA band have again similar dynamics, but differ from the measured singlet S_1 exciton lifetime from

streak camera experiments. The fluorescence lifetimes are longer compared to the ones extracted from TA spectroscopy. It has been reported that SSA is dependent on the repetition rate of the excitation source and the laser pulse fluence [145]. Mode-locked laser systems with kHz repetition rates achieve higher photon densities, where even at photon densities of $3.5 \cdot 10^{12}$ photons/cm^2 (1.8 µJ/cm^2) SSA is not completely absent. Even at low pump fluence as 1.8 µJ/cm^2, ASE can occur and influence the decay kinetics. As the pump fluence is increased to 14.6 µJ/cm^2, the transients have multi-component dynamics, that cannot be fitted in a single-exponential fashion. ASE is dominantly present and depopulates most of the excited states in the first few ps. In the measurements recorded with 14.6µJ/cm^2, the presence of ASE can be seen by a large drop of $\Delta T/T$ in the first few ps.

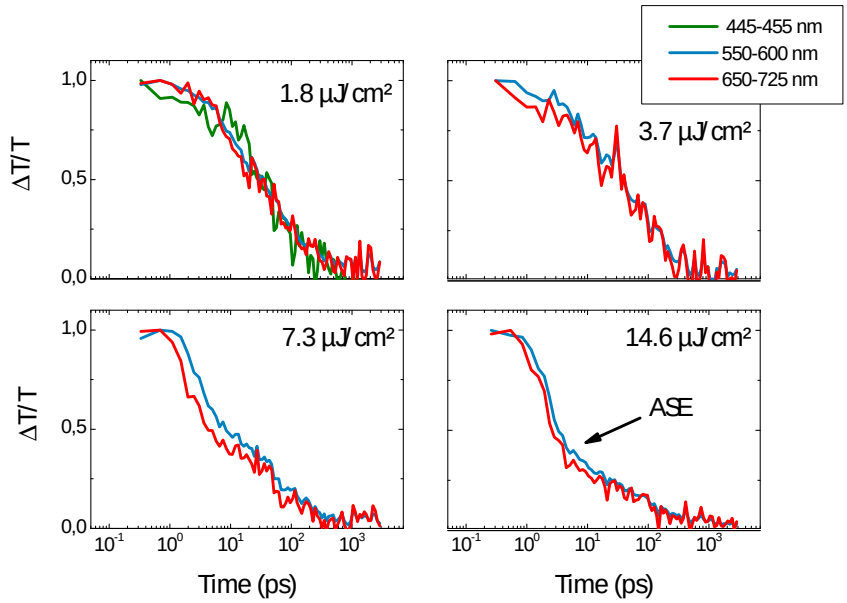

Figure 50: Kinetics probed at different wavelength regions in film and excited at different pump fluences.

Lanzani et al. have concluded that a close inter-chain packing can be disadvantageous to organic lasers since polaron pairs can be introduced as an additional species especially in the bulk. Yan et al. confirmed this by measurements of MEH-PPV dispersed in polystyrene, where the SE signal increased in blends and the PIA band assigned to polaron pairs vanished [146]. Typically, polaron pairs in conjugated polymers are reported to have a

distinct PIA band in the mid-visible region with a larger lifetime compared to the exciton lifetime. They stated that the key role in achieving a high gain is the control of morphology in organic semiconductors. As discussed in chapter 3.4.1, interchain packing plays a dominant role in the dynamics of BLUE-1 and BLUE-2. Polaron pairs are rather formed in solid state or poor solvents where aggregation allows interaction between conjugation segments packed adjacent to another [111]. There is no evidence that polaron pairs are generated in BLUE-1 as it was discussed in chapter 3.4.3. In addition, the kinetics of the TA spectroscopy do not reveal such a state and the dynamics can be only assigned to the singlet exciton. Figure 49 shows the kinetics of BLUE-1 in toluene at a concentration of 0.2 mg/ml. As the kinetics are probed further in the red, a deviation at later times from the single-exponential decay becomes more pronounced which is caused by triplet states that have their absorption peak at 820 nm (1.51 eV) as confirmed by PIA measurements and depicted in Figure 19 .

3.7 SUMMARY AND CONCLUSIONS OF CHAPTER 3

This chapter comprises the optical properties of polymers consisting of strictly alternating units of substituted indenofluorene and phenanthrene, namely BLUE-1 and BLUE-2, which only differ in the side chains attached to the backbone. TRPL spectroscopy showed that both polymers in solution behave similarly and their photoluminescence can be assigned to the singlet exciton emission. Transient spectra showed that the emission characteristics of BLUE-1 change at time delays of 4 ns and exhibit another emissive species. Measurements in solid-state were used to identify the second species and found to be rather a consequence of aggregation than the formation of geminate pairs or β-phase formation. The spectral dynamics of BLUE-2 in solid-state behave different, high pump powers transformed the spectrum and dynamics which can be assigned to the change of local packing by the low T_g. Furthermore phosphorescence and DF was detected, caused by radiative decay of triplet excitons or TTA, respectively. Next to the time-resolved spectroscopical investigations, ASE experiments on the polymers were performed with the variable stripe length medod. Thereby, BLUE-1 shows an outperforming gain parameter of g=154 cm^{-1}.

Using TA spectroscopy, the stimulated emission cross section was determined. It is commonly agreed that high gain in conjugated polymers can only be achieved by a high chromophore density with minimized intermolecular interaction. The second spectral component of BLUE-1 can be suppressed in solid-state by the addition of a high boiling point additive, which seems to prevent aggregation. This might lead to even higher gain values when spincast from solution with high boiling point additives.

4

DETERMINATION OF THE CHARGE CARRIER MOBILITY AND THE INFLUENCE OF HIGH MOBILITIES IN OPTOELECTRONIC DEVICES

4.1 INTRODUCTION

High charge carrier mobilities are desired for different optoelectronic applications. In organic field effect transistor (OFET)s high mobilities enable efficient current modulation and switching speeds [147]. Power conversion efficiencies in OSCs are also affected by the mobility. Low mobilities increase the dwell time in the device and therefore lower the extraction rate [148]. For the development of an organic laser diode, a high mobility in the emissive layer is essential for an effective transport of carriers to the recombination zone and for reaching singlet exciton densities that allow stimulated emission [149]. Engineering the charge transport properties of conjugated polymers is achieved by different approaches. It has been proven that short side chains attached to the polymer backbone can increase the mobility [150]. Also molecular weight dependence studies have shown, that high molecular weights lead to higher mobilities. By this approach hole mobilities in OFETs of 3.3 $cm^2/(Vs)$ were achieved by Tsao et al. [151]. They concluded that high molecular weights in donor-acceptor polymers have a higher tendency to crystalize and therefore elevate the intermolecular mobility, as well as the intramolecular transport along the polymer chain due to planarization of the backbone. Essentially, high charge carrier mobilities in disordered materials are achieved by increasing the transition rate of a carrier between two adjacent hopping sites as described by the Miller-Abraham equation. The overlap integral determines the transition rate. For organic semiconductors this is achieved by a closer spatial arrangement of the π-orbitals of adjacent chains. However, even amorphous polymers are able to achieve high mobilities of up to 0.01 $cm^2/(Vs)$, as determined by time-of-flight (TOF) [152, 35]. This chapter especially focuses on the charge carrier properties of BLUE-1 and its influence in optoelectronic applications. The devices were mainly prepared at the

Seoul National University with the assistance of Hyunkoo Lee and Donggu Lee from the department of electrical engineering under the guidance of Prof. Changhee Lee.

4.2 EXPERIMENTAL

4.2.1 *Time-of-flight technique*

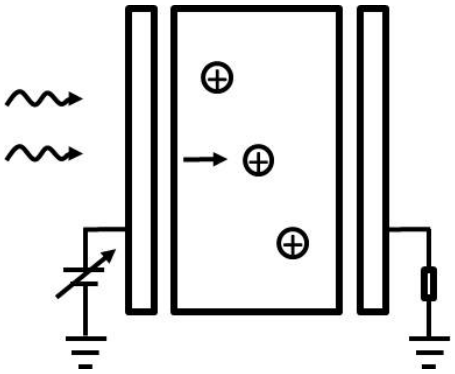

Figure 51: Device layout of time-of-flight experiment.

Films for TOF measurements were prepared by dropcasting the polymer from toluene solution (30 mg/ml) onto pre-cleaned ITO substrates. To better define the film thickness several layers of adhesive tape were put on each side of the ITO substrate. The polymer film was successively dried in a dry nitrogen glove box. The film thickness was determined to be $(17.5 \pm 0.5)\mu m$ by a Dektak profilometer. As counter electrode a 100 nm layer of aluminium was evaporated on top. Optical excitation was performed with the third harmonic of a nanosecond Nd:YAG (INDI Ray, Spectra Physics) laser system. The electrical signal was monitored with a TDS 524A Tektronix Oscilloscope.

4.2.2 *OLED preparation*

OLEDs were prepared on pre-patterned ITO substrates with a pixel area of 0.0196 cm^2. The substrates were cleaned by ultrasonification in different organic solvents for 10 minutes each in the following order: Isopropanol/deionized water/acetone/deionized water/methanol. Subsequently the substrates were treated with UV ozone for five minutes before the conduc-

tive polymer poly(3,4-ethylenedioxythiophene) poly(styrenesulfonate) (PEDOT:PSS) (Clevios P P VP Al 4083) was spincoated on top with a spinning speed of 4000 rpm for 30 s and annealed in a vacuum oven at a pressure of 10^{-3} mbar at 120 °C for 30 minutes. After annealing, active layers were spincast on top of PEDOT:PSS. Therefore the polymers were dissolved in toluene with a concentration of 10 mg/ml and deposited with a spinning speed of 2500 rpm for 120 s. The substrates were then transferred into a high vacuum evaporator, which allowed to deposit organic materials as well as metals by thermal evaporation without breaking the vacuum. Two different device layouts, with and without interlayer were chosen and their performance were compared. Device architectures of the OLEDs are sketched in Figure 52.

4.2.3 *OLED characterization*

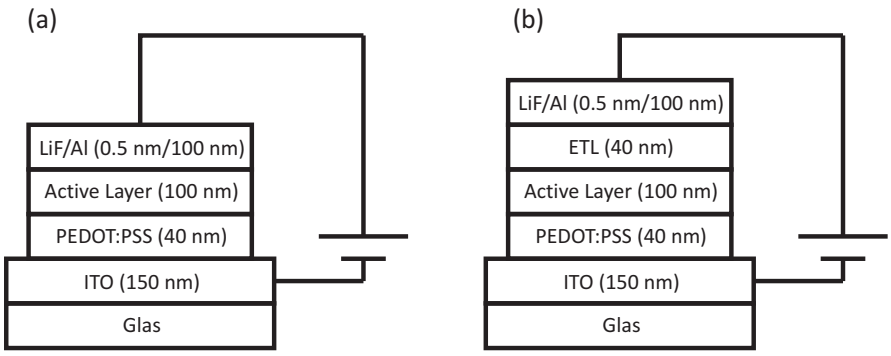

Figure 52: OLED device layouts.

Electroluminescence was characterized in a crystostate under a vacuum of 10^{-3} mbar. A calibrated photodiode with an active area of 1 cm^2 was attached to the cryostat and recorded the electroluminescence (EL). The current-voltage (IV) characteristics and light emission were simultaneously recorded. Devices were connected to a source-measure-unit (SMU), which monitored the current and the luminance as a function of the applied voltage. Electroluminescence spectra were taken with an electrospectrometer. OLED parameters were evaluated as described in chapter 2.6.

4.2.4 *Organic solar cell preparation and characterization*

Pre-patterned ITO substrates with a sheet resistance of 10 Ω/sq were cleaned in the same way as for OLED preparation. After UV ozone treatment for five minutes, PEDOT:PSS was spincast with a spinning speed of 4000 rpm for 30 s and annealed in a vacuum oven at 120 °C for 30 min. The substrates were taken out of the oven and were transferred into a N_2 glovebox where a blend solution of BLUE-1:PCBM from chlorobenzene was spincast on top with a spinning speed of 2000 rpm for 120 s. Thickness and mixing ratio were varied in order to find the optimal parameters. Substrates were then transferred into a high vacuum evaporator and lithium fluoride and aluminum were deposited with a thickness of 0.5 nm and 100 nm, respectively. The devices were transferred into a cryostat and IV characteristics were measured by a SMU, while illuminating the devices under a solar-simulator at AM 1.5 G. EQE spectra were measured by a home-built setup. The light of a halogen lamp was dispersed with a monochromator and the short circuit current J_{SC} was measured in dependence of the wavelength in order to determine the EQE spectrum.

4.3 DETERMINATION OF THE CHARGE CARRIER MOBILITY BY THE TIME-OF-FLIGHT TECHNIQUE

An important prerequisite for the application of conjugated polymers as active materials in organic lasers is a sufficiently high charge carrier mobility to allow fast injection of carriers into the organic material and successive transport of carriers to the recombination zone. Up to now only a few examples of materials that meet both, i.e. optical and electrical criteria, have been reported. Yap et al. have demonstrated excellent optical properties in combination with high charge mobilities in copolymers based on polyfluorene [35]. They demonstrated that tuning of the polymer composition and side chains attached to the backbone can lead to increased charge carrier mobilities, while preserving or even enhancing the gain properties. Indenofluorene copolymers can achieve similarly high charge carrier mobilities. The hole mobility of BLUE-1 was determined by the TOF technique frequently used to study charge transport in conjugated organic materials. For TOF experiments the material

is sandwiched between two electrodes, of which one electrode has to be semitransparent in order to photoexcite the material. A laser pulse of a few nanoseconds excites the active material in this device like structure (see Figure 51). Due to the applied bias excitons split into charges at the semitransparent-polymer interface and holes travel to the counter electrode. The mobility μ can be determined from the transit time t_{tr}, the applied electric field F and the thickness d of the polymer film.

$$\mu = \frac{d}{t_{tr} \cdot F}$$

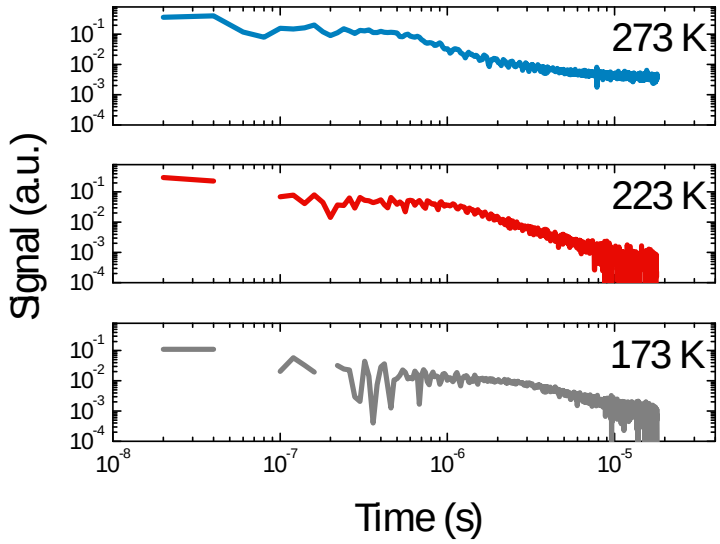

Figure 53: Time-of-flight transients of copolymer BLUE-1 at different temperatures and constant electric field. Note the gradually increasing transit time with lower temperature.

Figure 53 depicts TOF transients of a very thick film ($d \sim 17\mu m$) of BLUE-1 under constant electric field and constant excitation conditions but different sample temperature. The transients exhibit a plateau region followed by a current tail. The transit time of the fastest carriers was determined at the intersection of the tangents fitted to the plateau and the tail of the current transient in a double-logarithmic plot. For the highest temperature (273 K) shown in Figure 53 the transit time is close to 1 µs. Unfortunately, it was not possible to get meaningful transients at higher temperatures including room temperature (298 K), since the transit time approached the intrinsic RC time constant of the setup

and a clear plateau could not be resolved anymore. However, the hole mobility could be determined to 10^{-2} $cm^2V^{-1}s^{-1}$ at 273 K. Furthermore, the transit time gradually increases with lower temperature indicating a temperature-dependent hole mobility, while the field-dependence of the hole mobility was found to be very weak in the entire temperature range between 173 and 273 K. By plotting the extrapolated zero-field mobility versus $1/T^2$ in a semilogarithmic plot the energetic disorder σ corresponding to the width of the density of states can be evaluated within the framework of the Gaussian Disorder Model [153].

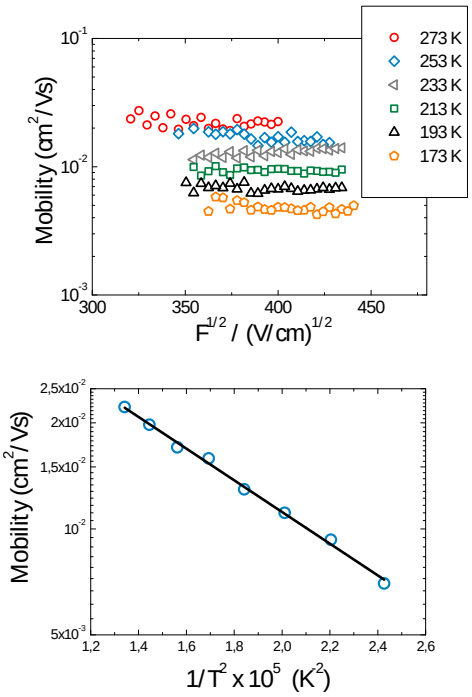

Figure 54: (a) Hole mobility versus $F^{1/2}$ parametric in temperature showing a virtually field-independent hole mobility exceeding 10^{-2} $cm^2/(Vs)$ at temperatures above 233 K. b) Mobility values plotted as a function of $1/T^2$ as typically done in the framework of the Gaussian disorder model. The energetic disorder σ can be obtained from a linear fit to the data.

For σ a comparably small value of only 42 meV was found, which indicates a rather narrow density of states and is in stark contrast to other blue-emitting conjugated polymers, where σ is typically around 100 meV as reported for poly(spirobifluorene), for instance [154]. The latter also exhibit the typical pronounced Poole-Frenkel type field-dependence of the hole mobility in

contrast to the indenofluorene-phenanthrene copolymers investigated this thesis. In fact, the hole mobility of $10^{-2} cm^2 V^{-1} s^{-1}$ is among the highest values observed by the time-of-flight technique for an amorphous blue-emitting conjugated polymer. Such high hole mobilities are typically obtained upon insertion of hole transporting comonomers such as triarylamine derivatives into the polymer backbone, since these facilitate hole transport by providing fast percolation pathways for charge carriers [155]. Furthermore, high mobilities and the absence of a pronounced field dependence have been observed in well-ordered materials, which allow for close interchain interaction with enhanced interchain charge transfer such as ladder-type conjugated polymers [156]. The high hole mobility of BLUE-1 and the absence of a field-dependence of the hole mobility indicate a rather efficient interchain charge carrier hopping, since no further hole transport units are present in the polymer that could promote charge transport. This, in combination with the rather narrow density of states for charge carriers and the absence of deep traps appear to be the main origin of the high hole mobility of BLUE-1. Yap et al. reported in their study on polyfluorene copolymers that careful tuning of the side chains and copolymer composition led to the formation of efficient transport paths, preferentially where polymer chains could come close enough together for efficient intercharge hopping [35]. Similar reasons may also account here as well for the high mobility. The indenofluorene comonomer can be considered a step-ladder-type oligophenylene, in which the phenylene units are forced into a planar structure due to the bridge-head carbon atoms. One may speculate that the planarized structure leads to enhance interchain interaction. This was demonstrated in previous time-resolved photoluminescence studies on poly(indenofluorene)s, which showed an aggregation-induced green emission, that was of different origin than the keto-defect emission often observed for blue-emitting polyfluorene materials [105] and is also clearly shown in chapter 3.4.2.

4.4 OLED CHARACTERIZATION OF DIFFERENT PIF-BASED COPOLYMERS

4.4.1 *Introduction*

The working principle of an OLED can be found in chapter 2.6. It generally relies on the thermionic emission and tunneling of charge carriers into the emissive layer and a subsequent bimolecular recombination of electrons and holes as described in the framework of Langevin recombination. Ideally, recombination creates a radiating exciton, which contributes to the light output. For this part three different active layers were studied in terms of electroluminescence and their corresponding efficiencies. The spectroscopic properties of BLUE-1 and BLUE-2 have been presented in chapter 3. Additionally another PIF based copolymer was characterized. Different to BLUE-1 and BLUE-2, the third polymer is a blend based on BLUE-2 with two different PIF based copolymers.

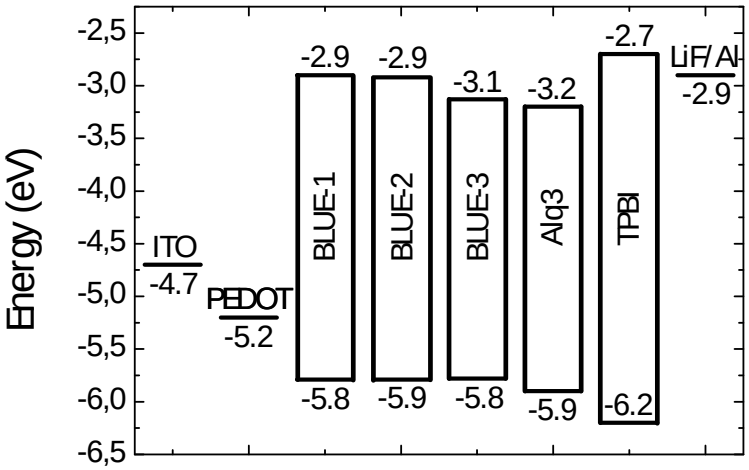

Figure 55: Energy level diagram of the materials used for OLED preparation.

The energy levels of the materials presented in this section are depicted in Figure 55. 1,3,5-tris(1-phenyl-1H-benzimidazol-2-yl)benzene (TPBI) with its HOMO and LUMO level at -6.20 eV and -2.70 eV respectively, was deployed due to its hole block-

ing and electron transport properties. In order to achieve high efficiencies, it was necessary to deploy an electron transport layer (ETL). With no interlayer incorporated, excitons created at the interface between cathode and polymer are quenched by the electrode and therefore they do not contribute to light emission. As cathode, a 0.5 nm thick layer of LiF and subsequently a layer of aluminum with a thickness of 100 nm was deposited by thermal evaporation.

4.4.2 *OLED characteristics of BLUE-1*

In the following the electroluminescent characteristics of BLUE-1 were studied. Figure 56 depicts some of the parameters that were evaluated. Three different layouts were chosen and fabricated. The device schemes are sketched in Figure 52. As reference, an OLED without an ETL was fabricated and compared to the diodes with ETLs. Aluminium-tris(8-hydroxychinolin) (Alq3) and TPBI served as electron injecting interlayers with a thickness of 40 nm. Without an ETL, there is no sufficient current flow observed and thus the reference device only achieved moderate device performance.

Alq3 with HOMO and LUMO levels of -5.9 eV and -3.2 eV was used in this study as an ETL. Apart from the purpose as transport layer it can also be deployed as emissive layers in electroluminescent devices. The electroluminescence spectrum in Figure 56 shows a peak at 530 nm (2.34 eV), characteristic for the emission of Alq3. Devices prepared with TPBI showed a higher EQE with 1.4 % compared to the Alq3 devices with 0.4 % at a current density of 1 mA/cm^2. Maximum EQE for Alq3 interlayers were achieved at high current densities, before the efficiency abruptly declined. The decrease of efficiency and brightness with increasing current densities is known as roll-off behavior. Roll-off is associated to two processes, to a charge imbalance within the emissive layer and an increase of nonradiative exciton quenching processes [79]. In singlet emitters SSA, singlet-polaron and field induced quenching increase with high current densities and are responsible for the roll-off. A more detailed analysis of the roll-off will be discussed later on. The mobility of TPBI and Alq3 are 10^{-5} cm^2/(Vs) and 10^{-6} cm^2/(Vs), respectively [83, 157]. The discrepancy of electron mobility compared to the

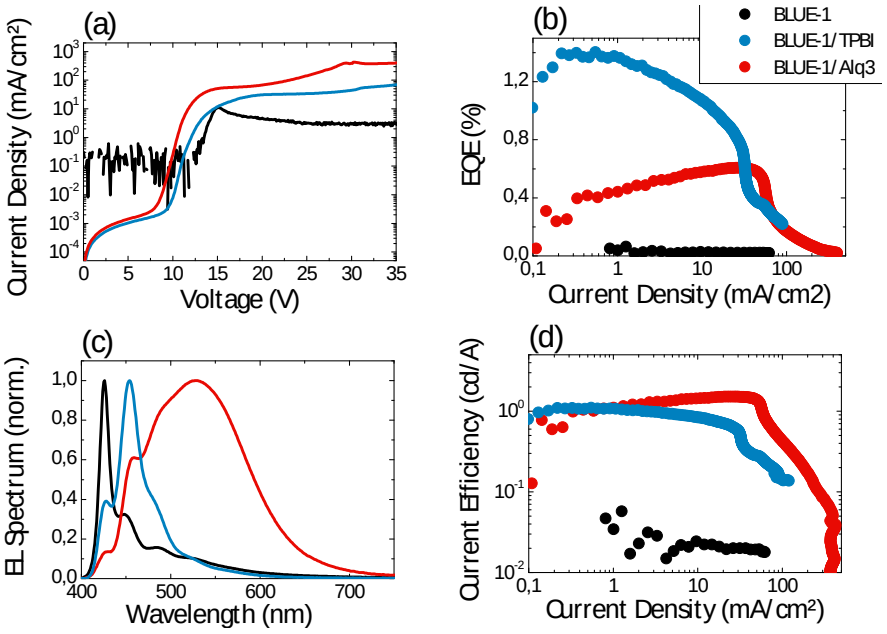

Figure 56: a) Current density, (b) EQE, (c) Luminance and (d) current efficiency of the fabricated devices. Comparison between different interlayers to a one without. The devices were fabricated with BLUE-1 as active layer.

hole mobility of BLUE-1 with 10^{-2} $cm^2/(Vs)$ causes that at high current densities space charges accumulate at the recombination zone, which at a certain threshold density quenches the light output. The rapid decrease of the EQE can also be recognized in the current-voltage characteristics, which appears as a deviation from the typical IV-curve. With Alq3 as interlayer, BLUE-1 is able to achieve higher current densities and has a lower turn-on voltage compared to the devices with TPBI.

The electroluminescence spectrum with different interlayers can be found in Figure 56 (c). The difference in the spectral appearance to the reference OLED can have manifold reasons. In the case of the TPBI interlayer, it is most likely effected by waveguiding. The additional layer can act similarly to a cavity, so that generated light experiences total reflections at the interfaces of the electrodes and organic layers. Also the mismatch in refractive index can enhance this effect. For Alq3 the low offset of the energy barriers allows to create excitons not only in the emissive layer, but also in the ETL. Therefore, the EL spectrum can be explained by a superposition of both materials. Apart from the spectral characteristics of BLUE-1, a broad and struc-

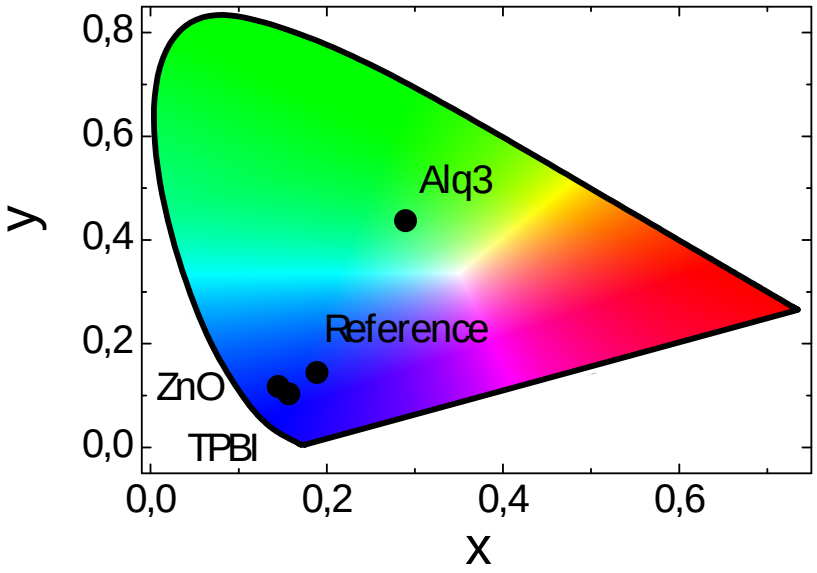

Figure 57: Color perception of BLUE-1 present on the CIE 1931 color space

tureless emission centered at about 530 nm (2.34 eV) can be seen. The HOMO offset of about 0.1 eV between BLUE-1 and Alq3 allows excitons also to recombine in the Alq3 layer. Figure 57 depicts the color perception of the human eye illustrated on the commission internationale de l'éclairage (CIE) 1931 color space and illustrates the color appearance of the different devices prepared from BLUE-1.

Apart from OLEDs of the above shown device architectures, inverted structures were also built and characterized. The bias was applied with reversed polarity, so that electrons were injected from the ITO electrode and holes from the aluminum side. Therefore different interlayers needed to be incorporated to overcome the injection barriers. On top of the ITO, a layer of zinc oxide (ZnO) nanoparticles was spincoated at a spinning speed of 2000 rpm for 60 s from a stabilized colloidal solution of n-butanol with two different concentrations of 5 mg/ml and 20 mg/ml. The thicknesses were found to be 25 nm and 45 nm for the concentrations of 5 mg/ml and 20 mg/ml respectively. Subsequently, the spincast layer was dried in a nitrogen filled oven at a temperature of 90 °C for one hour. The nanoparticles were prepared as described by Pacholski et al. [158] by Insun Park from the Department of Chemistry of Seoul National

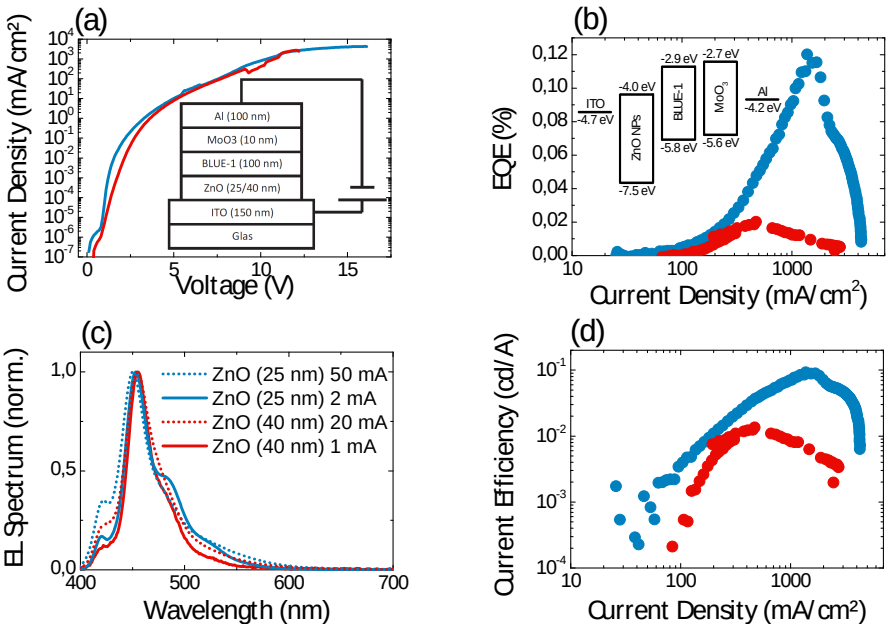

Figure 58: (a) Current density, (b) EQE, (c) Luminance and (d) current efficiency of the fabricated devices. As active layer polymer BLUE-1 was deployed with an inverted device architecture.

University. After spincasting BLUE-1, a layer of MoO_3 with a thickness of 10 nm and 100 nm aluminium were deposited by thermal evaporation. Transparency, low work function and the possibility to solution-process ZnO which has electron mobilities of over 1 $cm^2/(Vs)$ [159], makes it very suitable for optoelectronic devices. The energy level diagram, device layout and performance of the inverted OLED can be found in Figure 58. The ZnO layer with a thickness of 25 nm showed a better overall performance. The turn-on voltage was in comparison to the devices with TPBI as in interlayer, for both ZnO layer thicknesses at about 1 V, which is one order of magnitude lower to the TPBI interlayers and allowed to achieve high current densities of up to 4000 mA/cm^2. The maximum EQE was found to be at 0.12 % at a current density of 1381 mA/cm^2. A comparison of all characterized devices can be found in table 3. The emission spectrum did not differ to the devices prepared with TPBI as verified from the CIE color map in Figure 57. The high electron mobility and the low injection barriers, allow to drive the OLED with high current densities. The EQE increases with higher currents and behaves differently to the devices fabricated with TPBI interlayers, where the maximum EQE was already achieved at low currents and showed roll-off at higher current densities. The

gradual increase of the EQE with higher current densities and the better IV characteristics can be ascribed to a better charge carrier balance at higher currents. Furthermore, with higher currents, the recombination zone supposedly moved into the emission layer and away from ZnO, which leads to less quenching. However the lower EQE compared to the TPBI interlayer is a consequence of exciton-electrode quenching at the interface between ZnO and the organic layer. Further device engineering moving the recombination zone away from the electrode is a promising approach for higher quantum efficiencies at high current densities.

4.4.3 *OLED characteristics of BLUE-2*

Similarly, BLUE-2 devices were prepared from toluene and characterized as described above. As observed for BLUE-1, the OLED characteristics with an interlayer of TPBI are improved. BLUE-2 has a turn-on voltage at about 4.5 V and achieves a maximum EQE of about 1 %, which is in comparison to BLUE-1 about 0.4 % lower.

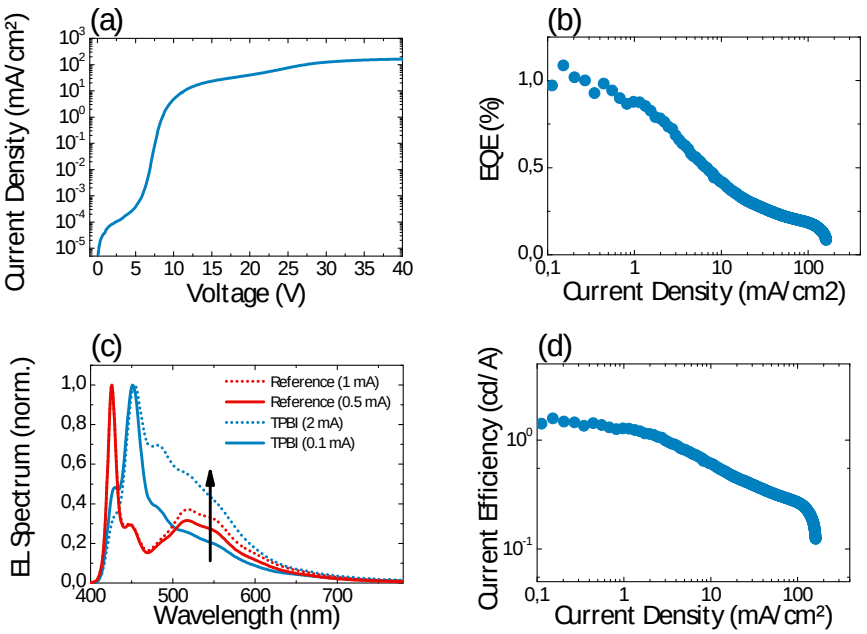

Figure 59: (a) Current density, (b) EQE, (c) Luminance and (d) current efficiency of the fabricated devices. As active layer polymer BLUE-2 was deployed.

The EL spectrum can be found in Figure 59 (c) which compares the spectral characteristics at different currents for OLEDs with and without TPBI interlayers. The spectrum of the reference diode has the same vibronic 0-0 and 0-1 progressions. Apart from the emission of the singlet exciton, BLUE-2 shows an additional broad emission band 530 nm (2.34 eV). The origin of the second emission component has already been discussed in the optical spectroscopy section in chapter 3 and is referred to oxidative defects within the polymer backbone. The spectrum suggests, that without thermal and optical stress of the materials, BLUE-2 already has structural defects. The spectroscopic studies do not show these defect sites without stressing, even though they might already be present in pristine films. When samples are electrically excited, the emission of light relies on the bimolecular recombination of electrons and holes. Emission of singlet excitons occurs from recombination of free charges, whereas green emission originates from recombination of a trapped polaron at the fluorenone position. Charge carrier transport in disordered materials is described by a hopping process within the framework of the Gaussian Disorder Model. If a charge carrier occupies a fluorenone site and if the energy offset of this site is too high, the trapped polaron cannot evade from this position and will radiatively decay by recombination with an electron. Studies on keto-defects in polyfluorenes have shown that defect sites act as traps for electrons as well as for holes [160]. From their studies, they were able to determine the trap concentration and concluded that even small amounts of trapping sites will influence the intrinsic blue emission in electroluminescent devices, even though the defect emission does not show up in the PL spectrum. Kuik et al. observed, that with higher current densities the green emission decreased relative to the blue emission. They explained their findings by assuming that the green emission feature is occurring from a fixed concentration of trap sites. Generally, higher current densities will increase the light emission since more excitons will radiatively recombine. Since the amount of traps is fixed, the amount of recombination sites is limited. The keto emission in their experiments at polyfluorenes had therefore a smaller contribution to the overall light output when higher currents were applied. Since BLUE-2 behaves differently, the amount of trap sites seems to have increased when going to higher current

regimes. Keto-defects do not only affect the optical properties in OLEDs, but also change the charge transport characteristics in conjugated polymers. In the same work mentioned before, they found that hole and electron transport in fluorenone is trap limited with an exponential trap distribution, whereas in pristine materials it is space-charge limited.

4.4.4 *Multilayer OLEDs- the impact of hole injection layers*

ETLs in OLEDs are essential in order to achieve high effiencies as discussed in the previous chapters and to prevent exciton quenching at the electrodes. OLED performance in general benefits from interlayers. Hole-injection layers for instance facilitate hole-transport into the emissive layer and lower the injection barrier at the anode. It has been shown that hole injection layers (HIL) not only support better charge carrier transport, but also increase the lifetime of an OLED [77]. Polymer based OLEDs have on the one hand the advantage of solution-processing, on the other hand they are impractical for multilayer devices. One possibility to overcome this obstacle is to process different layers from orthogonal solvents, presuming the materials are soluble in the given solvent. Thin film deposition from a dispersion of polymer nanoparticles and H_2O is another promising concept for multilayer processing [161]. However, this concept still lacks surface energy control at the interface as well as good film forming properties. Another method is to introduce groups such as oxetane into the polymer backbone that allow photochemical crosslinking and create insoluble polymer networks, which enables mulitlayer processing [162].

In this work, a crosslinkable hole injection layer (HIL) was used which can be crosslinked by heating to 180 °C for one hour in an inert atmosphere. The optical properties of HIL-2 are described in chapter 3.5.4. Films were prepared from toluene with a concentration of 5 mg/ml and spincoated with a spinning speed of 2000 rpm for 60 s. The thickness of HIL-2 was found to be at around 55 nm. Three different emissive layers were prepared and characterized regarding their optoelectronic properties. The device performance of a bi-layer comprising the emissive layer and an ETL of TPBI were compared to a tri-layer, where the emissive layer was sandwiched in between HIL-2

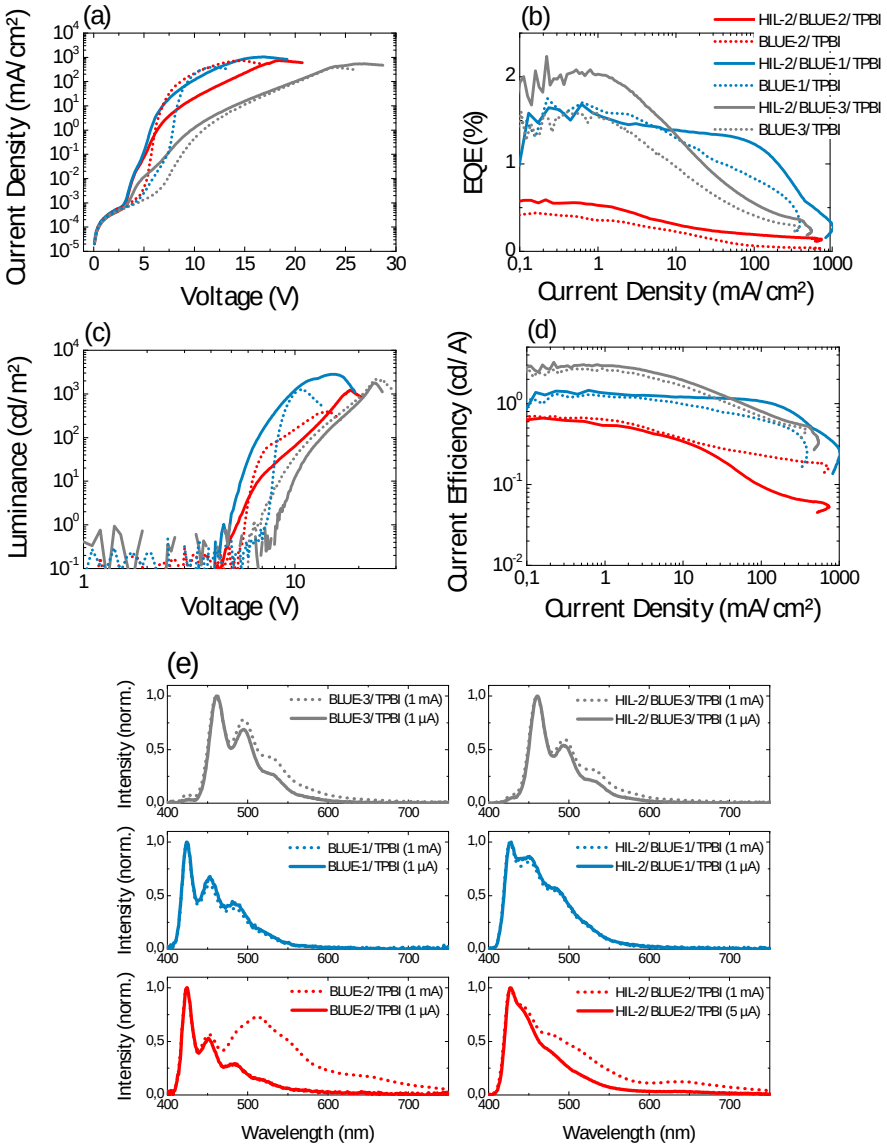

Figure 60: (a) Current density, (b) EQE, (c) Luminance and (d) current efficiency of the fabricated devices. Comparing BLUE-1, BLUE-2 and BLUE-3, respectively with and without HIL. Figure (e) is comparing the electroluminescence spectra.

after crosslinking and TPBI. The measurements and the device layout are summarized in Figure 60. The bi-layer devices of BLUE-1 and BLUE-2 when compared to the previous measured bi-layer devices resemble one another in respect to their opto-electronic performance and reproducibility of the experiments. The tri-layer diodes show that the device performance can be even enhanced compared to the previously characterized diodes. Turn-on voltages for all devices were found to be about 3.0 V. The EQE of the tri-layers increased or in the case of BLUE-1 are at least unchanged compared to the bi-layer devices. For all devices roll-off occurs at higher current densities, which indicates that HIL-2 regulates the balance of electron and hole in OLEDs.

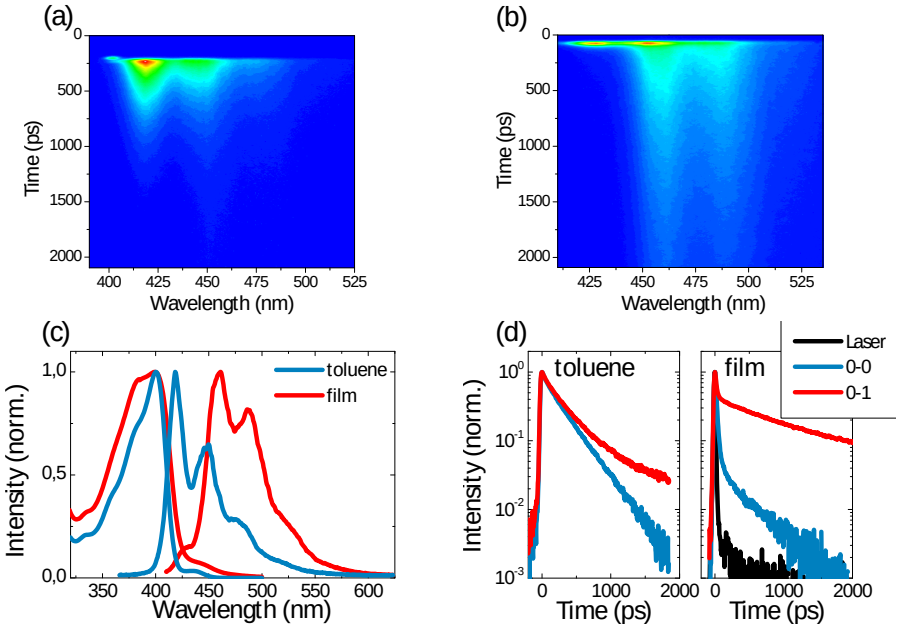

Figure 61: Photophysical properties of BLUE-3. (a) Streak camera image of BLUE-3 in toluene and on (b) film. (c) Absorption and fluorescence spectrum and (d) decay transients of 0-0 and 0-1 transition.

Apart from testing BLUE-1 and BLUE-2, a polymer blend, namely BLUE-3 was characterized. BLUE-3 consists of BLUE-2 and two different other PIF-copolymers, which were mixed in a defined ratio before processing. The concept behind the material's composition is to utilize FRET for color tuning and different hole transport units for better charge transport. Figure 61 illustrates the photophysical properties of BLUE-3 in toluene as well as in solid-state. Solid-state fluorescence shows, that the spec-

trum is strongly red-shifted in comparison to the measurements in solution. The streak camera images reveal that FRET is occurring when going from solution to solid-state. The lifetime of the donor polymer, which is dominantly emitting when measured in a dilute solution, is strongly quenched towards another emissive species. The acceptor polymer, which was invisible in the fluorescence spectrum in solution, experiences in return an increase of its lifetime in film. Intermolecular interaction enhances FRET to the acceptor polymer in the solid-state. Here, FRET is useful to create efficient electroluminescent devices. Figure 60 shows not only the performance of the previously described polymers, but also the optoelectronic properties of the blend. It has similar EQEs to BLUE-1, when both are prepared as bi-layers consisting of the emissive polymer and TPBI. When HIL-2 is additionally incorporated, the EQE is even increased up to 2 %. The emission spectrum for BLUE-1 and BLUE-2 is influenced by HIL-2 and vibronic progressions are blurred, whereas BLUE-3 is not affected by the HIL. The spectrum shows that the 0-0 transition is almost suppressed and energy transfer occurs very effectively also when electrically driven, which exemplifies an effective concept to enhance efficiencies in fluorescent OLEDs and to tune the color appearance. Surprisingly, the PLQE of BLUE-3 was found to be 17 % and is compared to BLUE-1 with 55 % and BLUE-2 with 66 % by far the lowest value, which does not correlate with the electroluminescent properties. In summary, BLUE-3 outperforms both copolymers in their quantum and current efficiencies in OLEDs. It illustrates that HILs can enhance device properties and shift the roll-off to higher current densities by balancing charge recombination.

material	specifics	EQE_{max} (%)	$L_{max}(cd/m^2)$	CE_{max} (cd/A)	$V_{turn\ on}$ (V)
BLUE-1	reference	0.06 @ 1 mA/cm^2	11 @ 15.1 V	0.05 @ 1.3 mA/cm^2	12.0
BLUE-1	Alq3	0.60 @ 37 mA/cm^2	693 @ 15.1 V	1.09 @ 0.2 mA/cm^2	7.8
BLUE-1	TPBI	1.39 @ 1 mA/cm^2	1178 @ 10.3 V	1.51 @ 28 mA/cm^2	9.1
BLUE-1	ZnO/inverted	0.12 @ 1381 mA/cm^2	1497 @ 11.2 V	0.09 @ 1381 mA/cm^2	0.8
BLUE-1	TPBI/HIL-2	1.71 @ 0.6 mA/cm^2	2805 @ 15.3 V	1.43 @ 0.23 mA/cm^2	2.9
BLUE-2	reference	0.06 @ 1.0 mA/cm^2	13 @ 23.3 V	1.00 @ 1.90 mA/cm^2	4.2
BLUE-2	TPBI	0.44 @ 0.2 mA/cm^2	391 @ 13.9 V	0.71 @ 0.22 mA/cm^2	4.5
BLUE-2	TPBI/HIL-2	0.60 @ 0.2 mA/cm^2	1220 @ 18.2 V	0.66 @ 0.16 mA/cm^2	3.0
BLUE-3	TPBI	1.60 @ 0.4 mA/cm^2	2150 @ 24.1 V	2.66 @ 0.20 mA/cm^2	6.4
BLUE-3	TPBI/HIL-2	2.08 @ 0.8 mA/cm^2	1773 @ 23.9 V	3.25 @ 0.22 mA/cm^2	3.2

Table 3: OLED characteristics. The table summarizes the OLED performance of BLUE-1, BLUE-2 and BLUE-3.

4.5 CONSEQUENCES OF RESULTS ON BLUE-1 FOR FUTURE LASING DIODES

For future organic lasing diodes, high charge carrier moblities are required, since stimulated emission can only be achieved at high exciton densities. Numerical studies on different organic semiconductors have shown that the minimum current densities are at least in the order of 200 A/cm^2 to accomplish exciton densities that would trigger ASE in a diode. However, at higher exciton densities, also bimolecular processes are further enhanced that can quench the light emission. At high currents, exciton quenching assigned to SSA, singlet-triplet annihilation (STA) and singlet-polaron annihilation (SPA) can occur. SPA is believed to be the major deactivation in fluorescent OLEDs at high current densities [85]. It is commonly agreed that SPA is caused at the interface of two different organic layers, where space charges accumulate at higher current densities due to the energy offset between both materials. The photophysical as well the optoelectronic experiments that were carried out, allow to make some estimations about BLUE-1 regarding its application in an electrically driven laser. The exciton density n_{ASE} that is required to reach the ASE threshold density E_{th}, when optically excited was calculated with the following equation:

$$n_{ASE} = E_{th} \cdot \frac{\lambda_p}{hc},$$

where λ_p is the wavelength of the pump laser. In this calculation λ_{ASE}=400 nm is used. The areal exciton density was found to be n_{ASE}=9.05$\cdot$ 10^{12} cm^{-2}. The same areal density in an electrically driven device, with taking into account that only a fraction of 25 % of all generated excitons are singlet states, translates into a current density in the order of J=39.3 $\cdot$ 10^3 A/cm^2. The exciton density for an electrically driven device was determined by [163, 10]:

$$n_{exciton} = \frac{1}{4} \cdot \frac{J}{e} \cdot \eta_{PL} \cdot \tau_{PL},$$

for the PLQE η_{PL}=0.55 and for the PL lifetime τ_{PL}=268 ps was used. The given calculation however sets only the lower limit for an electrically pumped device, since input parameters were extracted from a single slab waveguide and no bimolecular losses were additionally taken into account. When calculations are

carried out for a bi-layer of HIL-2 and BLUE-1, where the ASE threshold was found to be E_{th}=17.2 µJ/cm^2, the areal threshold exciton density corresponds to n_{ASE}=3.46 · 10^{13} cm^{-2} and the current density was found to be 150 · 10^3 A/cm^2. Such high current densities if at all can only be supplied by a pulsed source to prevent heating at the electrodes and a breakdown of the device. The regime of high densities will further introduce different exciton quenching processes as mentioned in the beginning with SPA as the major deactivation process. Therefore to prevent a high quenching rate by this type of interaction, high mobilities are a prerequisite which will additionally reduce the accumulation of space charges within the organic layer. SSA is another process that is expected to quench singlet emission. In the optical experiments that were carried out, the onset of SSA was found to be at about 10 µJ/cm^2 which occurs above the ASE threshold and therefore is expected to be of minor relevance. Additional loss processes that are expected to take place when going to an electrically driven device is exciton-electrode quenching. On the one hand they will enhance waveguide losses and suppress the ability of spectral collapse. On the other hand, the waveguide mode will shift closer to the electrode and with that ASE is less likely to occur. Therefore the incorporation of HIL-2 could be a promising approach for achieving ASE by introducing a distance to the electrode.

Figure 62 depicts the exciton density n_{ASE} that is required to achieve ASE when optically excited and the calculated current density in order to reach the same exciton densities in an electrically driven device. Apart from the given assumptions, the exciton densities of the previously characterized devices of BLUE-1 were determined and plotted in the same graph. From the calculations, one can see that there is still a gap between the exciton densities in OLEDs and the densities that can be achieved by optical excitation. Typically, with cavities such as distributed feedback gratings, the stimulated emission threshold can be lowered. Still, the corrugation of the active layer will lead to an inhomogeneous electric field distribution and with higher fields, a breakdown of the device will occur. Previous experiments have shown that OLEDs can achieve an EQE of about 2 % at current densities of 100 A/cm^2 with a pulsed source [164]. For the prospect of an electrically pumped laser, further

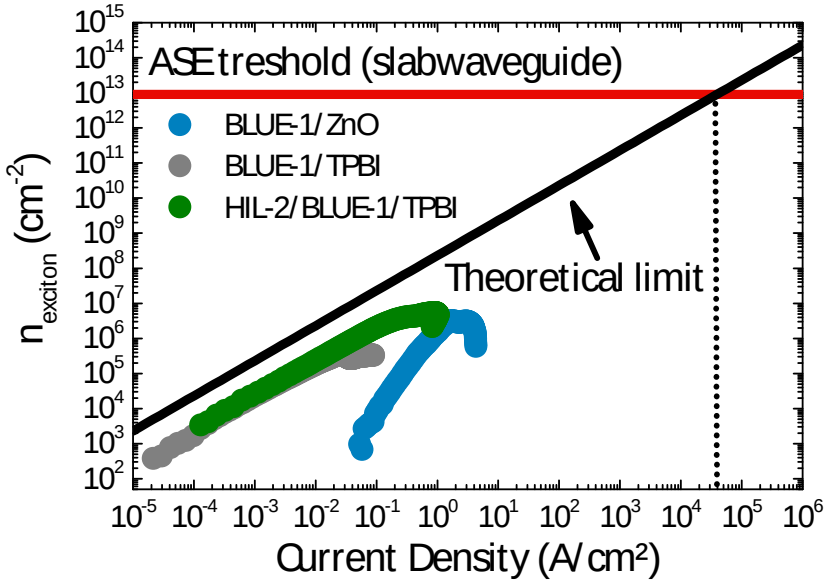

Figure 62: Estimation of exciton densities that are required to reach the ASE treshold in an electrically driven device. The red line presents the exciton density obtained from ASE experiments. The black line shows the theoretical limit of an electrical device, that an electroluminescent device prepared from BLUE-1 can achieve. The exciton densities of the prepared devices from BLUE-1 are illustrated as dots.

approaches regarding material design for lowering the treshold and increasing the gain as well device engineering need to be carried out.

4.6 EXCITON DISSOCIATION IN A WIDE BANDGAP POLYMER - IMPLICATIONS FOR ORGANIC SOLAR CELL PERFORMANCE

4.6.1 *Introduction*

For high power conversion efficiencies in OSCs, excitons created by photoexcitation, need to be efficiently dissociated at a donor-acceptor interface before charges can be extracted at the electrodes. As already mentioned in chapter 4.1, one loss mechanism in OSCs is non-geminate recombination at the donor-acceptor interface [148]. In order to overcome this obstacle high mobilities are required, which allow to increase the rate of charge extraction and by that remove the charges from the recombination zone. Conjugated polymers with absorption in the blue

region have due to their wide band gap only little overlap with the solar spectrum and therefore are not promising for OSCs. However, the high mobility of BLUE-1 makes it ideal to study the impact of mobility on exciton dissociation and on the efficiency of an polymer:fullerene blend organic solar cells. Optical spectroscopic studies were undertaken and OSCs from BLUE-1 were built and characterized. As acceptor material PCBM was chosen. The high electron affinity as well as its isotropic charge transport properties caused by the geometry of the molecule makes PCBM ideal for OSCs.

4.6.2 *Optical properties of BLUE-1 blended with PCBM*

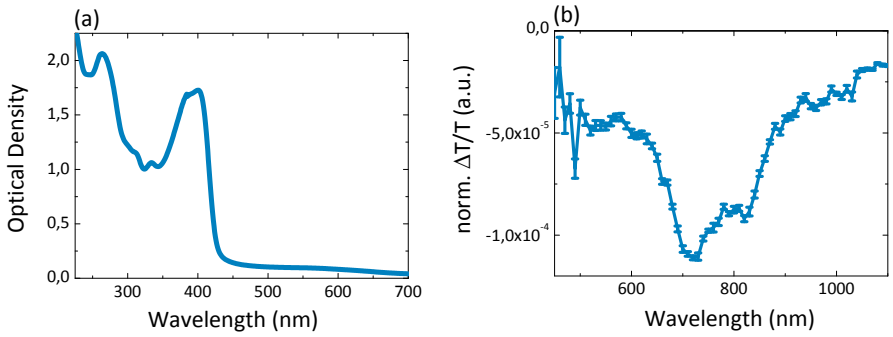

Figure 63: (a) Absorption spectra and photoinduced absorption spectra of a BLUE-1:PCBM blend.

The *steady-state absorption* as well as the *quasi steady-state* PIA spectrum of a BLUE-1:PCBM blend, mixed at a weight ratio of 50:50 at a polymer concentration of 10 mg/ml are shown in Figure 63. The film thickness was found to be about 250 nm. The absorption spectrum shows a superposition of both components. The absorption is mainly originating from the polymer with a broad and featureless absorption band at 400 nm (3.1 eV). PCBM absorbs in the UV region with a peak at around 264 nm (4.70 eV), which also can be seen in the UV/VIS spectrum. Furthermore the small tail beyond 450 nm (2.76 eV) arises from PCBM as well. The quasi steady-state PIA spectrum of the blend shows a broad absorption band peaked at 720 nm (1.72 eV), which did not appear in the PIA spectrum of the pristine polymer depicted in Figure 19. As quasi steady-state PIA allows to probe long-lived species, the absorption feature is most probably from dissociated excitons, i.e. polarons. The energy offset between the LUMO

levels is about 0.8 eV. Exciton binding energies in organic semiconductors are typically in the order of 0.5 eV. Consequently, when the energy offset at the heterojunction is greater than the binding energy, charge separation can be achieved [165]. If the band-edge offset is smaller, charge-transfer (CT)-states are stabilized at the interface. Apart from the broad emission band assigned to the polaron absorption, another feature seems to be present in the film that already was detected in the pure material and was assigned to long-lived triplet excitons.

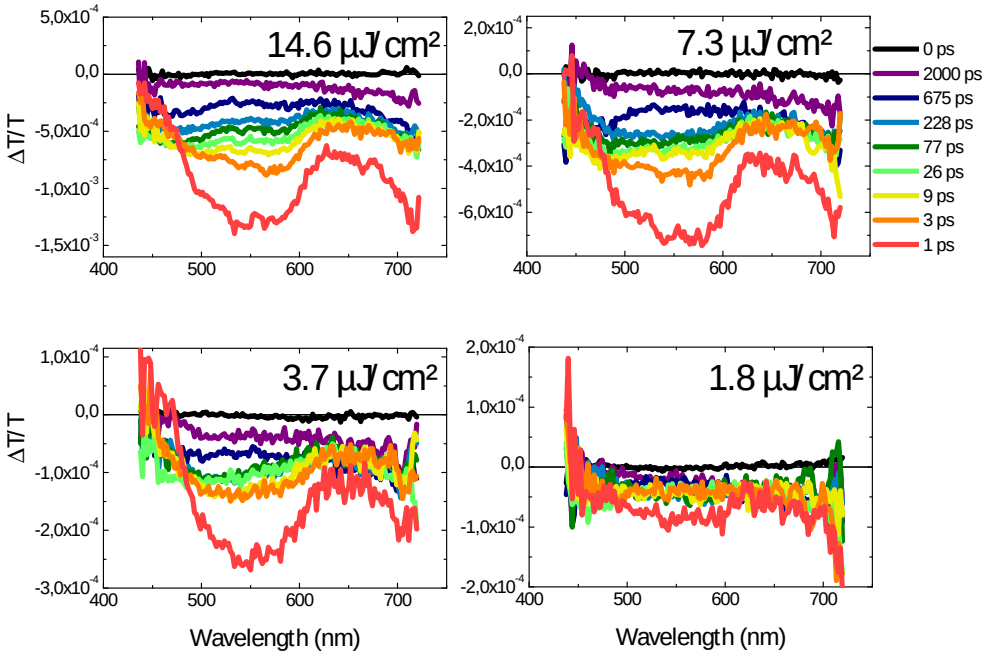

Figure 64: Transient absorption spectrum of BLUE-1 at different pump fluences.

TA spectroscopy allows to get deeper insights into exciton and charge dynamics. The transient spectra as well as the dynamics of the blend are depicted in Figure 64. The evolution of the spectra and the kinetics reveal that two different processes are taking place regardless of the spectral position probed. One occurring on an ultrafast timescale and the other one that can be traced up to several nanoseconds. Stimulated emission occurs in the first picoseconds at 450 nm (2.76 eV), depicted by a positive ΔT/T signal that disappears and rapidly transforms into a PIA. Stimulated emission in this spectral region is caused by the radiative decay of singlet excitons, most likely from polymer domains in

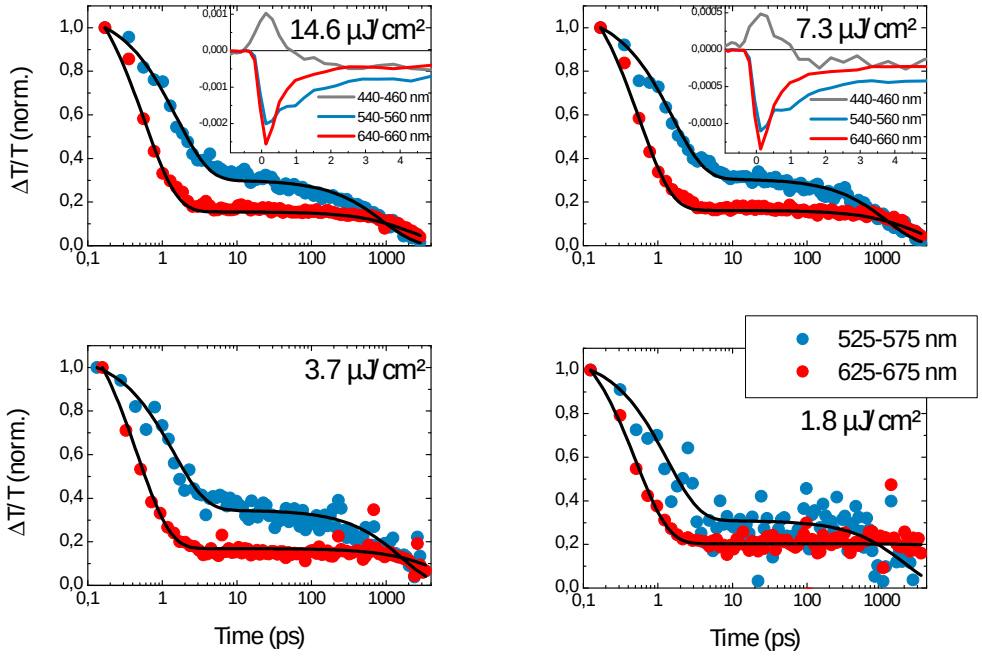

Figure 65: Transient absorption kinetics of BLUE-1 recorded at different pump fluences.

which singlet excitons have to diffuse before they can undergo separation. Following the transients at 450 nm (2.76 eV) and 550 nm (2.25 eV) very similar kinetics are observed, and both can be assigned to the kinetics of the singlet excitons. When probing the spectral region at 650 nm (1.91 eV), the transients behave differently to the singlet exciton. All transients were fitted with a bi-exponential function for different pump fluences. The decay constants and their corresponding amplitudes of the fits can be found in table 4. The short lifetime components were found to be τ_1=1.6 ps and τ_2=0.6 ps for the spectral regions of 550 nm (2.25 eV) and 650 nm (2.25 eV) respectively. τ_1 is not pump fluence dependent, whereas τ_2 increases with lower excitation intensities.

Extension of the spectral range of the supercontinuum probe beam, allowed to further analyze the spectral characteristics of the blend. Two different bands are present after photoexcitation. The band below 600 nm (2.07 eV) is getting more pronounced with higher fluences, whereas the second feature at 760 nm (1.63 eV) is independent on the pump fluence. The spectrum transforms from one with two absorption bands into a spectrum

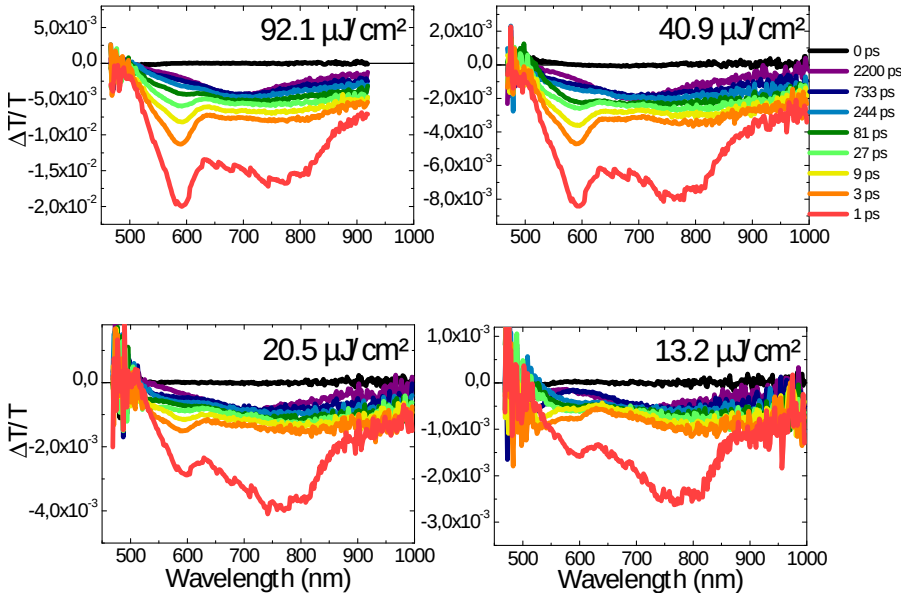

Figure 66: Transient absorption spectrum of BLUE-1:PCBM blend in dependence of the pump fluence.

with one broad absorption feature centered at 700 nm (1.77 eV), which remains at this position throughout the entire time range of the experiment. The long-lived species occurring at 700 nm (1.77 eV) coincides with the absorption band recorded with quasi steady-state PIA in Figure 63 and allows to assign the transformation of the long-lived component to polarons. The fractional change in transmission $\Delta T/T$ was measured in dependence of the pump fluence and allowed to determine the

E_p ($\mu J/cm^2$)	λ_{probe} (nm)	A1	τ_1 (ps)	A2	τ_2 (ps)
14.6	525-575	0.70	1.6	0.30	915.9
14.6	625-675	0.84	0.6	0.16	2319.8
7.3	525-575	0.70	1.5	0.30	1195.3
7.3	625-675	0.84	0.6	0.16	3189.7
3.7	525-575	0.65	1.4	0.35	1616.8
3.7	625-675	0.83	0.5	0.17	5707.9
1.8	525-575	0.69	1.3	0.31	2025.7
1.8	625-675	0.80	0.5	-	-

Table 4: Summary of the kinetics of BLUE-1:PCBM blend.

absorption cross section of the long-lived species as can be found in Figure 67.

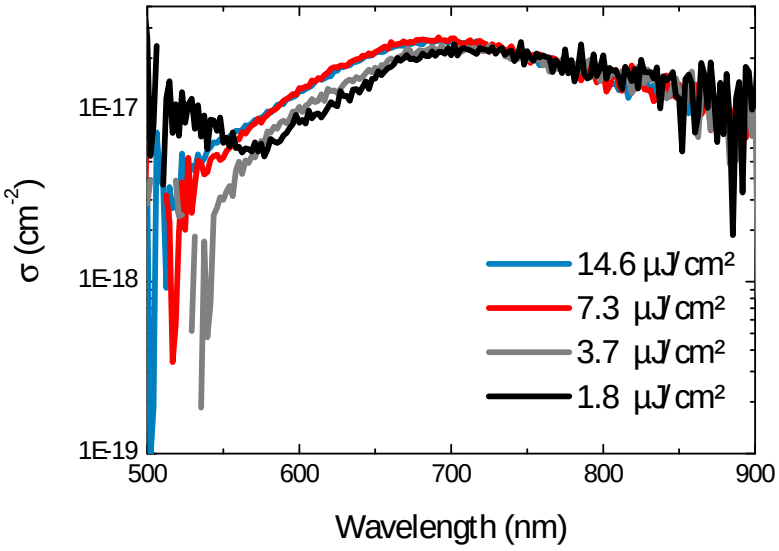

Figure 67: Cross section of the polaron absorption band. The spectra were recorded at a time delay of 2.2 ns.

The calculations were carried out for spectra taken at a time delay 2.2 ns. The cross section is found to be two order of magnitudes lower than the stimulated emission cross section σ_{SE} and interference and quenching by injection of charges upon interaction should be low for an electroluminescent device, especially when high current densities are applied, where the rate of interaction is expected to increase.

4.6.3 *Solar cell performance of BLUE-1:PCBM blends*

The working principle of an organic cell relies on efficient charge generation and charge extraction at the electrodes. In order to achieve efficient solar cell performance, photogenerated excitons need to be successively separated at the hetero-interface. The previously shown spectroscopic experiments on blends of BLUE-1:PCBM showed efficient exciton dissociation. Furthermore high charge carrier mobility is another prerequisite. However the energy bandgap of BLUE-1 does not allow to get high power conversion efficiencies due to the insufficient absorption of sun-

light by the polymer.

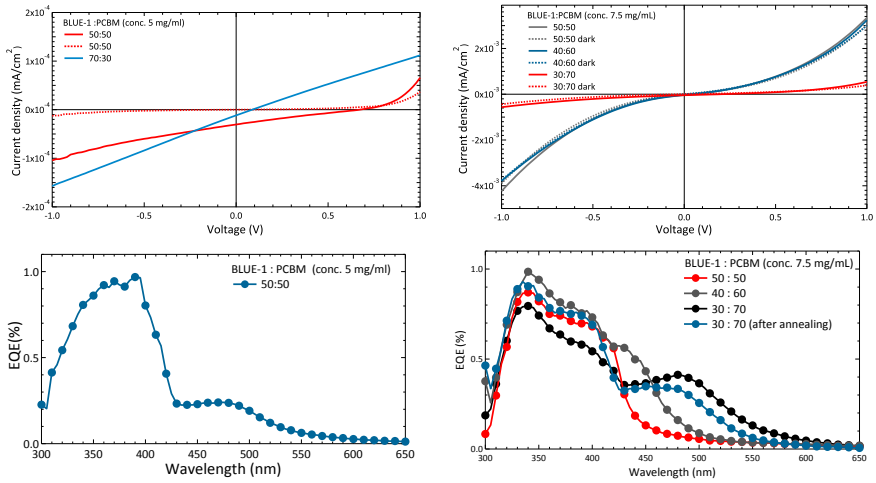

Figure 68: IV and EQE characteristics of organic solar cells using BLUE-1:PCBM blends.

BLUE-1 and PCBM were dissolved in chlorobenzene with different concentrations and different ratios of donor and acceptor material. The polymer concentration was kept constant at 5 mg/ml and 7.5 mg/ml. The IV-curves of both device batches as well their EQE are depicted in Figure 68. The low power conversion efficiency and the low EQE are assigned to different processes occurring in the material. TA spectroscopy on the blend has shown that excitons undergo charge transfer at the interface. Short circuit current J_{SC}, open circuit voltage V_{OC}, fill-factor (FF) and power conversion efficiency (PCE) are depicted in table 5.

c (mg/ml)	ratio	J_{SC} (mA/cm^2)	V_{OC} (V)	FF (%)	PCE (%)
7.5	50:50	0.0244	0.032	23	0.0002
7.5	40:60	0.0352	0.045	25	0.0004
7.5	30:70	0.0435	0.199	26	0.0022
5	50:50	0.0305	0.671	22	0.0046
5	30:70	0.0117	0.087	25	0.0003

Table 5: Solar cell performance of BLUE-1:PCBM.

Low FF and PCE, show that photogenerated charges are not efficiently extracted. High mobility on the one hand is a prerequisite for charge extraction, however non-geminate recombination, which represents another loss channel, is directly affected by the mobility and the rate increases with higher mobilities and charge densities. Furthermore high polaron densities decrease the internal field of the bulk material and with that increases the rate of bimolecular recombination [148]. The difference of charge carrier mobility between the active layer and PCBM exhibits another loss mechanism. Recently it was shown, that the right choice of electrodes is of importance, since open circuit voltage is decreased by injection barriers or by a very high mobility itself, which lowers the built-in field and a higher difusitivity increases difussion losses [166].

4.7 SUMMARY AND CONCLUSIONS OF CHAPTER 4

This chapter deals with the optoelectronic properties of BLUE-1 and BLUE-2. The charge carrier mobility of BLUE-1 was determined to be in the order of $\mu = 1.0 \cdot 10^{-2} cm^2/(Vs)$. The impact of high mobility was successively analyzed in optoelectronic devices. High mobility is one prerequisite in order to achieve lasing in the prospect of an electrically pumped laser. However, optoelectronic applications generally suffer from the imbalance of hole mobility and electron mobility such as in OLEDs and OSCs. In order to increase the efficiency of the photoemissive layer in OLEDs by deploying a material with a high charge carrier mobility, high efficiencies are only achieved by the incorporation of interlayers preventing quenching losses from the electrodes. It is further suggested that the interlayers need to have similar mobilities along with a low injection barrier. This will prevent the built-up of charges at the interface and the accumulation of space charges.

The spectroscopic experiments when blending BLUE-1 with PCBM showed that excitons are efficiently separated at the heterophase. However, the lack of efficient charge extraction is most likely caused by the imbalance of charge carriers between the donor and acceptor material. In addition, the choice of electrodes with low injection barriers is as important. A high injection barrier will cause an insufficient charge extraction and

thereby increase the polaron density upon charge separation. High polaron densities however, increase the rate of bimolecular recombination.

5

CONCLUSIONS AND OUTLOOK

This work aims to establish the relation between structure and function of conjugated polymers in the prospect of organic lasing. The task of this thesis was to identify and study materials that combine advanced optical properties such as high PLQE with excellent electrical properties, for instance. Two indenofluorene-phenanthrene copolymers, namely BLUE-1 and BLUE-2 were investigated. BLUE-1 showed promising optical as well as optoelectronic characteristics with a low ASE threshold of 4.5 $\mu J/cm^2$, a high optical gain of 154 cm^{-1} and a high charge carrier mobility in the order of $1 \cdot 10^{-2}$ $cm^2/(Vs)$. Until a few years ago, it was commonly agreed that such properties combined in one material are mutually excluded. Thus, a scientific challenge of this thesis was to understand how high gain and high mobility in conjugated polymers can be achieved. In addition to the determination of ASE characteristics and charge carrier mobility, excited states dynamics were investigated and the influence of charge carrier mobility on different optoelectronic applications was analyzed.

Throughout this work it was shown, that BLUE-1 and BLUE-2 differ in their photophysical as well as optoelectronic properties, although steady-state absorption and PL did not show significant differences between the two materials. Differential scanning calorimetry (DSC) measurements revealed glass transition temperatures T_g for BLUE-2 at 71 °C and a T_g for BLUE-1 at 287 °C, showing that the side chains influence the T_g significantly. The low T_g of BLUE-2 leads to morphological changes at high pump fluences causing parasitic emission from aggregates. BLUE-1 exhibited a second spectral component appearing and dominating the emission spectrum at time delays of 4 ns after excitation. This spectral component emerged slightly red-shifted to the 0-1 transition and with a different decay constant compared to the singlet exciton lifetime, unlike for BLUE-2 where such an emission was not observed. Upon the addition of a high boiling point additive to the solution used for spincoating, the feature could

be completely suppressed. The TRPL transients changed from a double-exponential to a single-exponential transient. The additive also influenced the steady-state absorption and emission spectra indicating a higher morphological order. The thorough characterization of both materials in the scope of this thesis, led to the conclusion that the second component is caused by aggregates in bulk. Time-resolved ASE experiments showed that the aggregates were not detrimental to the intensity dependent line-narrowing process. The results suggest that the additive suppresses aggregation, which is not only preferred towards higher ASE gain parameters, but also for the achievement of higher mobilities, since a higher degree of planarization typically leads to a faster transport along the polymer chain. In addition to the unprecedented gain values that BLUE-1 achieved, it has a high charge carrier mobility despite the absence of high order or crystallinity. Furthermore, the analyzation of the mobility in OLEDs and OSCs suggests, that organic optoelectronic devices can benefit from high mobilities. However, in OLEDs, high mobilities in the active layer can only improve the efficiency when electron and hole mobilities are balanced. This will prevent a built-up of charge carriers at the interface and lead to efficient light generation. First approaches with ZnO as ETL showed that high current densities can be achieved with the right choice of interlayers. High charge carrier mobilities of the photo-active layer in OSCs on the one hand lead to efficient charge separation and enhance charge extraction, on the other hand high charge carrier densities increase bimolecular recombination in a device. High mobilities can only increase solar cell performance, when charge extraction at the electrodes is efficient. Therefore, the right choice of electrodes with a low injection barrier is even more important when mobilities are very high.

A comparison to other state-of-the-art high gain ASE material, reveal that the materials in the scope of this thesis show unprecented gain values along with a low ASE threshold and low optical losses. However, the inability to demonstrate electrically pumped lasing in an organic driven device is generally a consequence of the low mobility in organic semiconductors. In this context, increasing the mobility without altering the PLQE is the ultimate challenge. A higher mobility allows higher current densities to be reached and reduces the built-up of space charges.

In conjugated polymers this can be achieved by increasing the molecular weight or varying the side chains attached to the polymer backbone, whereas smaller side chains typically show higher mobilities [150]. Alkyl side-chains on the indenofluorene backbone have shown higher tendencies of structural defects which harms the photostability. Therefore, it is suggested to substitute the alkyl side chains with chains of a higher steric demand. Para aryl-tert-butyl substitution for instance has shown a high degree of optical and thermal stabilities as in the case of BLUE-1. Electrical operation of an organic gain medium has to work not only at the limit of their luminescence and current density properties, but requires a high degree of thermal and optical stability. Therefore any form of secondary emission feature or quenching process occuring from aggregation or structural defects is malicious. In this context, BLUE-1 has already shown preferential optical properties, offering a high gain. For further improvements, it is suggested to substitute the linear alkyl chains at the indenofluorene backbone with side chains offering a higher stability against oxidation.

A further step towards an electrically driven device is the thorough understanding of the gain medium. The organic molecules have to withstand high current densities. Lowering the treshold of stimulated emission is achieved by low optical losses with the support of an efficient optical feedback. Optical gain is a consequence of chromophore density and thus related to the morphology. Theoretical studies should address the limit of the cross section of absorption and stimulated emission that can be reached along with the prefrential alignment of the molecules. Additionally the limits of charge transport should be studied that organic materials can supply. Future design of gain materials could benefit from the aforementioned studies.

For the realization of an organic laser that is purely electrically driven, further improvements are needed. The material BLUE-1 sets the direction towards high gain and high mobilities in conjugated polymers.

APPENDIX A

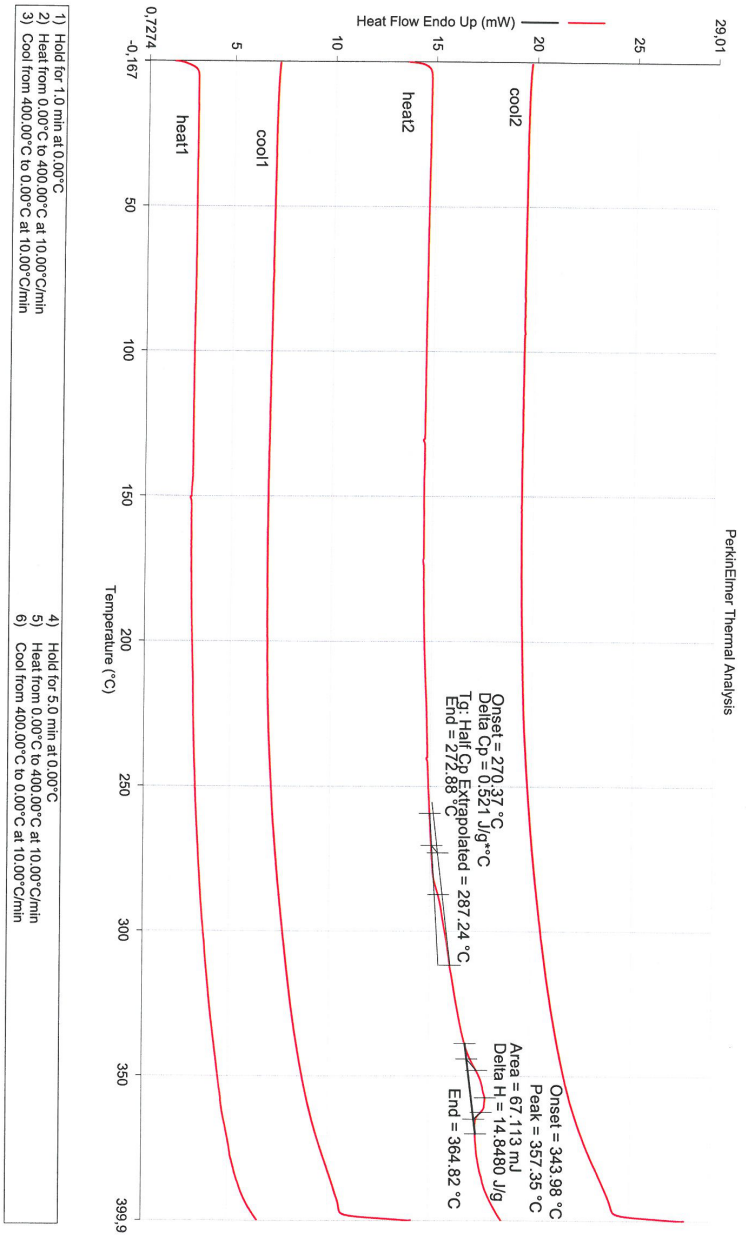

Figure 69: DSC measurements on BLUE-1.

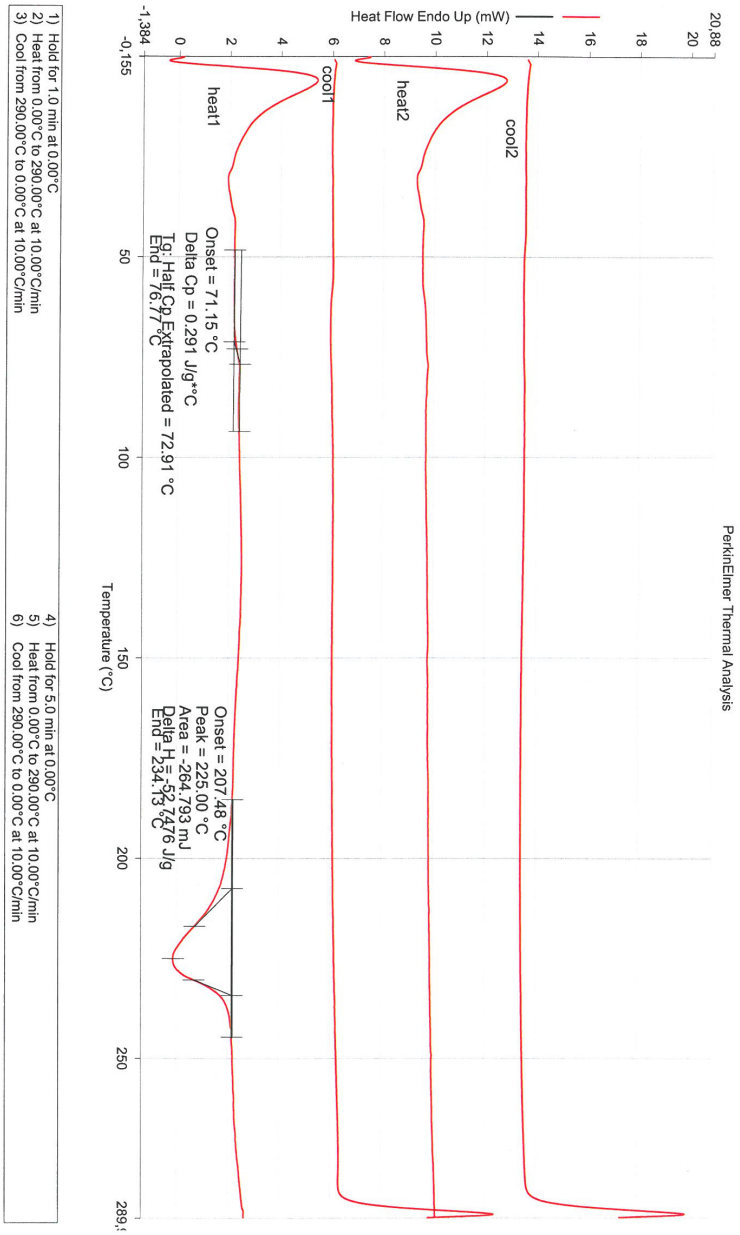

Figure 70: DSC measurements on BLUE-2.

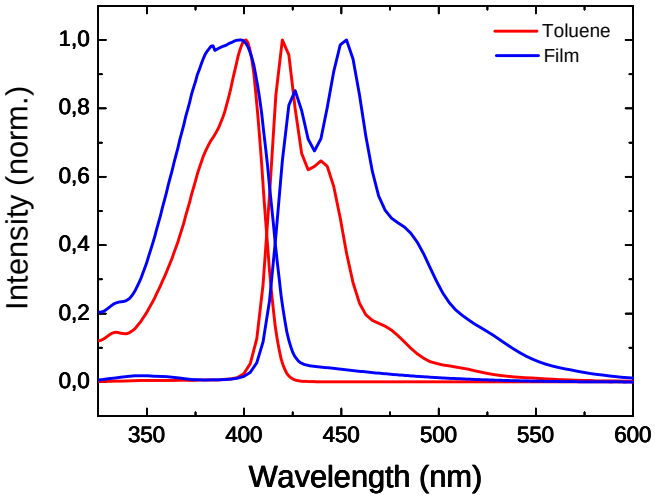

Figure 71: Comparison of absorption and emission spectra of BLUE-1 in toluene at a concentration of 0.1 mg/ml and in thin film.

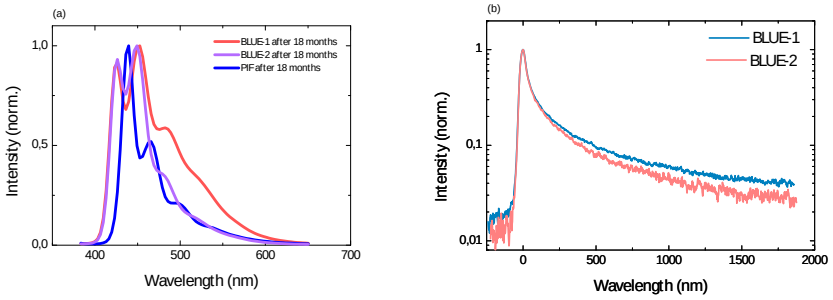

Figure 72: Figure (a) depicts the fluorescence spectrum of the different indenofluorene polymers stored under ambient conditions for 18 months. In Figure (b) decay transients of BLUE-1 and BLUE-2 are depicted that were stressed with UV light and stored under ambient conditions for 2 months prior to the measurements.

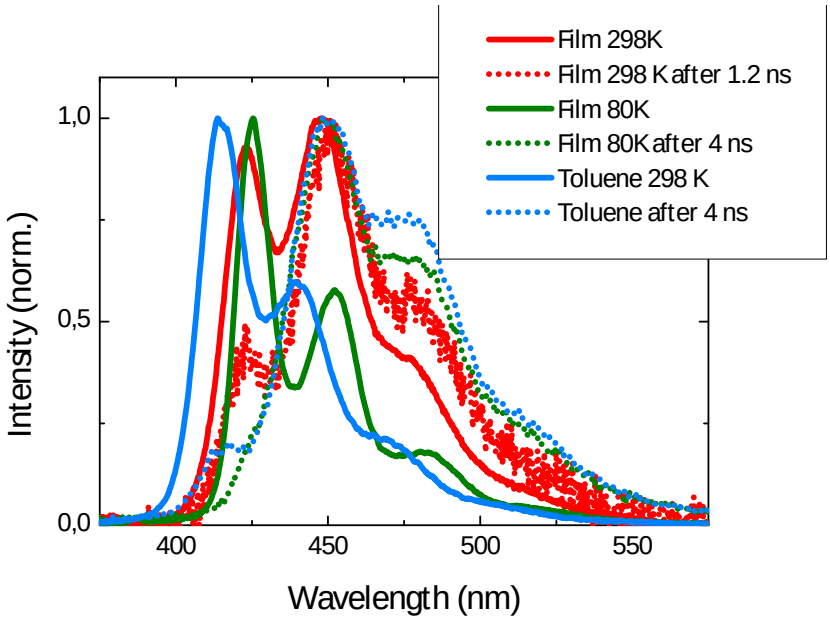

Figure 73: Transient photoluminescence spectra of BLUE-1 in toluene and in film at room temperature and 77 K.

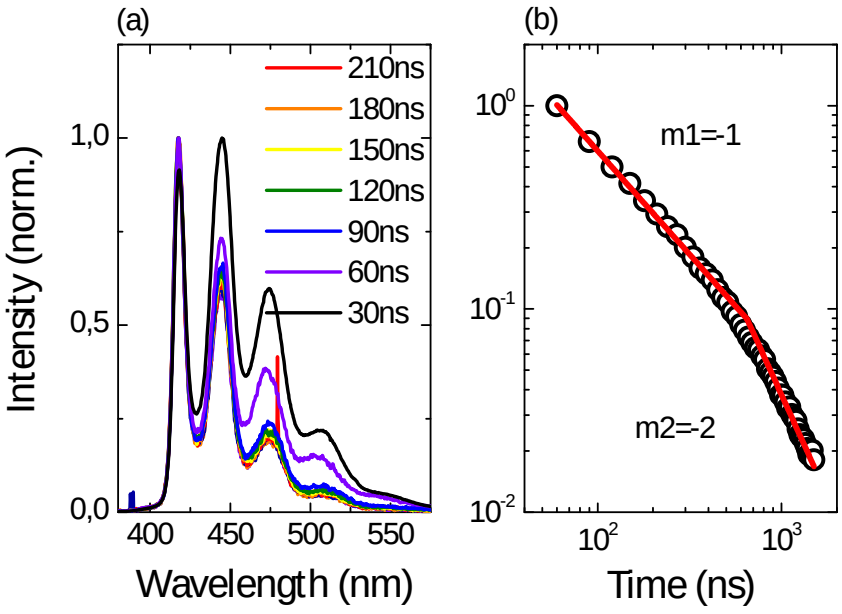

Figure 74: Delayed fluorescence measurements of BLUE-1 in MTHF with a concentration of 0.1 mg/ml.

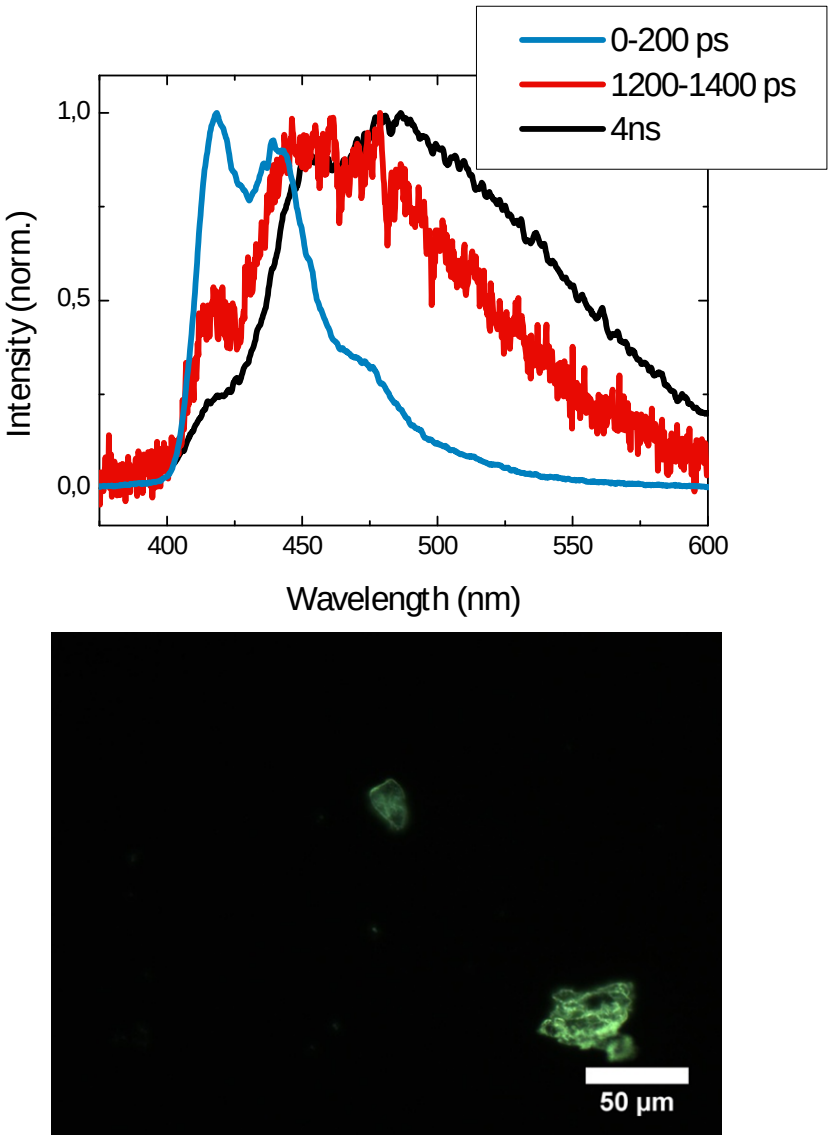

Figure 75: (a) Transient photoluminesence spectra of BLUE-1 dispersed in an inert matrix of Zeonex spincast on quartz. Figure (b) depicts a polarizing optical microscopy image of the same sample under crossed polarizers. The samples were prepared from toluene with a ratio of 100:1, with a Zeonex concentration of 10 mg/ml.

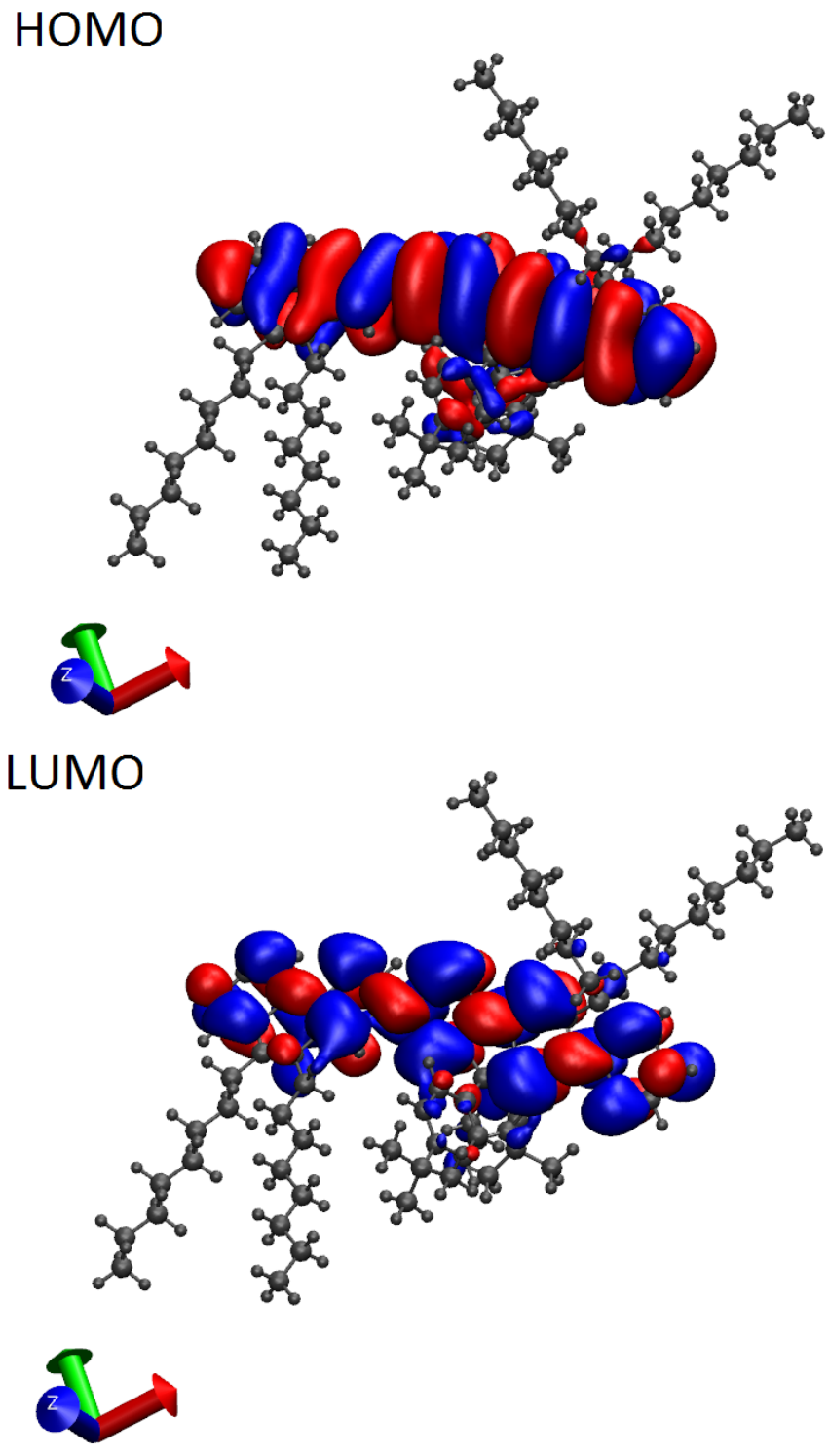

Figure 76: Calculated electronic structure of HOMO and LUMO for BLUE-1.

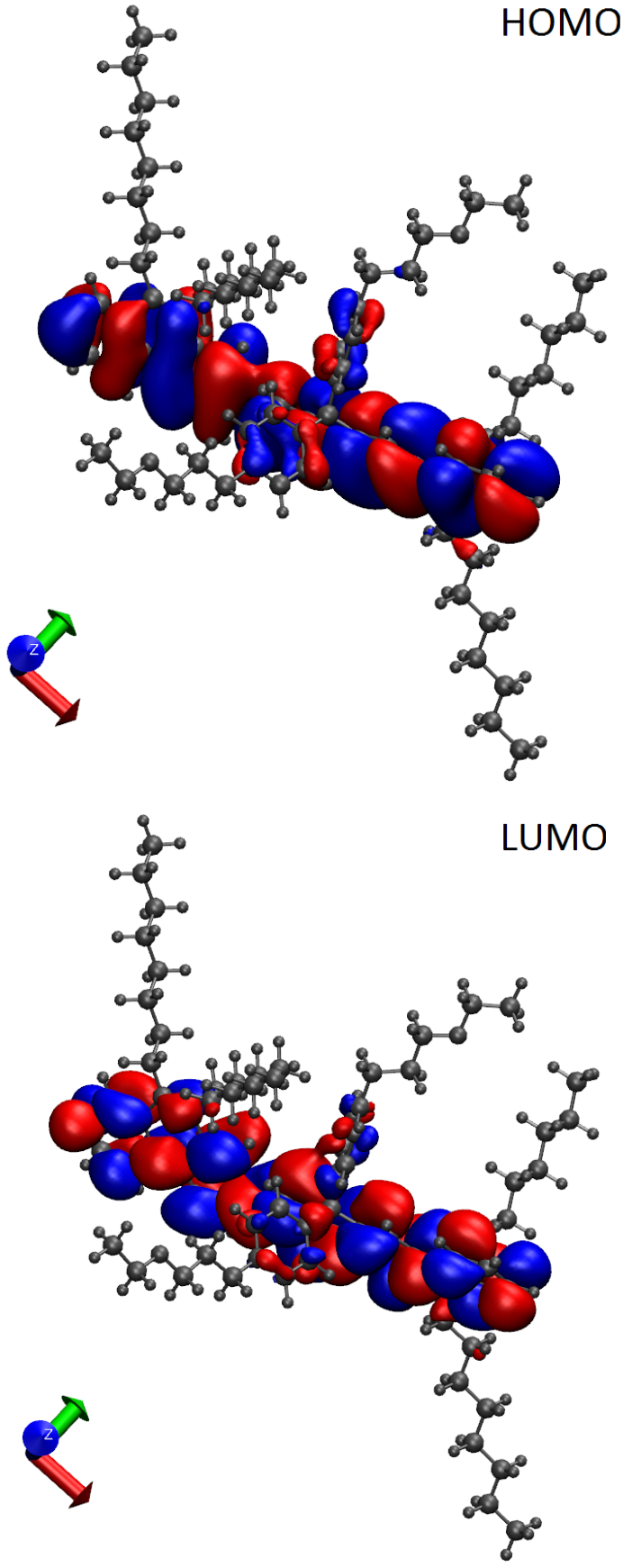

Figure 77: Calculated electronic structure of HOMO and LUMO for BLUE-2.

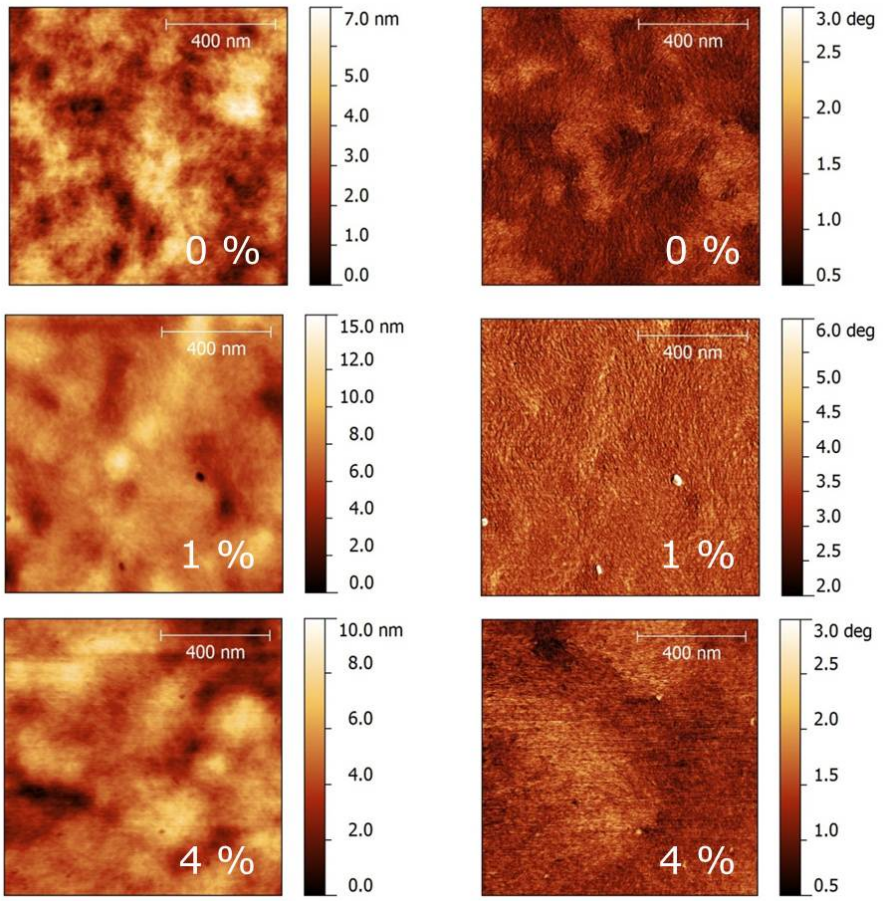

Figure 78: AFM measurements of BLUE-1 containing different volume fractions of DIO prior to spincoating. The samples were prepared from o-xylene with a concentration of 10 mg/ml.

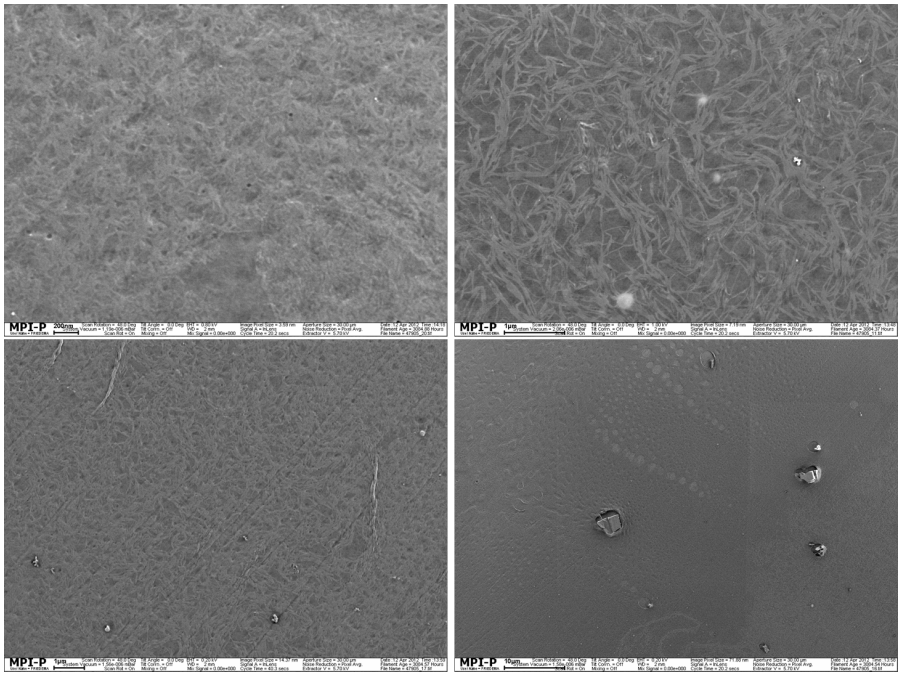

Figure 79: SEM recordings of BLUE-1 dropcasted from toluene with a concentration of 7.5 mg/ml.

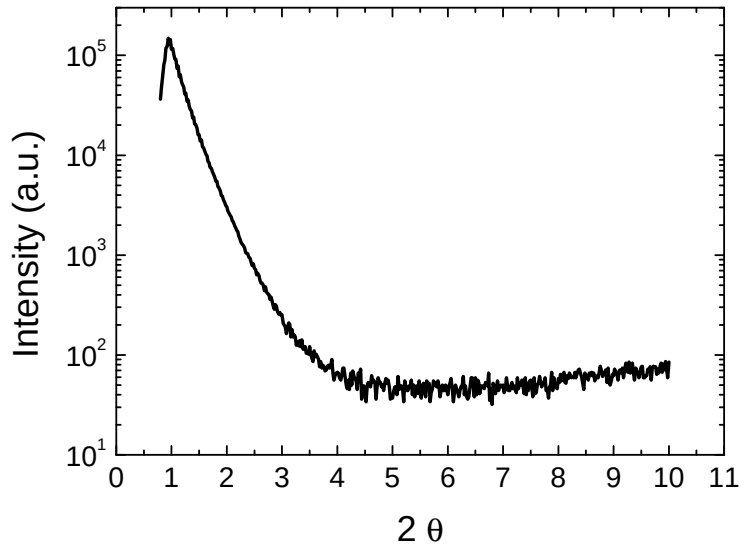

Figure 80: X-ray diffraction experiment on a spincast film of BLUE-1.

BIBLIOGRAPHY

[1] W. Demtröder, *Laser Spectroscopy*. Springer, 4th ed., 2008.

[2] H. Haken and H. C. Wolf, *Molekülphysik und Quantenchemie*. Berlin: Springer, 5th ed., 2006.

[3] Wikipedia, "Franck-condon prinzip," Apr. 2012.

[4] B. Valeur, *Molecular Fluorescence: Principles and Applications*. Wiley-VCH Verlag GmbH, 2001.

[5] M. Pope and S. C.E., *Electronic Processes in Organic Crystals and Polymers*. Oxford University Press, 2nd ed., 1999.

[6] F. Würthner, T. E. Kaiser, and C. R. Saha-Möller, "J aggregates: From serendipitous discovery to supramolecular engineering of functional dye materials," *Angewandte Chemie International Edition*, vol. 50, no. 15, pp. 3376–3410, 2011.

[7] W. Brütting and W. Rieß, "Grundlagen der organischen halbleiter," *Physik Journal*, vol. 7, no. 5, 2008.

[8] G. D. Scholes and G. Rumbles, "Excitons in nanoscale systems," *Nature Materials*, vol. 5, no. 9, pp. 683–696, 2006.

[9] F. Träger, *Springer Handbook of Lasers and Optics*. Springer, 2007.

[10] I. D. W. Samuel and G. A. Turnbull, "Organic semiconductor lasers," *Chemical Reviews*, vol. 107, no. 4, pp. 1272–1295, 2007.

[11] D. Neher, *Organic Semiconductors, SoSe 2010*. 2010.

[12] N. J. Turro, *Modern Molecular Photocehmistry*. Sausalito: University Science Books, 1991.

[13] J. R. Lakowicz, *Principles of fluorescence spectroscopy*. New York: Springer, 3rd ed., 2006.

[14] C. K. Chiang, J. Fincher, C. R., Y. W. Park, A. J. Heeger, H. Shirakawa, E. J. Louis, S. C. Gau, and A. G. MacDiarmid, "Electrical conductivity in doped polyacetylene," *Physical Review Letters*, vol. 39, no. 17, pp. 1098–1101, 1977.

[15] H. Shirakawa, E. J. Louis, A. G. MacDiarmid, C. K. Chiang, and A. J. Heeger, "Synthesis of electrically conducting organic polymers: halogen derivatives of polyacetylene, (ch)," *Journal of the Chemical Society, Chemical Communications*, no. 16, pp. 578–580, 1977.

[16] V. C. Sundar, J. Zaumseil, V. Podzorov, E. Menard, R. L. Willett, T. Someya, M. E. Gershenson, and J. A. Rogers, "Elastomeric transistor stamps: Reversible probing of charge transport in organic crystals," *Science*, vol. 303, no. 5664, pp. 1644–1646, 2004.

[17] H. Yan, Z. Chen, Y. Zheng, C. Newman, J. R. Quinn, F. Dotz, M. Kastler, and A. Facchetti, "A high-mobility electron-transporting polymer for printed transistors," *Nature*, vol. 457, no. 7230, pp. 679–686, 2009.

[18] D. Ghezzi, M. R. Antognazza, M. Dal Maschio, E. Lanzarini, F. Benfenati, and G. Lanzani, "A hybrid bioorganic interface for neuronal photoactivation," *Nat Commun*, vol. 2, p. 166, 2011. 10.1038/ncomms1164.

[19] M. Irimia-Vladu, N. S. Sariciftci, and S. Bauer, "Exotic materials for bio-organic electronics," *Journal of Materials Chemistry*, vol. 21, no. 5, pp. 1350–1361, 2011.

[20] S. C. B. Mannsfeld, B. C. K. Tee, R. M. S., C. V. H. H. Chen, S. Barman, B. V. O. Muir, A. N. Sokolov, C. Reese, and Z. Bao, "Highly sensitive flexible pressure sensors with microstructured rubber dielectric layers," *Nat Mater*, vol. 9, no. 10, pp. 859–864, 2010.

[21] Heliatek, "Heliatek sets new world record efficiency of 10.7% for its organic tandem cell," Apr. 2012.

[22] R. Bogue, "Developments in organic lasers and their role in sensing," *Sensor Review*, vol. 31, no. 1, pp. 13–17, 2011.

[23] J. Clark and G. Lanzani, "Organic photonics for communications," *Nature Photonics*, vol. 4, no. 7, pp. 438–446, 2010.

[24] I. A. Barlow, T. Kreouzis, and D. G. Lidzey, "High-speed electroluminescence modulation of a conjugated-polymer light emitting diode," *Appl. Phys. Lett.*, vol. 94, p. 243301, 2009.

[25] T. Rabe, "Quasi-continuous-wave operation of an organic thin-film distributed feedback laser," *Appl. Phys. Lett.*, vol. 89, p. 081115, 2006.

[26] M. Lu, S. S. Choi, U. Irfan, and B. T. Cunningham, "Plastic distributed feedback laser biosensor," *Applied Physics Letters*, vol. 93, no. 11, p. 111113, 2008.

[27] M. Ramuz, D. Leuenberger, R. Pfeiffer, L. Burgi, and C. Winnewisser, "Oled and opd-based mini-spectrometer integrated on a single-mode planar waveguide chip," *Eur. Phys. J. Appl. Phys.*, vol. 46, p. 12510, 2009.

[28] A. Rose, Z. Zhu, C. F. Madigan, T. M. Swager, and V. Bulovic, "Sensitivity gains in chemosensing by lasing action in organic polymers," *Nature*, vol. 434, no. 7035, pp. 876–879, 2005.

[29] J. Shinar and R. Shinar, "Organic light-emitting devices (oleds) and oled-based chemical and biological sensors: an overview," *J. Phys. D*, vol. 41, p. 133001, 2008.

[30] K. Mullen and U. Scherf, "Organic light emitting devices," 2006.

[31] N. Tessler, G. J. Denton, and R. H. Friend, "Lasing from conjugated-polymer microcavities," *Nature*, vol. 382, no. 6593, pp. 695–697, 1996.

[32] Y. Yang, G. A. Turnbull, and I. D. W. Samuel, "Hybrid optoelectronics: A polymer laser pumped by a nitride light-emitting diode," *Applied Physics Letters*, vol. 92, no. 16, pp. 163306–3, 2008.

[33] S. A. Jenekhe, "Polymer semiconductors: A fast mover with a bright spark," *Nat Mater*, vol. 7, no. 5, pp. 354–355, 2008.

[34] T.-Q. Nguyen, I. B. Martini, J. Liu, and B. J. Schwartz, "Controlling interchain interactions in conjugated polymers: The effects of chain morphology on exciton-exciton annihilation and aggregation in meh-ppv films," *The Journal of Physical Chemistry B*, vol. 104, no. 2, pp. 237–255, 1999.

[35] B. K. Yap, R. D. Xia, M. Campoy-Quiles, P. N. Stavrinou, and D. D. C. Bradley, "Simultaneous optimization of charge-carrier mobility and optical gain in semiconducting polymer films," *Nature Materials*, vol. 7, no. 5, pp. 376–380, 2008.

[36] M. Chakaroun, A. Coens, N. Fabre, F. Gourdon, J. Solard, A. Fischer, A. Boudrioua, and C. C. Lee, "Optimal design of a microcavity organic laser device under electrical pumping," *Optics Express*, vol. 19, no. 2, pp. 493–505, 2011.

[37] M. C. Gwinner, S. Khodabakhsh, M. H. Song, H. Schweizer, H. Giessen, and H. Sirringhaus, "Integration of a rib waveguide distributed feedback structure into a light-emitting polymer field-effect transistor," *Advanced Functional Materials*, vol. 19, no. 9, pp. 1360–1370, 2009.

[38] C. Karnutsch, C. Pflumm, G. Heliotis, J. C. Demello, D. D. C. Bradley, J. Wang, T. Weimann, V. Haug, C. Gartner, and U. Lemmer, "Improved organic semiconductor lasers based on a mixed-order distributed feedback resonator design," *Applied Physics Letters*, vol. 90, no. 13, p. 3, 2007.

[39] E. B. Namdas, M. Tong, P. Ledochowitsch, S. R. Mednick, J. D. Yuen, D. Moses, and A. J. Heeger, "Low thresholds in polymer lasers on conductive substrates by distributed feedback nanoimprinting: Progress toward electrically pumped plastic lasers," *Advanced Materials*, vol. 21, no. 7, p. 799, 2009.

[40] G. Heliotis, D. D. C. Bradley, G. A. Turnbull, and I. D. W. Samuel, "Light amplification and gain in polyfluorene waveguides," *Applied Physics Letters*, vol. 81, no. 3, pp. 415–417, 2002.

[41] C. Rothe, F. Galbrecht, U. Scherf, and A. Monkman, "The beta-phase of poly(9,9-dioctylfluorene) as a potential system for electrically pumped organic lasing," *Advanced Materials*, vol. 18, no. 16, p. 2137, 2006.

[42] C. Silva, R. D. M., A. S. H. L. M. D. C. Dhoot, N. C. Greenham, S. Arias, A. C.and Setayesh, K. Müllen, and F. R. H., "Exciton and polaron dynamics in a step-ladder polymeric semiconductor: the influence of interchain order," *Journal of Physics: Condensed Matter*, vol. 14, no. 42, p. 9803, 2002.

[43] C. Gartner, C. Karnutsch, U. Lemmer, and C. Pflumm, "The influence of annihilation processes on the threshold current density of organic laser diodes," *Journal of Applied Physics*, vol. 101, no. 2, 2007.

[44] E. J. W. List, C. H. Kim, A. K. Naik, U. Scherf, G. Leising, W. Graupner, and J. Shinar, "Interaction of singlet excitons with polarons in wide band-gap organic semiconductors: A quantitative study," *Physical Review B*, vol. 64, no. 15, p. 155204, 2001.

[45] A. Einstein, "Zur quantentheorie der strahlung," *Mitteilungen der Physikalische Gesellschaft Zurich*, vol. 18, pp. 121–128, 1916.

[46] U. Gubler and C. Bosshard, *Molecular Design for Third-Order Nonlinear Optics*. Springer-Verlag Berlin Heidelberg, 2002.

[47] A. J. Heeger, "Semiconducting and metallic polymers: The fourth generation of polymeric materials," *Nobel Lecture*, 2000.

[48] I. Bloch, *Licht-Atom Wechselwirkung im Zwei-Niveau System, WS 2003/04*. 2004.

[49] M. C. Petty, *Molecular Electronics - From Principles to Practice*. John Wiley & Sons, Ltd, 2007.

[50] K. Müllen and G. Wegner, *Electronic Materials: The Oligomer Approach*. Weinheim: Wiley-VCH, 1998.

[51] H. Bässler, "Charge transport in disordered organic photoconductors - a monte-carlo simulation study," *Physica Status Solidi B-Basic Research*, vol. 175, no. 1, pp. 15–56, 1993.

[52] P. W. M. Blom, M. J. M. de Jong, and M. G. van Munster, "Electric-field and temperature dependence of the hole mobility in poly(p-phenylene vinylene)," *Physical Review B*, vol. 55, no. 2, pp. R656–R659, 1997.

[53] B. Movaghar, B. Ries, and M. Grünewald, "Diffusion and relaxation of energy in disordered systems: Departure from mean-field theories," *Physical Review B*, vol. 34, no. 8, pp. 5574–5582, 1986.

[54] R. Richert, H. Bässler, B. Ries, B. Movaghar, and M. Grünewald, "Frustrated energy relaxation in an organic glass," *Philosophical Magazine Letters*, vol. 59, no. 2, pp. 95–102, 1989.

[55] B. Ries, H. Bässler, M. Grünewald, and B. Movaghar, "Monte carlo study of relaxation and diffusion in glassy systems," *Physical Review B*, vol. 37, no. 10, pp. 5508–5517, 1988.

[56] A. Miller and E. Abrahams, "Impurity conduction at low concentrations," *Physical Review*, vol. 120, no. 3, pp. 745–755, 1960.

[57] N. F. Mott and W. D. Twose, "The theory of impurity conduction," *Advances in Physics*, vol. 10, no. 38, pp. 107–163, 1961.

[58] N. Tessler, Y. Preezant, N. Rappaport, and Y. Roichman, "Charge transport in disordered organic materials and its relevance to thin-film devices: A tutorial review," *Advanced Materials*, vol. 21, no. 27, pp. 2741–2761, 2009.

[59] S. Heun, R. F. Mahrt, A. Greiner, U. Lemmer, H. Bässler, D. A. Halliday, D. D. C. Bradley, P. L. Burn, and A. B. Holmes, "Conformational effects in poly(p-phenylene vinylene)s revealed by low-temperature site-selective fluorescence," *Journal of Physics-Condensed Matter*, vol. 5, no. 2, pp. 247–260, 1993.

[60] R. Kersting, U. Lemmer, R. F. Mahrt, K. Leo, H. Kurz, H. Bässler, and E. O. Göbel, "Femtosecond energy relaxation in ?-conjugated polymers," *Physical Review Letters*, vol. 70, no. 24, pp. 3820–3823, 1993.

[61] S. C. J. Meskers, J. Hübner, M. Oestreich, and H. Bässler, "Time-resolved fluorescence studies and monte carlo simulations of relaxation dynamics of photoexcitations in a polyfluorene film," *Chemical Physics Letters*, vol. 339, no. 3, pp. 223–228, 2001.

[62] S. T. Hoffmann, H. Bässler, J.-M. Koenen, M. Forster, U. Scherf, E. Scheler, P. Strohriegl, and A. Köhler, "Spectral diffusion in poly(para-phenylene)-type polymers with

different energetic disorder," *Physical Review B*, vol. 81, no. 11, p. 115103, 2010.

[63] V. Coropceanu, J. Cornil, D. A. da Silva, Y. Olivier, R. Silbey, and J. L. Bredas, "Charge transport in organic semiconductors," *Chemical Reviews*, vol. 107, no. 4, pp. 926–952, 2007.

[64] I. D. W. Samuel, E. B. Namdas, and G. A. Turnbull, "How to recognize lasing," *Nature Photonics*, vol. 3, no. 10, pp. 546–549, 2009.

[65] S. Furumi, H. Fudouzi, H. T. Miyazaki, and Y. Sakka, "Flexible polymer colloidal-crystal lasers with a light-emitting planar defect," *Advanced Materials*, vol. 19, no. 16, p. 2067, 2007.

[66] M. Koschorreck, R. Gehlhaar, V. G. Lyssenko, M. Swoboda, M. Hoffmann, and K. Leo, "Dynamics of a high-q vertical-cavity organic laser," *Applied Physics Letters*, vol. 87, no. 18, pp. 181108–3, 2005.

[67] J. R. Lawrence, G. A. Turnbull, and I. D. W. Samuel, "Polymer laser fabricated by a simple micromolding process," *Applied Physics Letters*, vol. 82, no. 23, pp. 4023–4025, 2003.

[68] U. Scherf, S. Riechel, U. Lemmer, and R. F. Mahrt, "Conjugated polymers: lasing and stimulated emission," *Current Opinion in Solid State & Materials Science*, vol. 5, no. 2-3, pp. 143–154, 2001.

[69] M. A. Abkowitz, H. A. Mizes, and J. S. Facci, "Emission limited injection by thermally assisted tunneling into a trap-free transport polymer," *Applied Physics Letters*, vol. 66, no. 10, pp. 1288–1290, 1995.

[70] M. Schott, "Introduction to the physics of organic electroluminescence," *Comptes Rendus De L Academie Des Sciences Serie Iv Physique Astrophysique*, vol. 1, no. 4, pp. 381–402, 2000.

[71] G. E. Jabbour, B. Kippelen, N. R. Armstrong, and N. Peyghambarian, "Aluminum based cathode structure for enhanced electron injection in electroluminescent organic devices," *Applied Physics Letters*, vol. 73, no. 9, pp. 1185–1187, 1998.

[72] S. Bae, H. Kim, Y. Lee, X. Xu, J.-S. Park, Y. Zheng, J. Balakrishnan, T. Lei, H. Ri Kim, Y. I. Song, Y.-J. Kim, K. S. Kim, B. Ozyilmaz, J.-H. Ahn, B. H. Hong, and S. Iijima, "Roll-to-roll production of 30-inch graphene films for transparent electrodes," *Nat Nano*, vol. 5, no. 8, pp. 574–578, 2010.

[73] F. Bonaccorso, Z. Sun, T. Hasan, and A. C. Ferrari, "Graphene photonics and optoelectronics," *Nature Photonics*, vol. 4, no. 9, pp. 611–622, 2010.

[74] P. Langevin *Ann. Chim. Phys.*, vol. 28, p. 287, 1903.

[75] M. A. Baldo, M. E. Thompson, and S. R. Forrest, "High-efficiency fluorescent organic light-emitting devices using a phosphorescent sensitizer," *Nature*, vol. 403, no. 6771, pp. 750–753, 2000.

[76] C. W. Tang, S. A. VanSlyke, and C. H. Chen, "Electroluminescence of doped organic thin films," *Journal of Applied Physics*, vol. 65, no. 9, pp. 3610–3616, 1989.

[77] F. So and D. Kondakov, "Degradation mechanisms in small-molecule and polymer organic light-emitting diodes," *Advanced Materials*, vol. 22, no. 34, pp. 3762–3777, 2010.

[78] M. Kuik, L. J. A. Koster, A. G. Dijkstra, G. A. H. Wetzelaer, and P. W. M. Blom, "Non-radiative recombination losses in polymer light-emitting diodes," *Organic Electronics*, vol. 13, no. 6, pp. 969–974, 2012.

[79] N. C. Giebink and S. R. Forrest, "Quantum efficiency roll-off at high brightness in fluorescent and phosphorescent organic light emitting diodes," *Physical Review B*, vol. 77, no. 23, p. 235215, 2008.

[80] H. Nakanotani, H. S., and C. Adachi, "Singlet-singlet and singlet-heat annihilations in fluorescence-based organic light-emitting diodes under steady-state high current density," *Applied Physics Letters*, vol. 86, no. 21, pp. 213506–3, 2005.

[81] M. Deussen, M. Scheidler, and H. Bässler, "Electric field-induced photoluminescence quenching in thin-film light-emitting diodes based on poly(phenyl-p-phenylene vinylene)," *Synthetic Metals*, vol. 73, no. 2, pp. 123–129, 1995.

[82] M. Deussen, P. Haring Bolivar, G. Wegmann, H. Kurz, and H. Bässler, "Electric field-induced photoluminescence quenching in molecularly doped polymer light-emitting diodes," *Chemical Physics*, vol. 207, no. 1, pp. 147–157, 1996.

[83] B. J. Chen, W. Y. Lai, Z. Q. Gao, C. S. Lee, S. T. Lee, and W. A. Gambling, "Electron drift mobility and electroluminescent efficiency of tris(8-hydroxyquinolinolato) aluminum," *Applied Physics Letters*, vol. 75, no. 25, pp. 4010–4012, 1999.

[84] Y.-J. Pu, G. Nakata, F. Satoh, H. Sasabe, D. Yokoyama, and J. Kido, "Optimizing the charge balance of fluorescent organic light-emitting devices to achieve high external quantum efficiency beyond the conventional upper limit," *Advanced Materials*, pp. n/a–n/a, 2012.

[85] M. Ichikawa, R. Naitou, T. Koyama, and Y. Taniguchi, "Exciton dynamics in organic semiconductor devices: Investigation of exciton-charge carrier interactions as revealed by photoluminescence responses," *Japanese Journal of Applied Physics Part 2-Letters*, vol. 40, no. 10A, pp. L1068–L1070, 2001.

[86] H. Becker, S. E. Burns, and R. H. Friend, "Effect of metal films on the photoluminescence and electroluminescence of conjugated polymers," *Physical Review B*, vol. 56, no. 4, pp. 1893–1905, 1997.

[87] N. C. Greenham, R. H. Friend, and D. D. C. Bradley, "Angular dependence of the emission from a conjugated polymer light-emitting diode: Implications for efficiency calculations," *Advanced Materials*, vol. 6, no. 6, pp. 491–494, 1994.

[88] L. Xiao, S.-J. Su, Y. Agata, H. Lan, and J. Kido, "Nearly 100 % internal quantum efficiency in an organic blue-light electrophosphorescent device using a weak electron transporting material with a wide energy gap," *Advanced Materials*, vol. 21, no. 12, pp. 1271–1274, 2009.

[89] D. Marsitzky, J. C. Scott, J. P. Chen, V. Y. Lee, R. D. Miller, S. Setayesh, and K. Müllen, "Poly-2,8-(indenofluorene-co-anthracene) - a colorfast blue-light-emitting random

copolymer," *Advanced Materials*, vol. 13, no. 14, p. 1096, 2001.

[90] Y. W. Soon, T. M. Clarke, W. Zhang, T. Agostinelli, J. Kirkpatrick, C. Dyer-Smith, I. McCulloch, J. Nelson, and J. R. Durrant, "Energy versus electron transfer in organic solar cells: a comparison of the photophysics of two indenofluorene: fullerene blend films," *Chemical Science*, vol. 2, no. 6, pp. 1111–1120, 2011.

[91] T.-J. Ha, D. Sparrowe, and A. Dodabalapur, "Device architectures for improved amorphous polymer semiconductor thin-film transistors," *Organic Electronics*, vol. 12, no. 11, pp. 1846–1851, 2011.

[92] E. J. Meijer, D. M. De Leeuw, S. Setayesh, E. Van Veenendaal, B. H. Huisman, P. W. M. Blom, J. C. Hummelen, U. Scherf, and T. M. Klapwijk, "Solution-processed ambipolar organic field-effect transistors and inverters," *Nature Materials*, vol. 2, no. 10, pp. 678–682, 2003.

[93] K. Nakashima and I. Tanaka, "Phenanthrene and triphenylene as fluorescence probes for micellar systems," *Langmuir*, vol. 9, no. 1, pp. 90–95, 1993.

[94] Y. Kawamura, H. Sasabe, and C. Adachi, "Simple accurate system for measuring absolute photoluminescence quantum efficiency in organic solid-state thin films," *Japanese Journal of Applied Physics Part 1-Regular Papers Short Notes and Review Papers*, vol. 43, no. 11A, pp. 7729–7730, 2004.

[95] M. Campoy-Quiles, J. Nelson, P. G. Etchegoin, D. D. C. Bradley, V. Zhokhavets, G. Gobsch, H. Vaughan, A. Monkman, O. Inganas, N. K. Persson, H. Arwin, M. Garriga, M. I. Alonsos, G. Herrmann, M. Becker, W. Scholdei, M. Jahja, and C. Bubeck, "On the determination of anisotropy in polymer thin films: A comparative study of optical techniques," *Physica Status Solidi C Current Topics in Solid State Physics*, vol. 5, no. 5, pp. 1270–1273, 2008.

[96] S. Abe, M. Schreiber, W. P. Su, and J. Yu, "Excitons and nonlinear optical spectra in conjugated polymers," *Physical Review B*, vol. 45, no. 16, pp. 9432–9435, 1992.

[97] M. Wohlgenannt, W. Graupner, G. Leising, and Z. V. Vardeny, "Photogeneration and recombination processes of neutral and charged excitations in films of a ladder-type poly(para-phenylene)," *Physical Review B*, vol. 60, no. 8, pp. 5321–5330, 1999.

[98] M. Kaplanová and K. Cermák, "Effect of reabsorption on the concentration dependence of fluorescence lifetimes of chlorophyll a," *Journal of Photochemistry*, vol. 15, no. 4, pp. 313–319, 1981.

[99] J. M. Lupton, M. R. Craig, and E. W. Meijer, "On-chain defect emission in electroluminescent polyfluorenes," *Applied Physics Letters*, vol. 80, no. 24, pp. 4489–4491, 2002.

[100] U. Scherf and E. J. W. List, "Semiconducting polyfluorenes - towards reliable structure-property relationships," *Advanced Materials*, vol. 14, no. 7, p. 477, 2002.

[101] M. Sims, D. D. C. Bradley, M. Ariu, M. Koeberg, A. Asimakis, M. Grell, and D. G. Lidzey, "Understanding the origin of the 535 nm emission band in oxidized poly(9,9-dioctylfluorene): The essential role of interchain/inter-segment interactions," *Advanced Functional Materials*, vol. 14, no. 8, pp. 765–781, 2004.

[102] S. Gamerith, C. Gadermaier, U. Scherf, and E. J. W. List, "Emission properties of pristine and oxidatively degraded polyfluorene type polymers," *Physica Status Solidi a-Applications and Materials Science*, vol. 201, no. 6, pp. 1132–1151, 2004.

[103] J. M. Lupton, P. Schouwink, P. E. Keivanidis, A. C. Grimsdale, and K. Müllen, "Influence of dendronization on spectral diffusion and aggregation in conjugated polymers," *Advanced Functional Materials*, vol. 13, no. 2, pp. 154–158, 2003.

[104] L. M. Herz, C. Silva, R. T. Phillips, S. Setayesh, and K. Müllen, "Exciton migration to chain aggregates in conjugated polymers: influence of side-chain substitution," *Chemical Physics Letters*, vol. 347, no. 4-6, pp. 318–324, 2001.

[105] P. E. Keivanidis, J. Jacob, L. Oldridge, P. Sonar, B. Carbonnier, S. Baluschev, A. C. Grimsdale, K. Müllen, and

G. Wegner, "Photophysical characterization of light-emitting poly(indenofluorene)s," *Chemphyschem*, vol. 6, no. 8, pp. 1650–1660, 2005.

[106] F. B. Dias, A. L. Macanita, J. S. de Melo, H. D. Burrows, R. Guntner, U. Scherf, and A. P. Monkman, "Picosecond conformational relaxation of singlet excited polyfluorene in solution," *Journal of Chemical Physics*, vol. 118, no. 15, pp. 7119–7126, 2003.

[107] H. Bässler and B. Schweitzer, "Site-selective fluorescence spectroscopy of conjugated polymers and oligomers," *Accounts of Chemical Research*, vol. 32, no. 2, pp. 173–182, 1998.

[108] B. Schweitzer, V. I. Arkhipov, U. Scherf, and H. Bässler, "Geminate pair recombination in a conjugated polymer," *Chemical Physics Letters*, vol. 313, no. 1-2, pp. 57–62, 1999.

[109] L. Rothberg, *Semiconducting polymers : chemistry, physics and engineering Vol. I.* Wiley-VCH, 2007.

[110] W. Graupner, J. Partee, J. Shinar, G. Leising, and U. Scherf, "Dynamics of long-lived polarons in poly(para-phenylene)-type ladder polymers," *Physical Review Letters*, vol. 77, no. 10, pp. 2033–2036, 1996.

[111] J. Cabanillas-Gonzalez, G. Grancini, and G. Lanzani, "Pump-probe spectroscopy in organic semiconductors: Monitoring fundamental processes of relevance in optoelectronics," *Advanced Materials*, vol. 23, no. 46, pp. 5468–5485, 2011.

[112] M. Grell, D. D. C. Bradley, X. Long, T. Chamberlain, M. Inbasekaran, E. P. Woo, and M. Soliman, "Chain geometry, solution aggregation and enhanced dichroism in the liquidcrystalline conjugated polymer poly(9,9-dioctylfluorene)," *Acta Polymerica*, vol. 49, no. 8, pp. 439–444, 1998.

[113] C. Rothe, S. M. King, F. Dias, and A. P. Monkman, "Triplet exciton state and related phenomena in the ?-phase of poly(9,9-dioctyl)fluorene," *Physical Review B*, vol. 70, no. 19, p. 195213, 2004.

[114] A. Monkman, C. Rothe, S. King, and F. Dias, *Polyfluorene Photophysics Polyfluorenes*, vol. 212 of *Advances in Polymer Science*, pp. 187–225. Springer Berlin / Heidelberg, 2008.

[115] F. B. Dias, J. Morgado, A. L. Maçanita, F. P. da Costa, H. D. Burrows, and A. P. Monkman, "Kinetics and thermodynamics of poly(9,9-dioctylfluorene) β-phase formation in dilute solution," *Macromolecules*, vol. 39, no. 17, pp. 5854–5864, 2006.

[116] J. Peet, E. Brocker, Y. Xu, and G. C. Bazan, "Controlled beta-phase formation in poly(9,9-di-n-octylfluorene) by processing with alkyl additives," *Advanced Materials*, vol. 20, no. 10, pp. 1882–1885, 2008.

[117] B. J. A. Caputo, G. C. Welch, D. A. Kamkar, Z. B. Henson, T.-Q. Nguyen, and G. C. Bazan, "A dithienosilole-benzooxadiazole donor acceptor copolymer for utility in organic solar cells," *Small*, vol. 7, no. 10, pp. 1422–1426, 2011.

[118] A. P. Monkman, H. D. Burrows, L. J. Hartwell, L. E. Horsburgh, I. Hamblett, and S. Navaratnam, "Triplet energies of π-conjugated polymers," *Physical Review Letters*, vol. 86, no. 7, pp. 1358–1361, 2001.

[119] C. Rothe and A. Monkman, "Regarding the origin of the delayed fluorescence of conjugated polymers," *The Journal of Chemical Physics*, vol. 123, no. 24, pp. 244904–6, 2005.

[120] A. Endo, K. Sato, K. Yoshimura, T. Kai, A. Kawada, H. Miyazaki, and C. Adachi, "Efficient up-conversion of triplet excitons into a singlet state and its application for organic light emitting diodes," *Applied Physics Letters*, vol. 98, no. 8, pp. 083302–3, 2011.

[121] M. Scheidler, B. Cleve, H. Bässler, and P. Thomas, "Monte carlo simulation of bimolecular exciton annihilation in an energetically random hopping system," *Chemical Physics Letters*, vol. 225, pp. 431–436, 1994.

[122] J. S. Wilson, N. Chawdhury, M. R. A. Al-Mandhary, M. Younus, M. S. Khan, P. R. Raithby, A. Köhler, and R. H. Friend, "The energy gap law for triplet states in pt-containing conjugated polymers and monomers," *Journal*

of the American Chemical Society, vol. 123, no. 38, pp. 9412–9417, 2001.

[123] C. Kallinger, M. Hilmer, A. Haugeneder, M. Perner, W. Spirkl, U. Lemmer, J. Feldmann, U. Scherf, K. Müllen, A. Gombert, and V. Wittwer, "A flexible conjugated polymer laser," *Advanced Materials*, vol. 10, no. 12, p. 920, 1998.

[124] S. Riechel, C. Kallinger, U. Lemmer, J. Feldmann, A. Gombert, V. Wittwer, and U. Scherf, "A nearly diffraction limited surface emitting conjugated polymer laser utilizing a two-dimensional photonic band structure," *Applied Physics Letters*, vol. 77, no. 15, pp. 2310–2312, 2000.

[125] N. Tessler, "Lasers based on semiconducting organic materials," *Advanced Materials*, vol. 11, no. 5, pp. 363–370, 1999.

[126] F. Laquai, A. K. Mishra, K. Müllen, and R. H. Friend, "Amplified spontaneous emission of poly(ladder-type phenylene)s - the influence of photophysical properties on ase thresholds," *Advanced Functional Materials*, vol. 18, no. 20, pp. 3265–3275, 2008.

[127] B. H. Wallikewitz, M. de la Rosa, J. H. W. M. Kremer, D. Hertel, and K. Meerholz, "A lasing organic light-emitting diode," *Advanced Materials*, vol. 22, no. 4, p. 531, 2010.

[128] S. Schols, A. Kadashchuk, P. Heremans, A. Helfer, and U. Scherf, "Triplet excitation scavenging in films of conjugated polymers," *Chemphyschem*, vol. 10, no. 7, pp. 1071–1076, 2009.

[129] Y. Zhang and S. R. Forrest, "Existence of continuous-wave threshold for organic semiconductor lasers," *Physical Review B*, vol. 84, no. 24, p. 241301, 2011.

[130] J. Salbeck, M. Schorner, and T. Fuhrmann, "Optical amplification in spiro-type molecular glasses," *Thin Solid Films*, vol. 417, no. 1-2, pp. 20–25, 2002.

[131] F. Laquai, P. E. Keivanidis, S. Baluschev, J. Jacob, K. Müllen, and G. Wegner, "Low-threshold amplified spontaneous

emission in thin films of poly(tetraarylindenofluorene)," *Applied Physics Letters*, vol. 87, no. 26, 2005.

[132] H. Ma, A. K. Y. Jen, and L. R. Dalton, "Polymer-based optical waveguides: Materials, processing, and devices," *Advanced Materials*, vol. 14, no. 19, pp. 1339–1365, 2002.

[133] S. Reineke, F. Lindner, G. Schwartz, N. Seidler, K. Walzer, B. Lussem, and K. Leo, "White organic light-emitting diodes with fluorescent tube efficiency," *Nature*, vol. 459, no. 7244, pp. 234–238, 2009.

[134] M. D. McGehee, R. Gupta, S. Veenstra, E. K. Miller, M. A. Diaz-Garcia, and A. J. Heeger, "Amplified spontaneous emission from photopumped films of a conjugated polymer," *Physical Review B*, vol. 58, no. 11, pp. 7035–7039, 1998.

[135] http://wwwhome.math.utwente.nl/ hammerm/Metric/.

[136] M. Campoy-Quiles, G. Heliotis, R. D. Xia, M. Ariu, M. Pintani, P. Etchegoin, and D. D. C. Bradley, "Ellipsometric characterization of the optical constants of polyfluorene gain media," *Advanced Functional Materials*, vol. 15, no. 6, pp. 925–933, 2005.

[137] M. Campoy-Quiles, P. G. Etchegoin, and D. D. C. Bradley, "On the optical anisotropy of conjugated polymer thin films," *Physical Review B*, vol. 72, no. 4, p. 045209, 2005.

[138] I. B. Martini, I. M. Craig, W. C. Molenkamp, H. Miyata, S. H. Tolbert, and B. J. Schwartz, "Controlling optical gain in semiconducting polymers with nanoscale chain positioning and alignment," *Nat Nano*, vol. 2, no. 10, pp. 647–652, 2007.

[139] M. A. Díaz-García, F. Hide, B. J. Schwartz, M. R. Andersson, Q. Pei, and A. J. Heeger, "Plastic lasers: Semiconducting polymers as a new class of solid-state laser materials," *Synthetic Metals*, vol. 84, pp. 455–462, 1997.

[140] H. Kogelnik and C. V. Shank, "Coupled-wave theory of distributed feedback lasers," *Journal of Applied Physics*, vol. 43, no. 5, p. 2327, 1972.

[141] B. J. Schwartz, F. Hide, M. A. DiazGarcia, M. R. Andersson, and A. J. Heeger, "Stimulated emission and lasing in solid films of conjugated polymers: Ultrafast photophysics and photon confinement via scattering," *Philosophical Transactions of the Royal Society of London Series a-Mathematical Physical and Engineering Sciences*, vol. 355, no. 1725, pp. 775–787, 1997.

[142] S. Schols, S. Verlaak, C. Rolin, D. Cheyns, J. Genoe, and P. Heremans, "An organic light-emitting diode with field-effect electron transport," *Advanced Functional Materials*, vol. 18, no. 1, pp. 136–144, 2008.

[143] A. Charas, A. L. Mendonça, J. Clark, L. Bazzana, A. Nocivelli, G. Lanzani, and J. Morgado, "Stimulated emission and ultrafast optical switching in a ter(9,9?-spirobifluorene)-co-methylmethacrylate copolymer," *Journal of Polymer Science Part B: Polymer Physics*, vol. 49, no. 1, pp. 52–61, 2011.

[144] R. Xia, G. Heliotis, Y. Hou, and D. D. C. Bradley, "Fluorene-based conjugated polymer optical gain media," *Organic Electronics*, vol. 4, no. 2-3, pp. 165–177, 2003.

[145] Y. Zaushitsyn, K. G. Jespersen, L. Valkunas, V. Sundström, and A. Yartsev, "Ultrafast dynamics of singlet-singlet and singlet-triplet exciton annihilation in poly(3-2-methoxy-5 octylphenyl)thiophene films," *Physical Review B*, vol. 75, no. 19, p. 195201, 2007.

[146] M. Yan, L. J. Rothberg, E. W. Kwock, and T. M. Miller, "Interchain excitations in conjugated polymers," *Physical Review Letters*, vol. 75, no. 10, pp. 1992–1995, 1995. PRL.

[147] H. N. Tsao and K. Müllen, "Improving polymer transistor performance via morphology control," *Chemical Society Reviews*, vol. 39, no. 7, pp. 2372–2386, 2010.

[148] R. Mauer, I. A. Howard, and F. Laquai, "Effect of external bias on nongeminate recombination in polythiophene/methanofullerene organic solar cells," *The Journal of Physical Chemistry Letters*, vol. 2, no. 14, pp. 1736–1741, 2011.

[149] C. Gartner, C. Karnutsch, C. Pflumm, and U. Lemmer, "Numerical device simulation of double-heterostructure

organic laser diodes including current-induced absorption processes," *Quantum Electronics, IEEE Journal of*, vol. 43, no. 11, pp. 1006–1017, 2007.

[150] S. M. Tuladhar, M. Sims, J. Kirkpatrick, R. C. Maher, A. J. Chatten, D. D. C. Bradley, J. Nelson, P. G. Etchegoin, C. B. Nielsen, P. Massiot, W. N. George, and J. H. G. Steinke, "Influence of alkyl chain length on charge transport in symmetrically substituted poly(2,5-dialkoxy-p-phenylenevinylene) polymers," *Physical Review B*, vol. 79, no. 3, p. 10, 2009.

[151] H. N. Tsao, D. M. Cho, I. Park, M. R. Hansen, A. Mavrinskiy, D. Y. Yoon, R. Graf, W. Pisula, H. W. Spiess, and K. Müllen, "Ultrahigh mobility in polymer field-effect transistors by design," *Journal of the American Chemical Society*, vol. 133, no. 8, pp. 2605–2612, 2011.

[152] H. H. Fong, A. Papadimitratos, and G. G. Malliaras, "Nondispersive hole transport in a polyfluorene copolymer with a mobility of 0.01 cm(2) v-1 s(-1)," *Applied Physics Letters*, vol. 89, no. 17, p. 3, 2006.

[153] F. Laquai, G. Wegner, and H. Bässler, "What determines the mobility of charge carriers in conjugated polymers?," *Philosophical Transactions of the Royal Society a-Mathematical Physical and Engineering Sciences*, vol. 365, no. 1855, pp. 1473–1487, 2007.

[154] F. Laquai, G. Wegner, C. Im, H. Bässler, and S. Heun, "Nondispersive hole transport in carbazole- and anthracene-containing polyspirobifluorene copolymers studied by the charge-generation layer time-of-flight technique," *Journal of Applied Physics*, vol. 99, no. 3, 2006.

[155] F. Laquai and D. Hertel, "Influence of hole transport units on the efficiency of polymer light emitting diodes," *Applied Physics Letters*, vol. 90, no. 14, 2007.

[156] D. Hertel, U. Scherf, and H. Bässler, "Charge carrier mobility in a ladder-type conjugated polymer," *Advanced Materials*, vol. 10, no. 14, p. 1119, 1998.

[157] W.-Y. Hung, T.-H. Ke, Y.-T. Lin, C.-C. Wu, T.-H. Hung, T.-C. Chao, K.-T. Wong, and C.-I. Wu, "Employing ambipolar

oligofluorene as the charge-generation layer in time-of-flight mobility measurements of organic thin films," *Applied Physics Letters*, vol. 88, no. 6, pp. 064102–3, 2006.

[158] C. Pacholski, A. Kornowski, and H. Weller, "Self-assembly of zno: From nanodots, to nanorods," *Angewandte Chemie-International Edition*, vol. 41, no. 7, p. 1188, 2002.

[159] B. S. Ong, C. Li, Y. Li, Y. Wu, and R. Loutfy, "Stable, solution-processed, high-mobility zno thin-film transistors," *Journal of the American Chemical Society*, vol. 129, no. 10, pp. 2750–2751, 2007.

[160] M. Kuik, G.-J. A. H. Wetzelaer, J. G. Laddé, H. T. Nicolai, J. Wildeman, J. Sweelssen, and P. W. M. Blom, "The effect of ketone defects on the charge transport and charge recombination in polyfluorenes," *Advanced Functional Materials*, vol. 21, no. 23, pp. 4502–4509, 2011.

[161] T. Kietzke, D. Neher, K. Landfester, R. Montenegro, R. Guntner, and U. Scherf, "Novel approaches to polymer blends based on polymer nanoparticles," *Nat Mater*, vol. 2, no. 6, pp. 408–412, 2003.

[162] C. D. Muller, A. Falcou, N. Reckefuss, M. Rojahn, V. Wiederhirn, P. Rudati, H. Frohne, O. Nuyken, H. Becker, and K. Meerholz, "Multi-colour organic light-emitting displays by solution processing," *Nature*, vol. 421, no. 6925, pp. 829–833, 2003.

[163] R. C. G. Naber, M. Bird, and H. Sirringhaus, "A gate dielectric that enables high ambipolar mobilities in polymer light-emitting field-effect transistors," *Applied Physics Letters*, vol. 93, no. 2, pp. 023301–3, 2008.

[164] Y. Setoguchi and C. Adachi, "Suppression of roll-off characteristics of electroluminescence at high current densities in organic light emitting diodes by introducing reduced carrier injection barriers," *Journal of Applied Physics*, vol. 108, no. 6, pp. 064516–7, 2010.

[165] J. J. M. Halls, J. Cornil, D. A. dos Santos, R. Silbey, D. H. Hwang, A. B. Holmes, J. L. Brédas, and R. H. Friend,

"Charge- and energy-transfer processes at polymer/polymer interfaces: A joint experimental and theoretical study," *Physical Review B*, vol. 60, no. 8, pp. 5721–5727, 1999.

[166] W. Tress, K. Leo, and M. Riede, "Optimum mobility, contact properties, and open-circuit voltage of organic solar cells: A drift-diffusion simulation study," *Physical Review B*, vol. 85, no. 15, p. 155201, 2012.